CO-CRYSTALLIZATION, STRUCTURAL AND PHYSICOCHEMICAL ANALYSIS OF ACTIVE PHARMACEUTICAL INGREDIENTS FOR ENHANCED PROPERTIES

MAYANK JOSHI

A thesis submitted for the partial fulfillment of

the degree of Doctor of Philosophy

Department of Chemical Sciences

Indian Institute of Science Education and Research Mohali

Knowledge city, Sector 81, SAS Nagar, Manauli PO, Mohali 140306, Punjab, India.

November 2021

Dedicated to my Family...

Declaration

The work presented in this thesis entitled **"Co-Crystallization, Structural and Physicochemical Analysis of Active Pharmaceutical Ingredients for Enhanced Properties"** has been carried out by me under the guidance of **Dr. Angshuman Roy Choudhury** at the Indian Institute of Science Education and Research Mohali. This work has not been submitted in part or in full for a degree, a diploma, or a fellowship to any other university or institute. Whenever contributions of others are involved, every effort is made to indicate this clearly, with due acknowledgement of collaborative research and discussions. This thesis is a bona fide record of original work done by me and all sources listed within have been detailed in the bibliography.

MAYANK JOSHI

Date:
Place:

In my capacity as the supervisor of the candidate's thesis work, I certify that the above statements by the candidate are true to the best of my knowledge.

Dr. Angshuman Roy Choudhury
Assistant Professor
Department of Chemical Sciences
Indian Institute of Science Education and Research Mohali

Date:

Place:

ACKNOWLEDGEMENT

Many people have been contributory to the emergence of this thesis. It would not have been possible to write this doctoral thesis without the help and support of my teachers, family, friends and colleagues. I take this opportunity to make a sincere attempt to thank them all.

First of all, I would like to thank God for giving me the opportunity to pursue this research work and blessing me to accomplish it. It is a great pleasure to express my sincere thanks and a deep sense of gratitude to my research supervisor **Prof. A. R. Choudhury** for introducing me to the exciting field of X-ray Crystallography. He has been very kind to give me a lot of freedom for work and gaining knowledge in my research work. Without his constant support and encouragement, it would not have been possible to complete my research work and, finally, this thesis. His cheerfulness and jovial manner are greatly appreciated. I will always be grateful to **Dr. A. R. Choudhury** for his kind help for the time he spent explaining the various aspects of our field and improving crystallographic skills. I would like to express sincere thanks for helping in software learning. He has inspired me to work independently and to think in a broader way. Thank you, sir, for your kind, valuable support and for shaping my personality in total during my Ph.D. tenure. The influence will be a part of my nature forever.

I sincerely pay my gratitude to **Dr. Sanjay Singh** and **Dr. Santanu Kumar Pal**, members of my doctoral committee, for fruitful discussions during the yearly assessment of my work. **Prof. T. N. Guru Row** from the Indian Institute of Science is acknowledged as an external examiner for the DST INSPIRE review committee and his helpful comments during my evaluation.

I wish to express my heartfelt thanks and indebtedness to **Prof. Kaisar Raza, Prof. Arunika Mukhopadhaya** and **Dr. Aakanksha Gulati** for providing the apt guidance and research platform for biological evaluations. It is my great pleasure to thank **Prof. Raza**, the key person in my biological research work. His timely hints, suggestions, and help are unforgettable.

I would like to acknowledge our institute director, **Prof. J Gowrishankar**, for providing the space and research and infrastructural facilities. I am grateful to all the faculties of IISER for their teaching and constant encouragement. I acknowledge IISER Mohali for central X-ray diffraction and NMR facilities. A special thanks to **Dr. Angshuman Roy Choudhury** for their training and support in all aspects of using the facility. I thank all faculty members of the Department of Chemical Sciences for facilitating the use of various departmental instruments, including UV-VIS and FTIR spectrophotometers, TGA and DSC instruments, XtaLabmini tabletop X-ray diffractometer etc.

I thank **Dr. Sagarika Dev** for her help, encouragement, and providing a homely atmosphere, especially preparing veg food. My sincere thanks to **Dr. Hare Ram Yadav** and **Dr. Prasanta Bhowmik**, my ex-lab mate, for handling chemicals, managing lab and lab notes, using different instruments and their software, and developing curiosity. It was an enjoyable experience to work with them and learn. I am also thankful for my current lab-mate, **Ms. Labhini Singla**, for her help, helpful discussion and creating delightful entertainment in the lab. Other lab members who were there for a

short period, including **Dr. Dheeraj Das, Dr. Mrinal Adak, Dr. Virendra Kumar, Manish, Chesta, Pooja etc.**, are also acknowledged for the support and for making the working atmosphere in the lab extremely enjoyable and cheerful.

I wish to thank my friends **Bara Singh, Yogesh, Sandeep, Prabhakar, Prateek, Sai Srinivas, Feroz, Pravesh, Pavit, Arup, Atanu, Kirti, Shaina, Monika, Nisha, Dhananjay, Bankar, Subhash, Chandu, Sonam, Nitin, Prashant etc.** for their cheerful companionship. I have always been surrounded by a large number of good friends who made my life pleasant.

I am thankful to the Department of Science and Technology (DST), Government of India and IISER Mohali for a research fellowship and financial support to carry out the experimental work, giving me the fellowship on time and also for providing all the research facilities that enabled me to complete my Ph.D. I also thank all the staff members of stores, purchase office, administrative office, account section, library, animal house and computing facility of IISER Mohali for their help and co-operation with time.

I also thank **Mr. Alok Rohatgi, Mrs. Vibha Vyas** and **Mrs. Taruna Parekh** for introducing me to the world of science and creating and maintaining my interest in this field from the 11th class onwards. I cannot forget the contribution of my school teachers towards building my character. My warm regards to them for their love, affection and teaching during my school days.

I am thankful to all my teachers from the pharmacy, especially **Dr. Kaisar Raza, Dr. Vipin Bharadwaj, Dr. Devesh Sawant, Dr. Ruchi Malik, Dr. Umesh Gupta, Prof. M. L. Sharma, Dr. Sunita Panchawat, Dr. Joohee Pradhan, Dr. Lalit Singh Chouhan, Dr. C. P. Jain** and **Dr. B. S. Poonia** for creating interest in the field, always supporting and teaching me new skills.

I express my most profound sense of gratitude to my parents **Mr. Dhaneshwar Joshi** and **Mrs. Kamla Joshi**, sister **Mrs. Pragya Purohit**, brother-in-law **Mr. Vishal Purohit**, and sweet nephew **Mr. Nakshatra Purohit** for their never-ending support, encouragement, and care throughout this journey. My parent's patience, love, affection, and faith in freedom keep me alive and show me my way in life. I am thankful to my beloved wife, **Mrs. Srishty Joshi**, for her love and unconditional support in this journey.

Thanks to the creatures which were used as animal models for various studies. My sincere gratitude to those sacrificed animals from the core of my heart. Be their souls rest in peace. I especially thank **Mr. Dashrath** for his help in the handling of animals. Last but not least, I would like to express my deep sense of gratitude to one and all who have helped me complete my present research work successfully.

Synopsis

This thesis entitled "**Co-Crystallization, Structural and Physicochemical Analysis of Active Pharmaceutical Ingredients for Enhanced Properties"** consists of **two parts and 6 chapters**. **Part 1** is dedicated to the study of cocrystallization of Psychiatric Drugs Amoxapine (AMX), Doxepin (DOX) and Zaleplon (ZLP) while the **Part 2** deals with the cocrystallization and biological studies on antibiotic drugs Ofloxacin (OFX) and Levofloxacin (LFX). **Chapters 1** is a brief introduction to the field of pharmaceutical cocrystallization and its importance in the pharmaceutical industry. **Part 1** of the thesis is subdivided in three chapters, **Chapter 2**, **Chapter 3** and **Chapter 4**. The **Chapter 2** describes the cocrystallization and structural analysis of Amoxapine while the **Chapter 3** covers the cocrystallization studies on Doxepin and the **Chapter 4** depicts the structural studies of cocrystals of Zaleplon. **Part 2** of the thesis is subdivided in two chapters, **Chapter 5**, and **Chapter 6**. The **Chapter 5** is dedicated towards the cocrystallization and biological study of Ofloxacin and the **Chapter 6** is dedicated to the cocrystallization and biological property studies on Levofloxacin.

Chapter 1 is a brief introduction to cocrystals, its importance and usefulness in the pharmaceutical industry. Cocrystallization is utilized to combine and optimize the properties of different compounds for specific applications such as improving energetic materials, pharmaceuticals and other compounds. One of the most widely studied applications of cocrystallization is the formation of novel materials using active pharmaceutical ingredients (API's) for modifying the structure and physical properties of the API's. Cocrystallization influences the physical properties *viz*; solubility, melting point, stability and bioavailability. The objective of pharmaceutical cocrystallization is to produce novel cocrystal analogs that have enhanced properties compared to the pure API's without making and/or breaking any covalent bonds. In the last couple of decades several different drug molecules were targeted for cocrystallization to improve their physical properties. Herein, in this thesis we have used drugs of two categories: (1) psychiatric drugs like Amoxapine (AMX), Doxepin (DOX) and Zaleplon (ZLP); (2) antibiotic drugs like Ofloxacin (OFX) and Levofloxacin (LFX). The basis of selection of these drugs was their poor solubility and dissolution rate in water.

Chapter 2 of **Part 1** of this thesis unravels the study of cocrystallization of Amoxapine (AMX), which is a benzoxazepine derivative and exhibits anti-depressant properties. AMX has very low solubility in water and low dissolution rate. We have cocrystallized AMX with natural acids as coformer using ethanol as solvent; by solvent drop grinding method. We have used powder X-ray diffraction patterns of the novel salts to identify the formation of a new solid phase, different from the starting materials. DSC analysis also indicated different melting point of newly formed solid compared to AMX and the coformers. Single crystals of salts of AMX with natural acids were grown by solvent evaporation method. Crystal structure of AMX: D (-) Tartaric acid, AMX: Fumaric acid, AMX: Maleic acid, AMX: Succinic acid and AMX: Malonic acid were determined by single crystal X-ray diffraction

(SCXRD) and their structures were analyzed in detail. Solubility and intrinsic dissolution rate (IDR) of salts were determined in PBS7 at 37 ˚C and it found 4.1 to 193.7 times higher solubility and 13.1 to 283.2 times enhanced IDR.

Chapter 3 of **Part 1** of this thesis describes the study of cocrystallization of Doxepin (DOX), which is a dibenzoxazepine derivative tricyclic antidepressant used to treat depression, anxiety and insomnia. DOX has some physical challenges like low solubility, poor bioavailability and liquid state of existence at room temperature. Cocrystallization of DOX with natural acid has been performed by solvent evaporation method. Three solid salts of DOX were prepared with oxalic acid, terephthalic acid and 4-nitrobenzoic acid. These salts have been characterized using PXRD and DSC methods. Detailed structural analysis has been performed using SCXRD method. We have determined the solubility and it was found to be enhanced by 1.2 to 11.2 times. We have also determined IDR of these salts in PBS7 by USP II method.

Chapter 4 of **Part 1** of this thesis is about the study of cocrystallization of Zaleplon (ZLP), which is nonbenzodiazepine hypnotic, and is used in the treatment of insomnia. ZLP faces some challenges in physical properties like poor water solubility and dissolution rate. Cocrystallization of ZLP with natural acids has been synthesized by solvent evaporation method. These solids were characterized by PXRD and DSC analysis. Single crystals of ZLP cocrystal with fumaric acid, terephthalic acid, oxalic acid and malonic acid were grown by slow evaporation method. Single crystal structure is determined by SCXRD and detailed analysis was performed. We have experimentally determined the solubility of all the cocrystals and ZLP and found an increase in solubility by 2.8 to 18.8 times. We have also determined IDR of all compounds in PBS7 and enhanced dissolution rate was found up to 4.41 times.

Chapter 5 of **Part 2** of this thesis is focused on the study of cocrystallization of Ofloxacin (OFX), which is a broad-spectrum fluoroquinolone antibiotic agent, which is used to treat various microbial infections. We have cocrystallized OFX with naturally occurring acids *via* solvent drop grinding method. These salts have been characterized by PXRD and DSC. Significant size of single crystal of these salts could not be grown. We have performed solubility test on all developed salts and pure drug and got enhanced solubility for all salts by 10.4 to 21.1 times. We have also determined IDR experiment on all solid phases and have found increased by 21.2 to 42.9 times. Microbiological activity of all salts has been seen with determination of MIC in gram negative bacteria *E. coli* and *S. typhymurium.* OFX: pimelic acid has shown improved MIC in case of *E. coli* while all salts of OFX have shown better MIC results in case of *S. typhimurium*.

Chapter 6 of **Part 2** of this thesis presents the study of cocrystallization of Levofloxacin (LFX), which is synthetic fluoroquinolone class of broad-spectrum antibiotic. LFX is the more potent with low water solubility and poor dissolution rate. Salts of LFX was formed with naturally occurring and

pharmacologically acceptable acids by solvent drop grinding method. All salts were characterized through PXRD and DSC. We could successfully grow five single crystals of LFX with D (-) tartaric acid, maleic acid, pimelic acid and 3-nitrobenzoic acid by slow evaporation method. These are crystallized in chiral space groups. Solubility and IDR also determination for LFX salts and LFX in PBS7 at body temperature 37 ˚C using UV−vis spectroscopy and found significantly improved these physical properties by many folds. MIC of LFX salts was determined in *E. coli* and *S. typhymurium* with significant improvement in LFX: succinic acid salt. On the basis of these results, 3 salts were selected for cell line study in caco2 liver cell line and IC_{50} value of LFX: Maleic acid and LFX: Succinic acid was found more potent then pure LFX. Pharmacokinetics and biodistribution studies are performed in Balb/c mice in one compartment oral modal and single point biodistribution is determined in the heart, liver, kidney and brain of mice. We have seen substantial results of pharmacokinetic parameters and biodistribution in vital organs. LFX: succinic acid and LFX: maleic acid salts have shown better results as an alternative of LFX.

Contents

Chapter 3: Cocrystals of Doxepin with Improved Solubility for Enhanced Pharmaceutical Applicability

Chapter 1

Introduction

Chapter 1

1.1 Solid Doses Forms

The solid-state of a material, whether inorganic ionic substances or covalently bonded organic molecules, exists in varied structures (polymorphs),[1] which, although consisting of the same chemical composition, may exhibit miscellaneous physical properties. A compound in its solid-state exists as either a crystalline material or as an amorphous substance. The amorphous form is well-defined as a solid with a narrow distribution range, meaning there is no ordered arrangement of atoms in the three-dimension. On the other hand, crystalline form has an ordered array of atoms or molecules in space.[2] Amorphous form of material has greater mobility in comparison to the crystalline phase. It does not diffract X-rays in a well-defined periodicity, as shown in Figure 1.1.[3] A substance that occurs in a crystalline form can exist in various forms giving rise to different polymorphs demonstrating differences in the molecular arrangement. Still, each state has the same elemental composition. This phenomenon is called polymorphism.[1,4] Thermodynamically, only a single polymorph is regarded as a stable form under some specified conditions. In common practice, as per the laws of kinetics, the metastable polymorphic states of a compound can coexist with other more stable forms.[5,6]

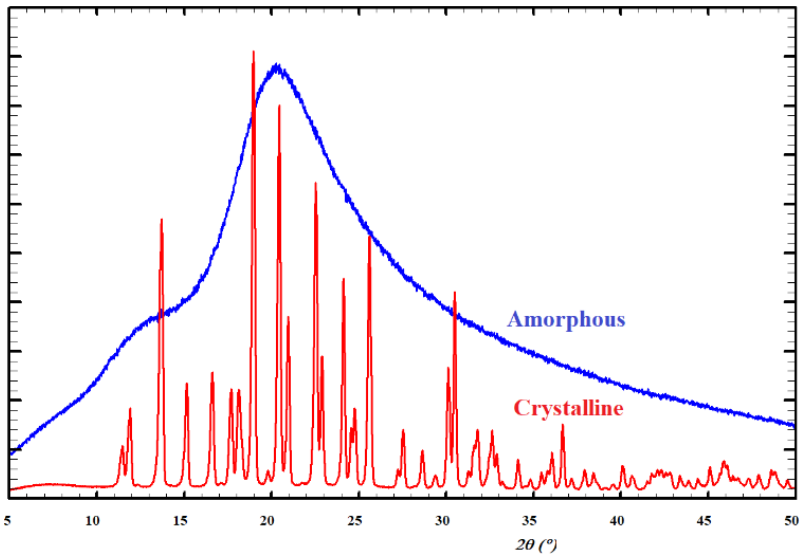

Figure 1.1: X-ray diffraction patterns of amorphous and crystalline materials.

Active pharmaceutical ingredients (APIs) are rarely administered alone; instead, they are given as part of a formulation combined with nonmedicinal agents that serve diverse and specialized pharmaceutical functions. Selective use of these pharmaceutical ingredients or excipients produces various types of dosage forms. The pharmaceutical constituents solubilize, suspend, thicken, dilute, emulsify, stabilize, preserve, color and flavor API into effective and attractive dosage forms.[7] All dosage forms show unique physical and pharmaceutical characteristics. The suitable design and formulation of a dosage form involve considering the physical, chemical, and biological aspects of drug substances and pharmaceutical components to produce the product. The drugs and pharmaceutical materials must be compatible with each other to create a drug product that is stable, safe, attractive, productive and easy to administer.[8] The product should be manufactured with appropriate measures of quality control and packaged to keep the product stable. The product should be labelled appropriately to use correctly and stored under environments that maximize shelf life.[9,10]

The formulation of a drug matter into a dosage form requires us to establish the framework of the desired product development. Several initial formulations are developed and examined for selected features, e.g., drug release profile, bioavailability, clinical effectiveness etc.[11] Hereafter, we scale up the production for pilot plant studies. The formulation, which best meets the goals for the product is selected to be its master formula. Each batch of product manufactured afterward must meet the conditions established in the master formula.[12] There are many different forms in which a drug agent may be placed for the convenient and efficacious treatment of disease. Before a drug candidate is formulated into dosage forms, various factors like the physiochemical properties of the drug substance and different therapeutic considerations.[9] If the medication is proposed for systemic use and oral administration is desired. We generally prepare tablets and capsules because they are effortlessly handled by the patient and are most appropriate in the self-administration of medication. If a drug constituent has to be applied in an emergency where the patient may be unconscious and unable to take medicine orally, then the drug is prepared to give in the form of an injection. But the most preferred route of administration of the drug is oral and solid dosage form (Tablet or capsule) because they are handily carried, readily identified, and easily taken.[13] These are favoured over liquid dosage forms due to the convenience of having the supply. There is no need to use measuring devices, which may be inconvenient and result in less than accurate dosing.[14] Maximum tablets and capsules are tasteless when swallowed, which is not the case with oral liquid medication. These solid dosage forms have abundant features like shapes and color, identification code embossed or imprinted on their surface, available in various dosage strengths, and provide the prescriber with accurate, individualized dosage for the patient.[15] From a pharmaceutical standpoint, solid dosage forms are efficiently and productively manufactured. They are packed and shipped by manufacturers at lower cost and with less breakage when compared to the liquid state. They are more stable and have a longer shelf life also than their liquid counterparts. Suppose the patient cannot swallow an intact solid dosage form. In that case, an alternative product is also possible such as

a chewable tablet, instant dissolving tablet, oral or nasal inhalation solution, oral liquid, suppository, or injection. These solid dosage forms are given mainly in three states, i.e., powder, tablets and capsules.[16]

1.1.1 Powder

Most of the active and inactive pharmaceutical ingredients occur in the solid state as amorphous powders or crystalline forms of various structures. A powder is a dosage form made of a solid or mixture of solids reduced to a finely divided state and proposed for internal or external use.[17] The term "powder" in pharmacy may be used to describe the physical form of material, i.e., a dry substance composed of finely divided particles or, it may be used to designate a type of pharmaceutical preparation, i.e., a medicated powder intended for internal (oral powder) or external (topical powder) use.[18] Anciently solid drugs were administered in the form of powder from natural sources as plant barks (cinchona), root (ashwagandha), leaves (senna) etc. Historically powders were used to administer insoluble drug-like calomel, mercury, bismuth salt and chalk.[19,20] Internal route of administrations is oral, intranasal and inhalation, whereas externally used as topical powder. We can easily alter the dose quantity of powder which is not the case with tablets or capsules, so the powder has significance in clinical studies. The dose of powder drug can be adjusted for children and infants or mixed with another suitable compound to make it more accepted. It is ideal for bulky medications where it is challenging to prepare tablets and capsules. Powders provide a quick onset of action because they are readily dispersed due to large surface area and require only dissolution, not disintegration, before absorption.[21,22] Even though the therapeutic use of medicinal powders is limited. It is used to prepare other dosage forms as fillers, granules, tablets, capsules, solutions, suspensions, ointments, creams, etc.

1.1.2 Tablets

Tablets are solid dosage forms generally prepared with the help of appropriate pharmaceutical excipients. Tablets might vary in size, shape, color, weight, hardness, thickness, disintegration, dissolution rate, and other characteristics, depending on their envisioned use and method of production.[23] Generally, tablets are made for oral administration of the drug, while some are administered sublingually, buccally, or vaginally.[24] Tablets are prepared mainly by compression, with an inadequate number prepared by molding. The compressed tablets are manufactured with tablet machines capable of employing tremendous pressure in compacting the powdered or granulated material. The shape and dimensions of tablets are determined by using various shaped punches and dies. Molded tablets are prepared by tablet machinery on a large scale or by hand on a small scale, forcing dampened powder material into a mold from which the formed tablet is then ejected and allowed to dry. Some tablets are scored or grooved, which lets them be easily broken into two or more parts.[25,26] This enables the patient to swallow reduced portions as may be desired or when prescribed. Some coated tablets are not scored since they may have special coatings and drug release features. They are not proposed to be broken or cut manually by the patient that would be compromised by altering the tablet's physical integrity.[27]

1.1.3 Capsules

Capsules are the solid dosage forms where therapeutic agents or inert ingredients are enclosed in a small gelatin shell. Capsule shells of gelatin may be hard or soft, depending on the composition. The gelatin shells may be composed of two pieces, a body and a cap, or they may be composed of a single sample. Two-piece capsules are generally referred to as hard gelatin capsules, and one-piece capsules are regularly referred to as soft gelatin capsules. These dosage forms are intended to be swallowed whole.[28] However, it is relatively common in hospitals and extended care facilities to open capsules or crush tablets to blend with food or drink, exclusively for children or other patients unable to swallow solid dosage forms. This practice should be done with the permission of the pharmacist since the drug release physical characteristics of certain dosage forms can be altered and can adversely affect the patient's wellbeing.[29]

1.2 Challenges of Solid Dosage Form and Solution

The oral route of drug administration has been the most desirable and preferred route of administering therapeutic agents for their therapeutic effects. Still, the poor water solubility of the drug is a significant challenge for formulations. The solubility is understood as a maximum quantity of solute that can dissolve in a certain amount of solvent or quantity of solution at a specified temperature.[30] As the solubility increases, bioavailability increases. Solid dosage forms are administered orally; about 40 % suffer from lower water solubility and fall under BCS class II and IV.[31] In the last ten years, ~13% compound annual growth increased for the solubility enhancer.[32] In research and development, around 80% of drug candidates, are poorly soluble in water, which can cause difficulties in the effectiveness of oral pharmaceutical dosage forms. It results in poor oral dissolution rate, stability, absorption, distribution, bioavailability and excretion of APIs.[33]

Biopharmaceutics classification system (BCS) was first devised in 1995 and categorize the drug into four classes according to their solubility and permeability as shown in table 1.1.[34] solubility related challenges are faced in the BCS Class II and Class IV drugs (where the rate of dissolution becomes the limiting step for the absorption of drug) which encompass many medicines like Gliclazide, Glipizide, Nimodipine, Felodipine, Zaltoprofen, Flurbiprofen, Indomethacin, Ibuprofen, Ketoprofen and Diclofenac etc.[35]

Table 1.1: BCS classification of drug.

Class	Permeability	Solubility
I	High	High
II	High	Low
III	Low	High
IV	Low	Low

Poorly soluble drugs are often a challenge for the pharmaceutical industry. The improvement of drug solubility and its oral bio-availability remains one of the most challenging aspects of the drug development process, especially for the oral drug delivery system. We need to adopt various traditional

and newer methods to solve the problem of poor aqueous solubility. These methods include solid dispersion, complexation, liquisolid, hydrotropy, salt formation, cocrystallization, and self-emulsifying strategies, commonly referred to for solubility enhancement of BCS class II and IV compounds.[36] In the process of drug absorption, dissolution rate has a vital role for lipophilic drugs for maximal therapeutic effect.[37] Dissolution rate is the process when the solute particles (here drug) go into a solution over time. The dissolution of the drug is related to drug solubility.[38] Hence, solubility plays a significant role in the control of the dissolution speed. Henceforth it's required to improve the absorption and bioavailability of poorly water-soluble drugs by using various technologies.[39]

These technologies involve changes in physical properties by particle size reduction, polymorphism, co-solvency, cocrystallization, hydrotropy, pH alteration, micronization, changing the dielectric constant of the solvent, changes into amorphous forms, and salt formation. Chemical modifications using surfactants, complexation, hydrates or solvates, soluble pro-drugs, selective adsorption on insoluble carriers, functional polymer technology, precipitation inhibitors, solvent deposition, ultrasonic waves, spherical agglomeration, co-precipitation process, lipid-based delivery system, microemulsion, micellar, porous microparticle, floating drug delivery system, solid dispersions, vascular approaches can be targeted to progress the bioavailability of poorly solvable molecules.[40–42] The basic techniques followed by all the currently available technologies engaged in solubility and dissolution enhancement maximize bioavailability and therapeutic efficacy.

1.3 Crystal Engineering of Solid Active Pharmaceutical Ingredient

The concept of crystal engineering[43] has emerged since 1989 as a massive tool in developing novel crystalline phases of various combinations of different materials to control and manipulate the physical and chemical properties of already existing materials. scientific community as well as by regulatory bodies tries to define cocrystals. According to US-FDA, cocrystals are "*solids that are crystalline materials composed of two or more molecules (API and excipient) in the same crystal lattice*." This definition in their guidance document has been a matter of concern by the researchers working in this field. Its consequences were carefully debated in the Indo-US Bilateral Meeting by several leading academic and industrial groups working in the area of cocrystals. Solid form in a drug product that is a new cocrystal entity is considered a new polymorph (solvate/hydrate) of the active pharmaceutical ingredient (API). The scientific community has defined cocrystals as "*solids that are crystalline single-phase materials composed of two or more different molecular and/or ionic compounds generally in a stoichiometric ratio, which are neither solvates nor simple salts."*[44] This definition excludes simple salts, hydrates, and solvates, but these could be cocrystals in the "solvated/hydrated salt cocrystals" case.[45] The multicomponent systems like solid solutions, inclusion complexes and dispersions are not encompassed in the above-proposed definition. European Medicines Agency has given a similar definition in a paper, which defined cocrystals as "*homogenous (single-phase) crystalline structures made up of two or more components in a definite stoichiometric ratio, where the arrangement in the crystal lattice is not based on ionic bonds, and components of a cocrystal*

may nevertheless be neutral as well as ionized" .[46] FDA definition present a plain view. At the same time, other definitions include additional supramolecular features of cocrystals.

Cocrystal can be designed by applying the principles of supramolecular chemistry to change the solid-state properties of an API. Selection of suitable coformer is important, which shows compatibility to form a supramolecular synthon with API molecules.[47] These supramolecular synthons, as shown in Figure 1.2, are of two types (i) *Homosynthons*: when the same complementary functional groups are present between two molecules, e.g., carboxylic acid-dimer, amide-dimer; (ii) *Heterosynthons*: when different but complementary functional groups present between two molecules, e.g., carboxylic acid-amide, carboxylic acid-aromatic nitrogen, alcohol-aromatic nitrogen, and alcohol-amine. CSD survey suggests that the probability of occurrence of carboxyl-pyridine heterosynthon is more expected than acid-acid homosynthon.[48]

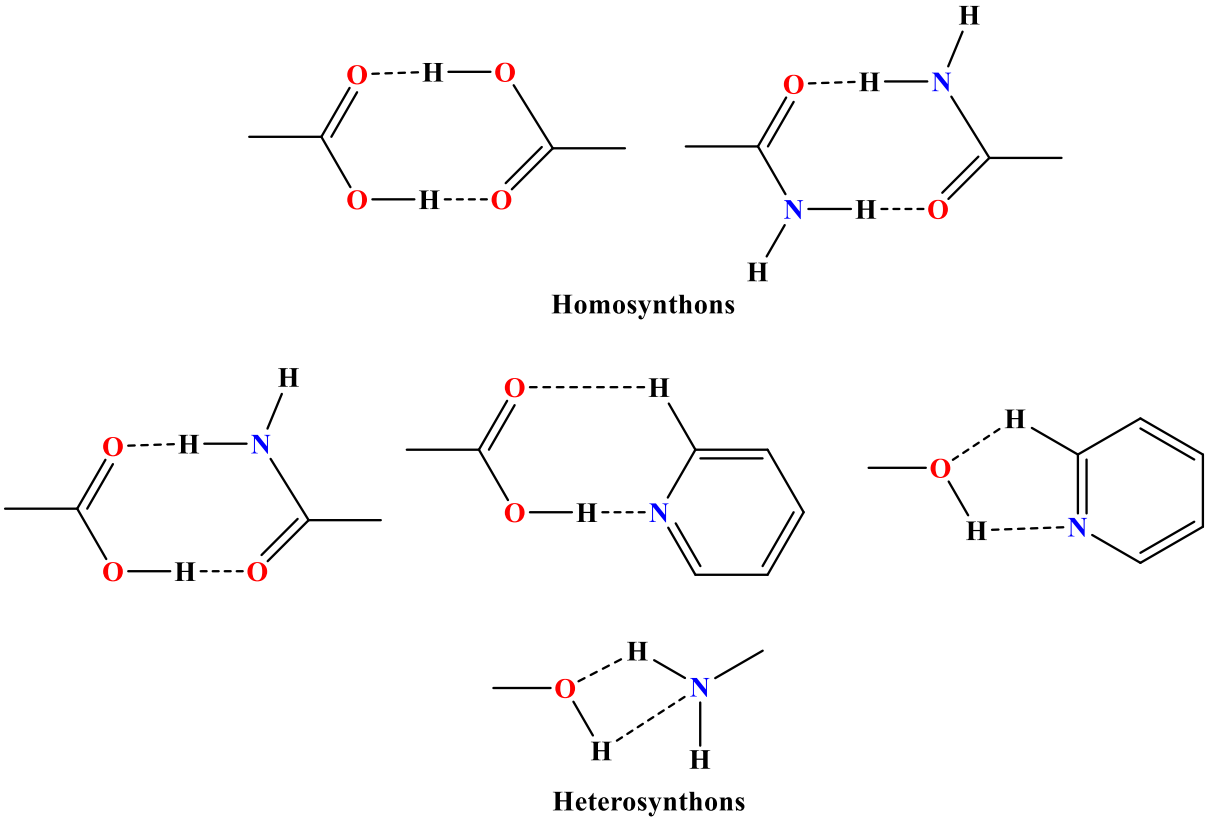

Figure 1.2: Pictural representation of homosynthons and heterosynthons.

An additional approach to predicting cocrystal formation is ΔpK_a rule of three, as shown in Figure 1.3. According to this rule, if the difference ΔpKa between the pKa of the base and pKa of the acid is more than three, then the salt formation will prevail, whereas if ΔpKa is less than 1, that will generally result in the construction of a cocrystal. In contrast, when the ΔpK_a is between 1-3, it will result in material encompassing cocrystals or salts, shared protons, or intermediate ionization states, which can be named salt-cocrystal hybrids.[49,50] Some studies suggest that ΔpK_a more than four will exclusively result in ionized acid-base complexes, whereas ΔpK_a less than -1 will result in nonionized acid-base complexes as cocrystals or solvates or hydrates.[51]

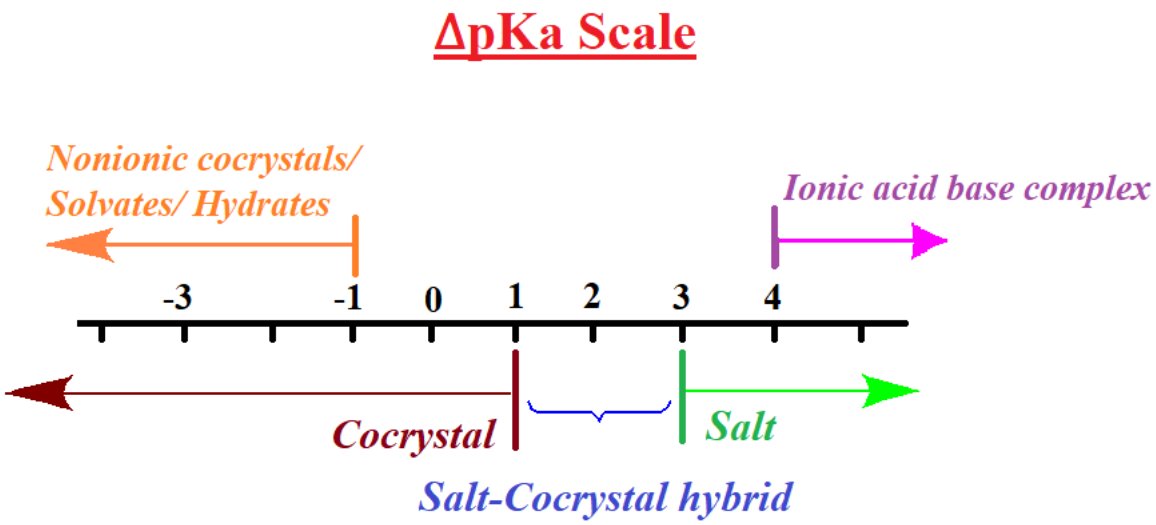

Figure 1.3: ΔpK_a rule of three for prediction of cocrystallization.

The application of crystal engineering includes designing multicomponent crystalline phases of a combination of two or more compounds[52] to form a sizeable metal-organic framework (MOF)[53] and covalent organic framework (COF).[54] The concept of the development of different crystalline phases of several biologically significant molecules to boost their physical properties has directed researchers across the globe to a new area of cocrystallization of drugs with other biologically acceptable molecules.[55–58] Cocrystallization and salt formation of various pharmaceutically important molecules have emerged as an expanding field of contemporary research.[44,59] Cocrystallization of antibacterial agents,[44] antifungal drugs,[60] different antidepressants,[61] antitubercular[62] and various other types of drugs[63,64] have been reported to have better solubility, dissolution rate, thermal and environmental stability and bioavailability. Recent efforts on cocrystallization of fluconazole by Karanam et al. resulted in new fluconazole polymorphs under different coformers.[65] They have developed four new polymorphs of fluconazole and studied their structural aspect. They developed new salts of enrofloxacin, and these are found highly soluble than pure drug.[66] This study indicated that the crystal engineering approach might apparently fail to generate the targeted cocrystal but eventually result in a new crystalline phase (polymorph) of the native drug.

Pharmaceutical cocrystal formation was introduced into the vocabulary of pharmaceutical research by Örn Almarsson and Michael J. Zaworotko.[67] They used the crystal engineering concept to design various types of derivatives of the pharmaceutically active compound to modify their physical and pharmacokinetic properties.[68–72] In recent years cocrystallization concept has been established as a general method for modification, even though primarily by trial and error, the solid-state properties of APIs.[73] Harry Brittain and co-workers contribute to giving the cocrystal system for pharmaceutical applicability[74–76] and predicting its importance in new drug development.[77]

1.4 Classification of work

Many active pharmaceutical ingredients (API's) pose challenges due to their low water solubility, poor aqueous dissolution rate and low bioavailability. We have identified a few such drugs which have lower water solubility. We tried to use an approach of cocrystallization to address this problem. We have selected two different classes of drugs, namely psychiatric drugs and antibiotics, as shown in Figure 1.4. In the first class of drugs, we have chosen amoxapine (AMX), doxepin (DOX) and zaleplon (ZLP). AMX and DOX are antidepressant drugs, but ZLP is a hypnotic drug used to treat insomnia. The second class contains antibiotics drugs ofloxacin (OFX) and levofloxacin (LFX).

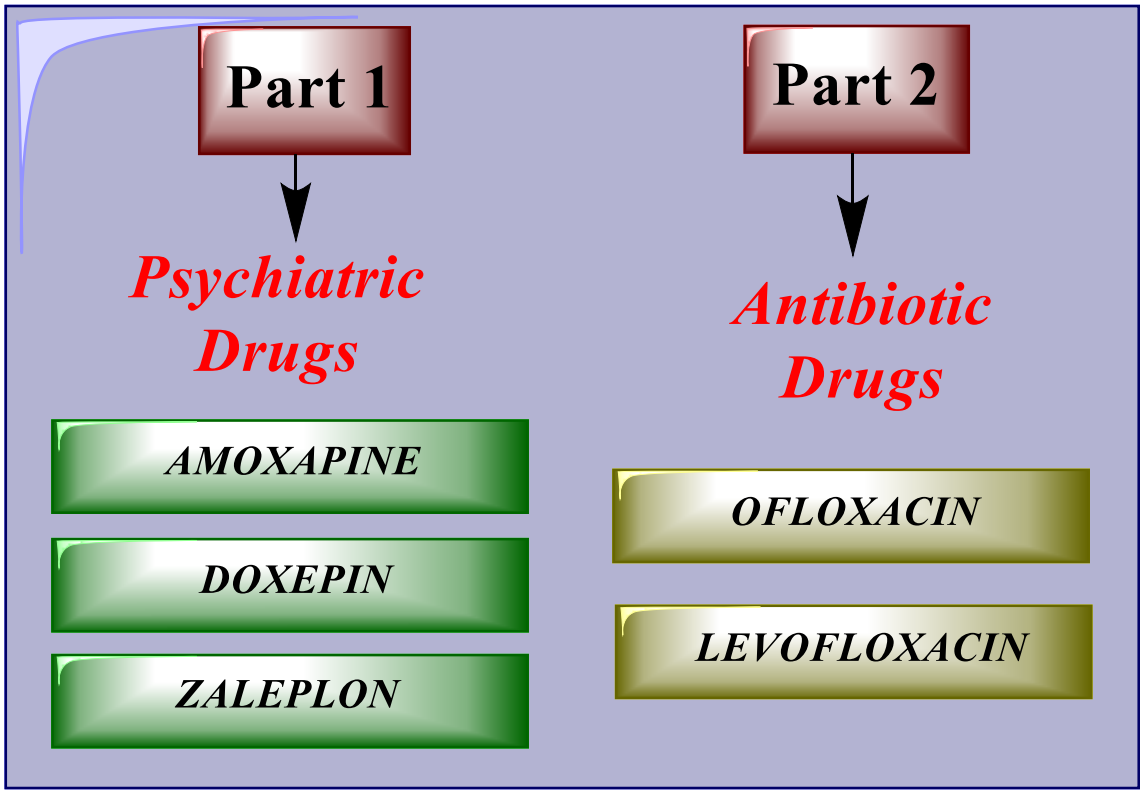

Figure 1.4: Classification of work.

1.5 Workflow

The methodology used in this thesis includes cocrystallization of the selected drug molecule with the biologically accepted coformer molecule by solvent drop grinding method or a solvent evaporation method. The salt/cocrystal formed by solvent drop grinding method or solvent evaporation method has been characterized initially by powder X-ray diffraction patterns and differential scanning calorimetry. Once the formation of a new solid phase is confirmed, single crystals of salt/cocrystals were grown using types of solvent systems to study the structural insight of the molecules. We collected the single-crystal X-ray diffraction data for newly developed single crystals and determined the interaction pattern in crystal packing. We have generated the Hirshfeld surface area by these X-ray diffraction data to analyze the intermolecular interaction between two molecules across the molecular surface. Further, we focused on determining the physical properties of newly developed salts/cocrystals to determine the changes in the properties of the salts/cocrystals compared to the corresponding API.

In the second part of the thesis, we will demonstrate the biological properties of these new derivatives of antibiotic drugs, both *in-vitro* and *in-vivo*. We have determined its minimum inhibitory concentration in *E. Coli* and *S. Typhimurium* bacteria for the microbiological study. Then we have studied IC_{50} value in caco2 liver cell line infected with *S. Typhimurium* to see its effect in mammalian cell line infection. Further, we determined the pharmacokinetic parameters in the animal model. We have also determined the area under the curve (AUC), the volume of distribution (V_d), biological half-life ($t_{1/2}$), elimination rate (K), and clearance (Cl) in Balb/c mice. We have performed a biodistribution study in the Balb/c mice one compartment oral model. We have determined single-point biodistribution in vital organs like the heart, liver, kidney, and brain. These studies would highlight the purpose and importance of our cocrystallization of drugs to improve their physical and biological properties.

PART-I

Psychiatric Drugs

Chapter 2

Salts of Amoxapine with Improved Solubility for Enhanced Pharmaceutical Applicability

Chapter 2

2.1 Introduction

Amoxapine (AMX; 2-chloro-11-(piperazine-1-yl)dibenzo[b,f][1,4]oxazepine) is a tricyclic dibenzoxazepine based antidepressant drug which is generally used for the treatment of depression.[78] Amoxapine has been used as a rapidly acting antidepressant agent over other cyclic antidepressants available in 1980 and became popular in the United States.[79] The *N*-desmethyl analogue of loxapine, named amoxapine[80] (Figure 2.1), showed neuroleptic action and antidepressant activity[81], especially in psychotic depression.[80] Various activities of AMX like noradrenaline reuptake inhibition,[82] 5-HT2 receptor antagonism,[83] and dopamine D2 receptor antagonism[84] have been studied. AMX blocks the reuptake of the neurotransmitter norepinephrine, with little effect on serotonin.[85] AMX may be an atypical antipsychotic agent because it antagonizes dopamine D2 receptor.[86]

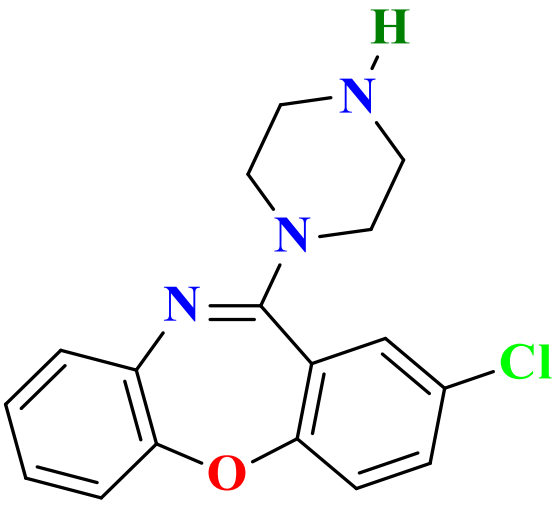

Figure 2.1: Structure of Amoxapine drug molecule.

Crystal engineering plays a significant role in the efficient design and synthesis of pharmaceutical cocrystals.[87] In recent decades, there has been a considerable increase in the study and use of multicomponent solid forms of pharmaceuticals to achieve improved physical properties by the academic community and pharmaceutical industry.[88–91] Cocrystallization of active pharmaceutical ingredients is conducted with pharmaceutically acceptable co-formers, generally recognized as safe materials.[92] The concept and application of cocrystallization to modify physical properties are far from

new development. These include aqueous solubility, dissolution rate, melting point, bioavailability, physicochemical stability and tablet compression-manufacturability.[93–96] In this context, a recent perspective has decorated the definition and classification of cocrystals.[44]

AMX has poor water solubility and low bioavailability.[97] These problems of AMX can be solved by cocrystallization of AMX with organic acids. These coformers are generally recognized as safe (GRAS) in the list of The Food Safety and Inspection Service (FSIS) regulations.[98] We have selected D (-) tartaric acid, D (+) tartaric acid, Fumaric acid, Maleic acid, Succinic acid, Citric acid, Malonic acid, L (-) Malic acid and Adipic acid for our experiments. Using the salt form is one of many possible routes to achieve improved aqueous solubility, e.g., the use of amorphous form, crystalline form, solvate form, or different polymorphs could all help with this problem.

2.2 Experimental Section

2.2.1 Materials

Amoxapine (99.9% pure) was bought from Sigma-Aldrich. The cocrystal formers were purchased from various commercial suppliers such as Adipic acid (99.5% purity) from Sigma Aldrich; D (-) Tartaric acid (99% purity) from Spectrochem Pvt. Ltd., India; Fumaric acid (99% purity), Maleic acid (99.5% purity) and Succinic acid (99.5% purity) from Sisco Research Laboratories Pvt. Ltd., India; D (+) Tartaric acid (99.5% purity) from Qualigens Fine Chemicals Pvt. Ltd., India and Citric acid (99.7% purity), Malonic acid (99% purity), L (-) Malic acid (99.5% purity), Di-sodium hydrogen phosphate anhydrous (99% purity) and potassium dihydrogen phosphate anhydrous (99% purity) from Hi-media laboratories Pvt. Ltd. Analytical grade solvents Ethanol (99.9% purity) and Methanol (99.9% purity) were obtained from Merck, Millipore Corporation, USA.

2.2.2 Synthesis of Salts

The salts were synthesized by the solvent drop grinding method. An equimolar mixture of the AMX and a coformer (one among maleic acid, fumaric acid, citric acid, succinic acid, D-(-)-tartaric acid, (+)-tartaric acid, adipic acid, l-malic acid and malonic acid) was made by accurate weighing. 100 µL of ethanol was added to the mixture using a micro pipette and was ground in agate mortar and pestle till a free-flowing powder was formed. The same was followed about five to six times till a new single-phase was obtained. Powder X-ray diffraction data were recorded after a new single-phase was obtained. Once a new single-phase was formed, then the resulted mixture was used for DSC. A portion was dissolved in various solvent systems and kept for a single crystal's growth by a slow evaporation process.

2.2.3 Powder X-ray Diffraction (PXRD)

PXRD data of AMX and salts were recorded on a Rigaku Ultima IV diffractometer with parallel beam geometry equipped by a Cu K_α source, 2.5° primary and secondary solar slits, 5° in-plane divergence slit with 10mm height limit slit, sample rotation stage (120 rpm) attachment and DTex Ultra

detector. The data were collected over 2θ range 5° – 50° with a scanning speed of 2° per minute with 0.02° steps.

2.2.4 Thermal Analysis

Perkin-Elmer DSC8000 was used to determine the melting points and thermal properties of the complexes/salts. All the samples (2-5 mg) were heated at 5 ºC / min heating rate in sealed aluminum pans. The melting points and the melting enthalpies of AMX and their salts were obtained from the Differential Scanning Calorimetry (DSC) data.

2.2.5 Single Crystal X-ray Diffraction (SCXRD)

Single crystal X-ray diffraction data were collected using a Rigaku XtaLABmini X-ray diffractometer equipped with Mercury CCD detector with graphite monochromatic Mo-Kα radiation (λ = 0.71073 Å) at 100.0 (2) K using ω scans. The data were reduced using CrysAlisPro 1.171.38.46, and the space group determination was done using Olex2.[99] The crystal structures were solved using ShelXT[100] and were refined using ShelXL[101] through the Olex2 suite. All the hydrogen atoms were geometrically fixed and refined using the riding model. Absorption correction was done by the multi-scan method. Data collection, crystal structure solution and refinement details for all the salts are listed in Table 2.3. All the packing and interaction diagrams have been created using Mercury 3.9 and 4.0.[102]

Single crystal of 1:1 salt of AMX with D (-) tartaric acid was grown in dimethyl sulfoxide (DMSO) solvent (stirred at 90 ºC). The clear solution was then cooled to room temperature. Then this solution was kept for slow evaporation at room temperature. Good quality single crystals were obtained after 15-20 days. Crystals of AMX with fumaric acid 1:1 salt were gained from the Water: Methanol (1:1) mixture at 4 ºC in the refrigerator. Another crystal of AMX with maleic acid in 1:1 salt was grown in a 1:1 water: ethanol mixture at 4 ºC. Crystals of AMX: succinic acid and AMX: malonic acid were found in water at 4 ºC. Good quality single crystals were found after 10-15 days.

2.2.6 Hirshfeld Surface Analysis

Hirshfeld surfaces and 2D fingerprint plots on the single crystal data were generated using Crystal Explorer 17.5 package.[103–105] All the intermolecular interactions between AMX and corresponding co-former were studied using Hirshfeld surfaces, and these intermolecular interactions were located within crystal packing. The function d_{norm} is a ratio of the distances of any surface point to the nearest interior (d_i) and exterior (d_e) atom and the van der Waals radii of the atoms. The normalized contact distance (d_{norm}) could be expressed following the equation:

$$d_{norm} = \frac{d_i - r_i^{vdW}}{r_i^{vdW}} + \frac{d_e - r_e^{vdW}}{r_e^{vdW}}$$

Where r_e^{vdW} and r_i^{vdW} denote the corresponding van der Waals radii of atoms. The negative value of d_{norm} indicates that the sum of d_i and d_e is shorter than the sum of the relevant van der Waals radii, which is considered the closest contact and visualized in red. The white color represents intermolecular distances close to van der Waals contacts with d_{norm} equal to zero. In contrast, contacts more extended than the sum of van der Waals radii with positive d_{norm} values are colored with blue. D_i versus d_e's plot

is a fingerprint plot that identifies the different intermolecular interactions between AMX and surrounding molecules in the crystal lattice. The short and directional interactions are depicted via sharp spikes and vice versa. We have drawn the fingerprint plots between the atoms present in the AMX salt and we have studied the interaction between all the atoms inside and outside of Hirshfeld surfaces. These interactions between all the atoms are plotted and which compares the relative contributions, giving a holistic view.

2.2.7 Partition Coefficient

The partition coefficient of AMX and AMX salts was determined by the slow stirring method.[106] We had taken a conical flask and added 10 mg of pure AMX or the novel salts, 10 mL of phosphate buffer solution at pH 7 and 10 mL n-octanol. Individual conical flasks were stirred at 300 RPM for 24h. After that, we separated the phases by separating the funnel. These phases were diluted 100 times by corresponding solvents, and the absorbance was recorded by UV-Vis spectrophotometry.[107] Concentration of AMX in each phase was calculated by fitting this value in calibration curves, and partition coefficient (P) was calculated using the following formula and hence the value of $log_{10}P$ was calculated.

$$\mathrm{P} = \frac{Concentration\ of\ drug\ in\ octanol}{Concentration\ of\ drug\ in\ PBS7}$$

2.2.8 Solubility Analysis using UV-Vis Spectroscopy

The solubility of the AMX salts and AMX was determined by using UV−Vis spectroscopy. The calibration curves were drawn for AMX and AMX salts using known concentrations and measuring the absorbance at λ_{max} in phosphate buffer solution at pH 7 on Lab India UV3200 UV-Vis spectrophotometer.[108] Concurrently saturated solutions of pure AMX and all AMX salts were prepared by stirring (1500 rpm for 24 h) an excessive amount of the compound in 2 mL of phosphate buffer solution at pH 7 in 5 mL sealed vials at 37 °C. These solutions were then centrifuged at 10000 rpm for 15 min, and the supernatant solution was diluted 10000 times using phosphate buffer solution at pH 7. The absorbance of the diluted solution was measured at the respective λ_{max} of salts, and the concentration of the AMX and salts were determined using the calibration curves. The solubility was calculated by multiplying the concentration with the dilution factor.

2.2.9 Intrinsic Dissolution Rate (IDR)

The intrinsic dissolution rate was determined using Lab India 8000+ Dissolution Tester. 100 mg of AMX and AMX salts were compressed to make a 3.288 cm^2 pellet using a hydraulic press at a pressure of 2 ton/$inch^2$ for two minutes. The pellet was compressed to provide a flat surface. The pellet was dropped into 1 L of phosphate buffer solution pH 7 at 37 °C, with the paddle rotating at 100 RPM. A 5 mL portion of the dissolution medium was withdrawn and replenished with an equal volume of fresh medium at a regular interval. The same was done up to 24 hrs. The amount of drug dissolved in the solution after each time interval was calculated using the calibration curve by UV–VIS spectroscopy. Then, the concentration of the drug at each interval was calculated and plotted against

time. The linear region of the dissolution profile was used to determine the intrinsic dissolution rate (IDR) of the AMX and its salts.[109]

2.3 Results & Discussion

Amoxapine (pK_a = 8.83) is likely to form salts with GRAS organic acids having pK_a ranging from 1.9 to 6.4, which are not so strong to cause harm to AMX and the cells. According to the ΔpK_a rule of 3,[50,110,111] salt formation occurs at least three units pK_a[111] difference, whereas ΔpKa of <1 means it forms a neutral cocrystal. ΔpK_a 1−3 means this is a grey zone of transitional proton states. This concept is also observed in the case of AMX (Table 2.1). Noticeably, salt formation is detected in the case of all acids which are used as co-formers.

Table 2.1: pKa and ΔpKa values of AMX and co-formers used in this study

Name	pK_a	ΔpK_a
Amoxapine	8.83	-
D (-) Tartaric acid	2.89, 4.40	5.94, 4.43
D (+) Tartaric acid	2.89, 4.40	5.94, 4.43
Fumaric acid	3.03, 4.44	5.80, 4.39
Maleic acid	1.90, 6.07	6.93, 2.76
Succinic acid	4.20, 5.60	4.63, 3.23
Citric acid	3.13, 4.76, 6.39	5.70, 4.07, 2.44
Malonic acid	2.83, 5.69	6.0, 3.14
L (-) Malic acid	3.40, 5.20	5.43, 3.63
Adipic acid	4.43, 5.41	4.4, 3.42

2.3.1 Powder X-ray Diffraction

The powder pattern of AMX, corresponding acid and salts are shown in Figures 2.2A and B. The generation of a new salt through solvent-assisted grinding has been confirmed by the PXRD pattern of the product of the grinding experiment. The PXRD pattern of all the salts was different from the starting materials, and no peak of the starting material was found as impurity also. The difference in powder pattern compared to AMX and acid indicated the formation of a novel solid form which DSC supports.

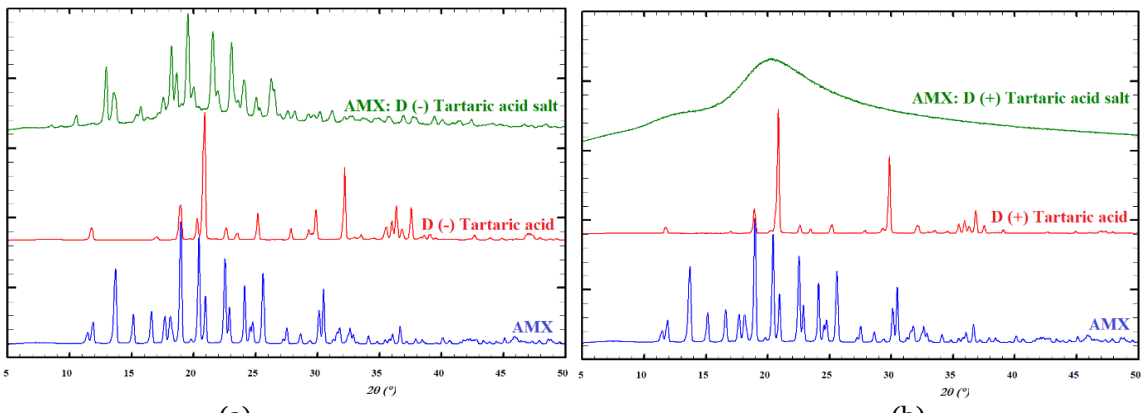

(a) (b)

Figure 2.2A: PXRD patterns of salts of AMX in comparison with AMX and coformers.

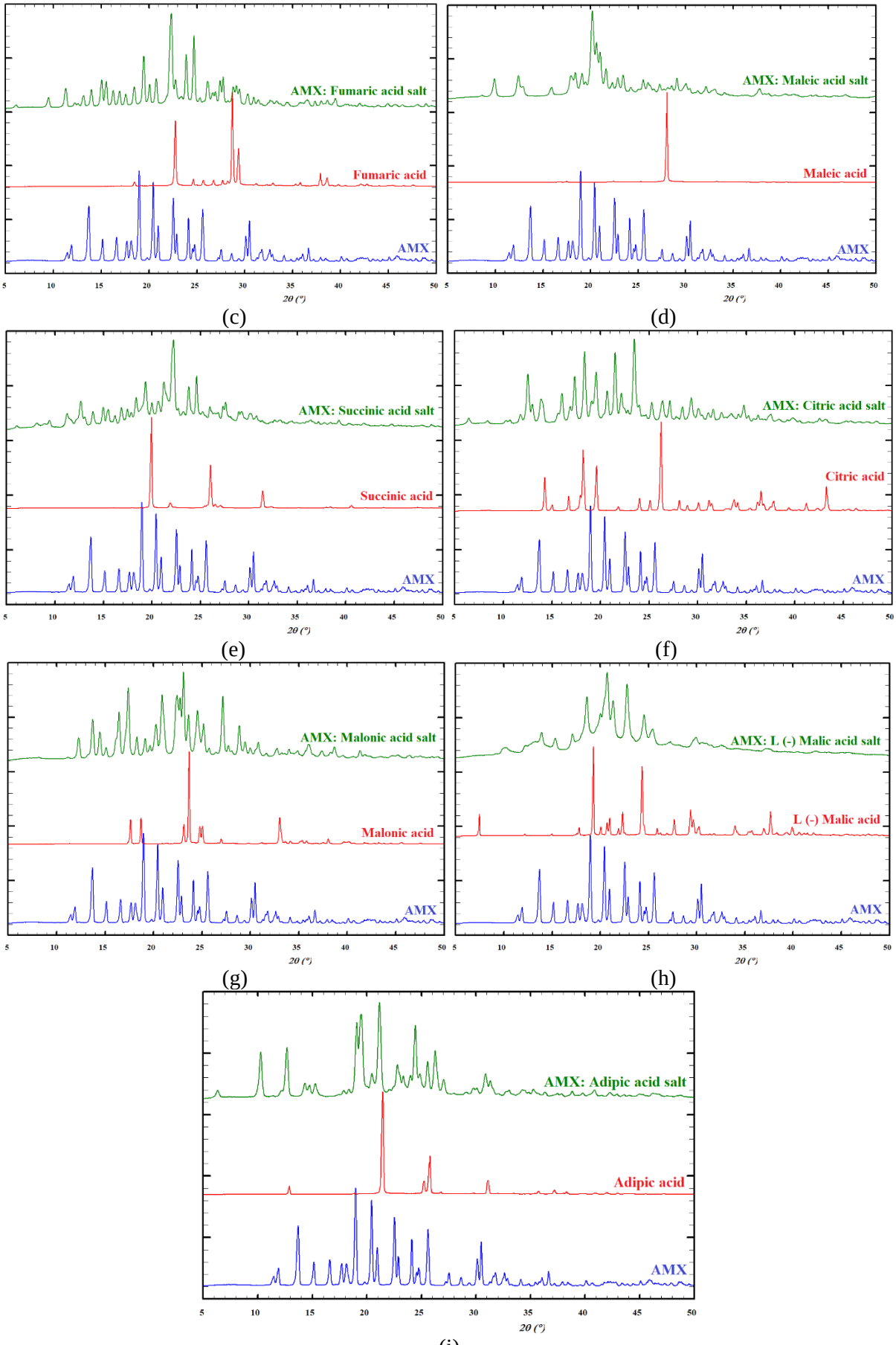

Figure 2.2B: PXRD patterns of salts of AMX in comparison with AMX and coformers.

2.3.2 Thermal Analysis

The DSC data on Amoxapine displayed a sharp endotherm at 183.1 ˚C without any phase transformation. The melting point of the salts of AMX with D (-) tartaric acid, D (+) tartaric acid, Fumaric acid, Maleic acid, Succinic acid, Citric acid, Malonic acid, L (-) Malic acid and Adipic acid was found to be 147.2, 147.1, 127.2, 183.3, 95.8, 209.5, 162.3, 173.0 and 193.0 ˚C, respectively as shown. The representative DSC traces are provided as a supporting information [Figure S2.1 – S2.10 on page 3 – 7] in the enclosed DVD. The citrate salt of AMX has demonstrated the highest melting point 209.5 ˚C and the succinate salt of AMX has presented the lowest melting point 95.8 ˚C. DSC thermograms and melting point and melting enthalpies are listed in Table 2.2.

Table 2.2: Melting point and melting enthalpies of AMX and its salts.

Name	Melting point of AMX/ Coformer (ºC)	Melting point of salt with AMX (ºC)	Melting enthalpies (J/g)
Amoxapine	183.1		114.4
D (-) tartaric acid	173	147.2	83.0
D (+) tartaric acid	206	147.1	45.1
Fumaric acid	287	127.2	13.9
Maleic acid	135	183.3	21.8
Succinic acid	184	95.8	23.4
Citric acid	153	209.5	442.6
Malonic acid	135	162.3	11.6
L-Malic acid	131	173.0	60.4
Adipic acid	152	193.0	96.6

2.3.3 Crystal Structure Description

We have produced nine novel cocrystals of AMX with D (-) tartaric acid, fumaric acid, maleic acid, succinic acid and malonic acid, characterized by powder X-ray diffraction (PXRD) and DSC. Single crystals, suitable for structure determination, could be grown only for five cocrystals. Single crystals of these five salts were grown by slow evaporation method at 4 ºC and room temperature by using different solvent systems (AMX: D (-) tartaric acid crystal in DMSO; AMX: fumaric acid crystal in the water-methanol mixture; AMX: maleic acid crystal in the water-ethanol combination; AMX: succinic acid and AMX: malonic acid single crystals in an aqueous solution). Crystallographic data and hydrogen bonds are listed in Tables 2.3 and 2.4 for salts of AMX with D (-) tartaric acid, fumaric acid, maleic acid, succinic acid and malonic acid.

2.3.3.1 AMX: D (-) tartaric acid salt

The asymmetric unit of this salt encompasses two molecules of AMX^+ cation and one molecule of D (-) tartrate anion (Figure 2.3a). This salt crystallizes in monoclinic lattice and $P2_1$ chiral space group. The acidic proton of the D (-) tartaric acid molecule is transferred to N of the piperazine ring of

the AMX and forms strong hydrogen bonding. The main intermolecular force present between N–H of AMX and O of D (-) tartaric acid is hydrogen bonding like N3–H3A···O5, N3–H3A···O7, N3–H3B···O3, N6–H6B···O8, N6–H6A···O4. We have seen intramolecular hydrogen bonding in D (-) tartaric acid molecule between hydroxyl and carboxylic acid group O5–H5A···O3 and O6–H6C···O7. All the hydrogen-bonded interactions as per the symmetry operations are tabulated in Table 2.4. AMX molecules are connected in a layered channel by weak van der Waals' forced like C–H···C and C–Cl···π interactions as shown in Figure 2.3b. Here weak bonding played a prominent role in holding the parallel AMX molecules in a layer. AMX and D (-) tartaric acid molecules formed channels in the crystal packing. They were connected by strong and weak intermolecular forces like hydrogen bonds and van der Waals' forces, as seen in Figure 2.3c along the 'b' axis.

Table 2.3: Crystallographic data of AMX salts.

Parameter	**AMX: D (-) Tartaric acid**	**AMX: Fumaric acid**	**AMX: Maleic acid**	**AMX: Succinic acid**	**AMX: Malonic acid**
Empirical formula	$2(C_{17}H_{17}ClN_3O)^+$, $(C_4H_4O_6)^{2-}$	$2(C_{17}H_{17}ClN_3O)^+$, $(C_4H_3O_4)^-$, $(C_2HO_2)^-$, $2(H_2O)$	$(C_{17}H_{17}ClN_3O)^+$, $(C_4H_3O_4)^-$	$2(C_{17}H_{17}ClN_3O)^+$, $(C_4H_4O_4)^{2-}$, $5(H_2O)$	$2(C_{17}H_{17}ClN_3O)^+$, $(C_3H_2O_4)^{2-}$, $2(H_2O)$
CCDC number	2080711	1590199	1590200	1590201	1812331
Formula weight	777.64	429.85	429.85	835.72	767.65
Crystal system	Monoclinic	Triclinic	Monoclinic	Monoclinic	Monoclinic
Space group	$P2_1$	$P\ \bar{1}$	$P2_1/c$	$P2_1/c$	$P2_1/c$
a (Å)	10.1249 (5)	9.2238(2)	20.5724(6)	15.7210(2)	21.3450(7)
b (Å)	8.8710 (5)	12.4815(2)	9.8586(3)	19.4546(3)	9.9547(3)
c (Å)	19.9737 (10)	17.0725(3)	9.7866(3)	25.7568(4)	17.4738(6)
α (°)	90	86.2850(10)	90	90	90
β (°)	91.138 (4)	89.375(2)	97.143(3)	97.940(2)	102.057(3)
γ (°)	90	82.224(2)	90	90	90
V (Å^3)	1793.64(16)	1943.33(6)	1969.46(10)	7802.1(2)	3631.0(2)
Z	2	4	4	8	4
ρ_{calc} (g/cm^{-3})	1.440	1.469	1.450	1.423	1.404
Temperature (K)	100.0(2)	100.0(2)	100.0(2)	100.0(2)	100.0(2)
μ/ mm^{-1}	0.245	0.237	0.234	0.236	0.241
2θ$_{min, max}$ ()	5.024, 49.996	5.062, 65.696	5.746,65.678	5.078, 65.546	4.928, 65.604
F (000)	812.0	896.0	896.0	3520.0	1608.0
h$_{min,max}$; k$_{min,max}$; l$_{min,max}$	-12, 12; -7, 10; -23, 23	-14,14; -18,17; -25,25	-30, 31; -14, 14; -14, 14	-23, 23; -28, 29; -38, 38	-32, 31; -14, 14; -26, 26
Total no. of reflections	13729	43941	43349	183373	67443
R_{int}	0.0562	0.0249	0.0525	0.0528	0.0546
No. of unique reflections	5106	13758	7218	28243	12968
R_1 [I>2σ(I)]	0.0425	0.0419	0.0677	0.0699	0.0695
wR2 (all data)	0.1138	0.1190	0.1989	0.2243	0.2009
GooF on F^2	1.064	1.063	1.076	1.037	1.035
Δρ$_{max,min}$/eÅ^{-3}	0.54, -0.52	0.61, -0.29	0.50, -0.37	1.19, -0.60	1.19, -0.51

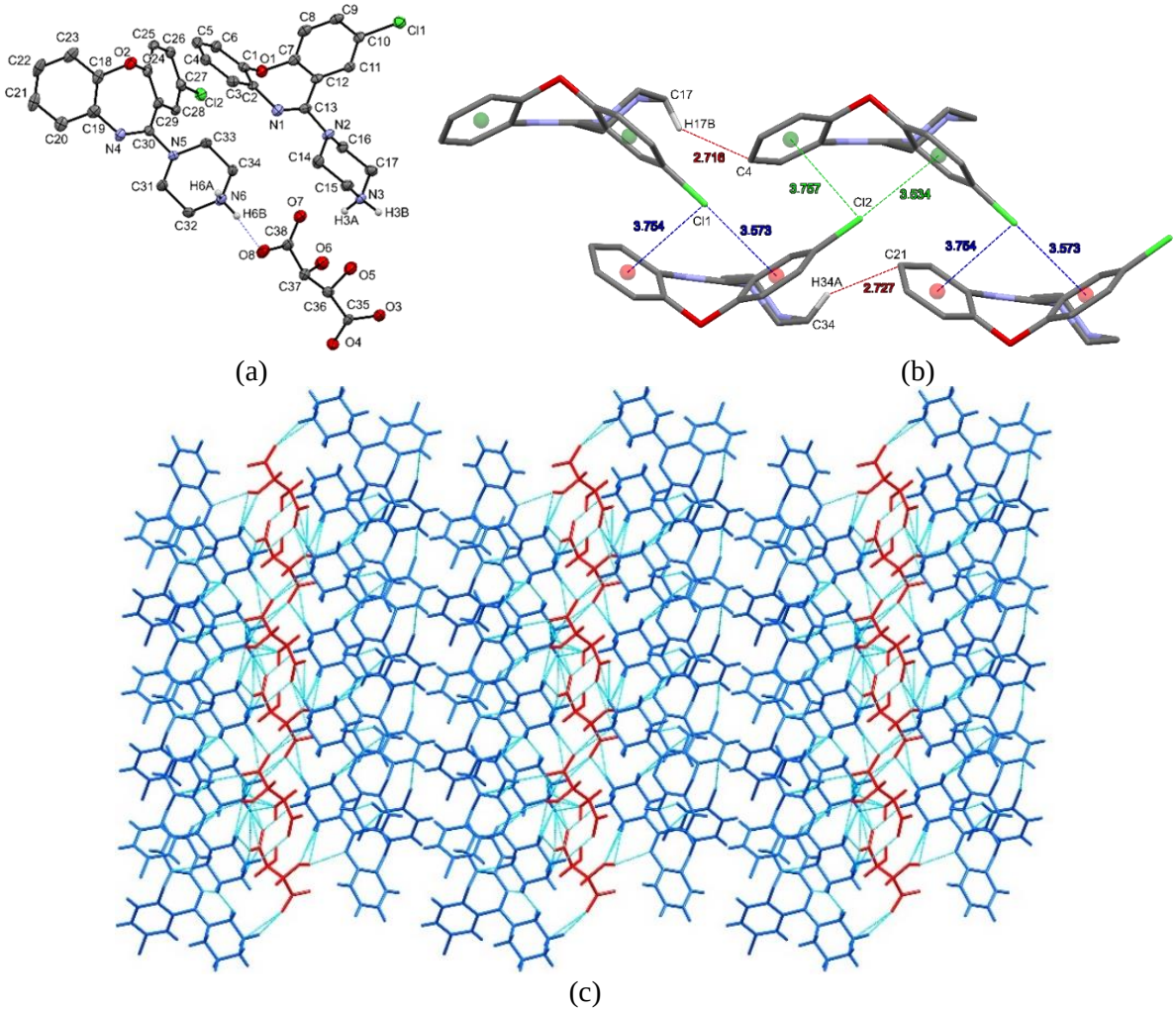

Figure 2.3: (a) The asymmetric unit of AMX: D (-) tartaric acid cocrystal. (b) Intra layer interaction between drug molecules. (c) Layers of AMX and fumaric acid water channel in crystal packing along 'b' axis.

2.3.3.2 AMX: Fumaric acid salt

The asymmetric unit of this structure (triclinic system, $P\ \bar{1}$ space group) contained two molecules of AMX^+ cation, one mono-fumarate anion and half molecule of fumarate anion and two molecules of water (Figure 2.4a). AMX^+ is connected to fumarate anion by N6–H6A···O7 hydrogen bond and with water molecule *via* N6–H6B···O10 hydrogen bond. The carboxylate anions are hydrogen-bonded to each other (O4–H4···O8), and the water molecules are hydrogen-bonded to the carboxylate anions (O7···H10B–O10) as well. Water molecules are also hydrogen-bonded among them (O10–H10A···O9). Two AMX^+ ions are organized antiparallel in the lattice and are connected by weak C–H···Cl hydrogen bond and C–H···π interactions (Figure 2.4b). Alternate layers of acid water channel and drug molecules are found in the crystal packing (Figure 2.4c), where the hydrogen bonds are responsible for the interlayer connectivity. Acid and water molecules are bonded by strong hydrogen bonds, while AMX^+ ions are attached by weak interactions (C–H···Cl and C–H···π) in the same layer.

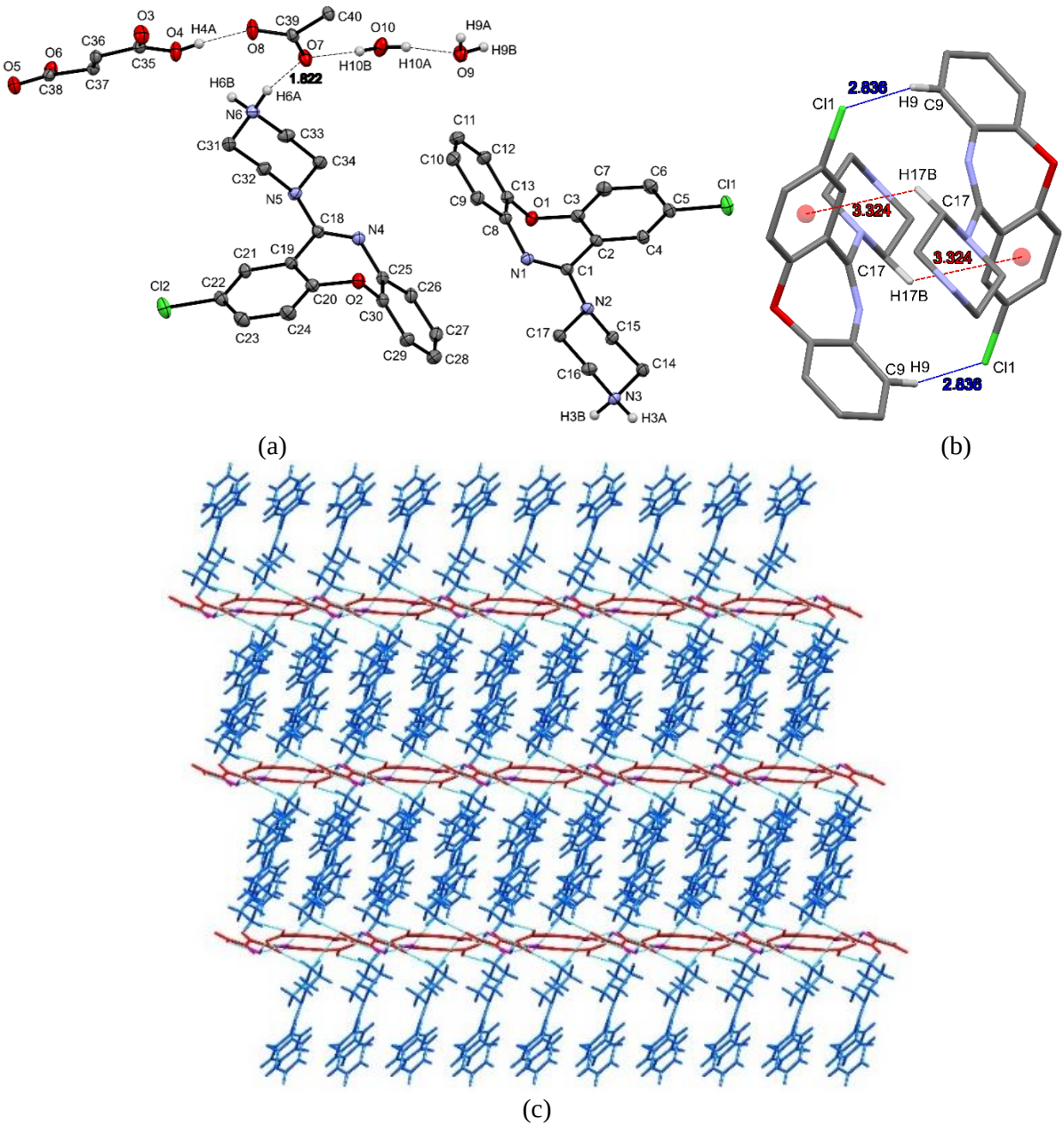

Figure 2.4: (a) The asymmetric unit of AMX: fumaric acid cocrystal. (b) Intra layer interaction between drug molecules. (c) Layers of AMX and fumaric acid water channel in crystal packing along 'c' axis.

2.3.3.3 AMX: Maleic acid salt

One molecule of each AMX^+ cation and the maleic acid anion is present in the asymmetric unit (monoclinic, space group $P2_1/c$) (Figure 2.5a). AMX^+ and maleic acid are linked *via* N3–H3A···O3 and N3–H3B···O4 hydrogen bonds. The intramolecular hydrogen bond is also present in maleic acid O5–H5···O2 (Table 2.4). In the same layer of AMX^+, cations are arranged parallelly by week interactions like C–H···Cl and C–H···π, while the two layers of cations are connected by weak C–H···π and π···π interaction (Figure 2.5b). AMX+ cations are organized parallelly in this crystal packing, so a piperazine ring is present on the same side. They formed two layers of AMX^+, attached by one layer of maleic acid (Figure 2.5c).

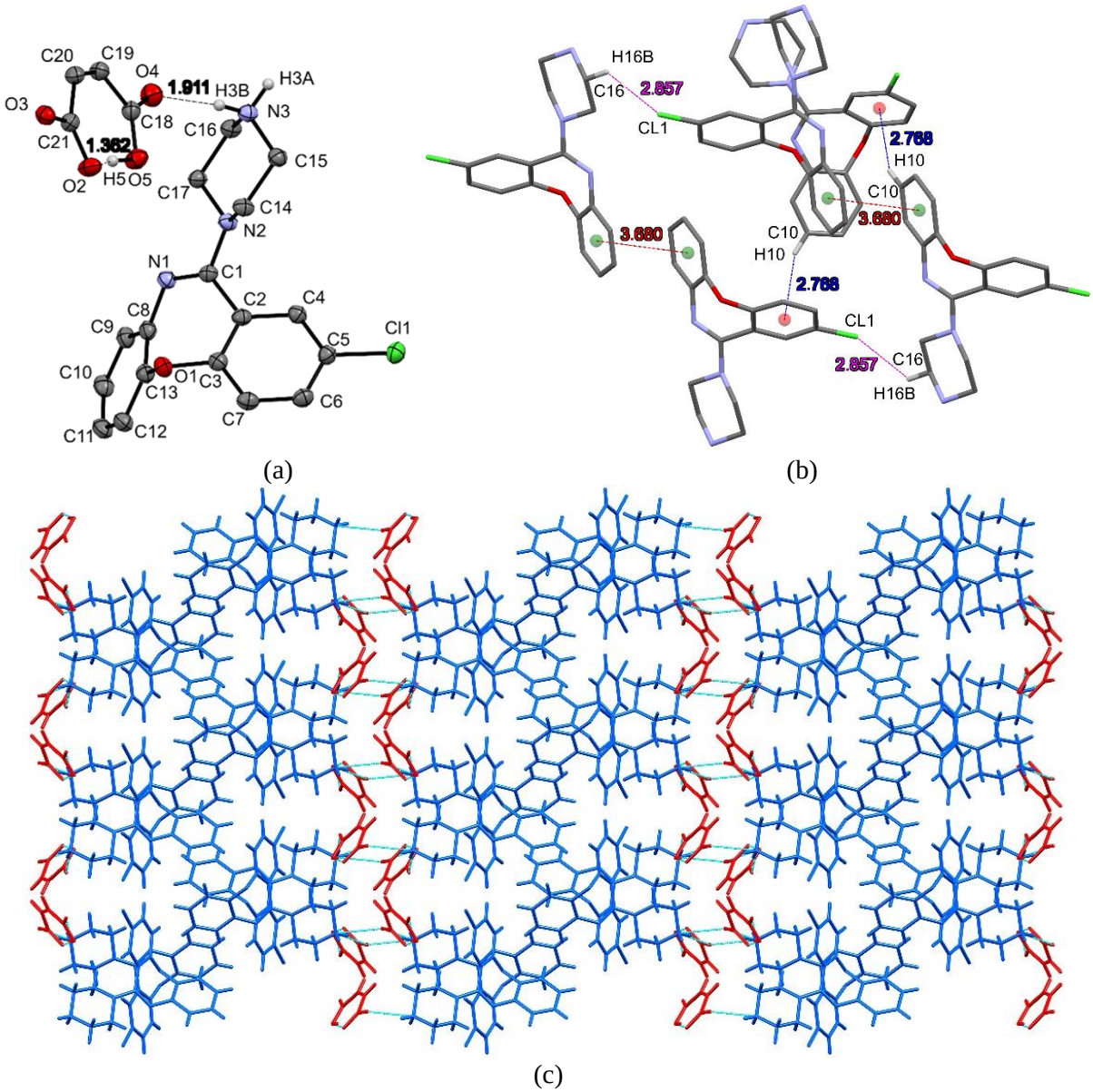

(a) (b)

(c)

Figure 2.5: (a) asymmetric unit of AMX: maleic acid cocrystal. (b) Intra layer interaction of AMX. (c) Interlayer interactions along the 'c' axis and AMX and maleic acid layers in crystal packing along the 'c' axis.

2.3.3.4 AMX: Succinic acid salt

The asymmetric unit of this crystal has four molecules of AMX^+ cation, two molecules of disuccinate anion and ten molecules of water (monoclinic, $P2_1/c$ space group) (Figure 2.6a). AMX^+ and succinate anions are linked *via* strong hydrogen bonds (N3–H3A···O5, N6–H6B···O12, N9–H9B···O9 and N12–H12A···O8). AMX^+ and water molecules are interlinked by N3–H3B···O13, N6–H6A···O14, N9–H9A···O18 and N12–H12B···O19 hydrogen bonds (Table 2.4). Two AMX^+ molecules are arranged antiparallel in a layer, interconnected by C–H···π, C–H···Cl and C–H···O interactions (Figure 2.6b). Layers of AMX^+ and succinic acid water channels are arranged alternately in crystal packing because API is arranged antiparallel in the same layer (Figure 2.6c).

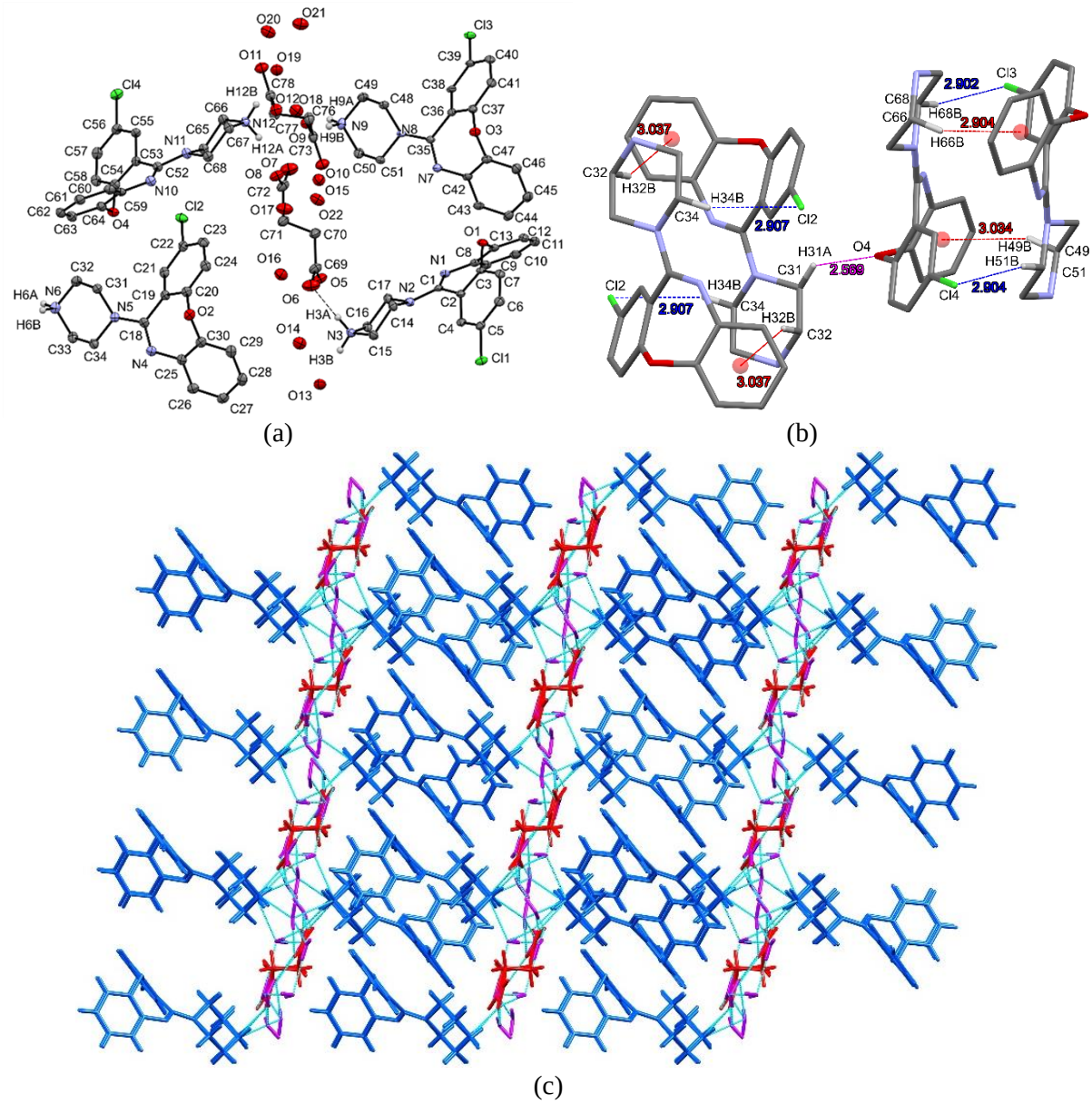

Figure 2.6: (a) Asymmetric unit of AMX: Succinic acid cocrystal. (b) Intra layer interaction of AMX molecules. (c) Layers of AMX and succinic acid water channel in crystal packing along 'b' axis.

2.3.3.5 AMX: Malonic acid salt

The asymmetric unit contains two molecules of AMX^+ cation, one molecule of malonate anion, and three water molecules (monoclinic, $P2_1/c$) (Figure 2.7a). AMX^+ cations are connected to malonate anions by strong hydrogen bonding (Table 2.4) N3–H3A···O4, N3–H3A···O6, N3–H3B···O3, N6–H6A···O5, N6–H6A···O6, N6–H6B···O3 and N6–H6B···O4. Hydrogen bonds also interconnect water molecules. AMX^+ cations are organized in a partially parallel pattern in the same layer and connected by C–H···π and C–H···O (Figure 2.7b), creating a chain of molecules. Two layers of AMX^+ are also linked by a different C–H···π interaction. Two layers of AMX^+ in the lattice are associated by C–H···O and C–H···π interactions as they are parallelly arranged, further connected to malonic acid and water molecules present in the channel by strong hydrogen bonds (Figure 2.7c).

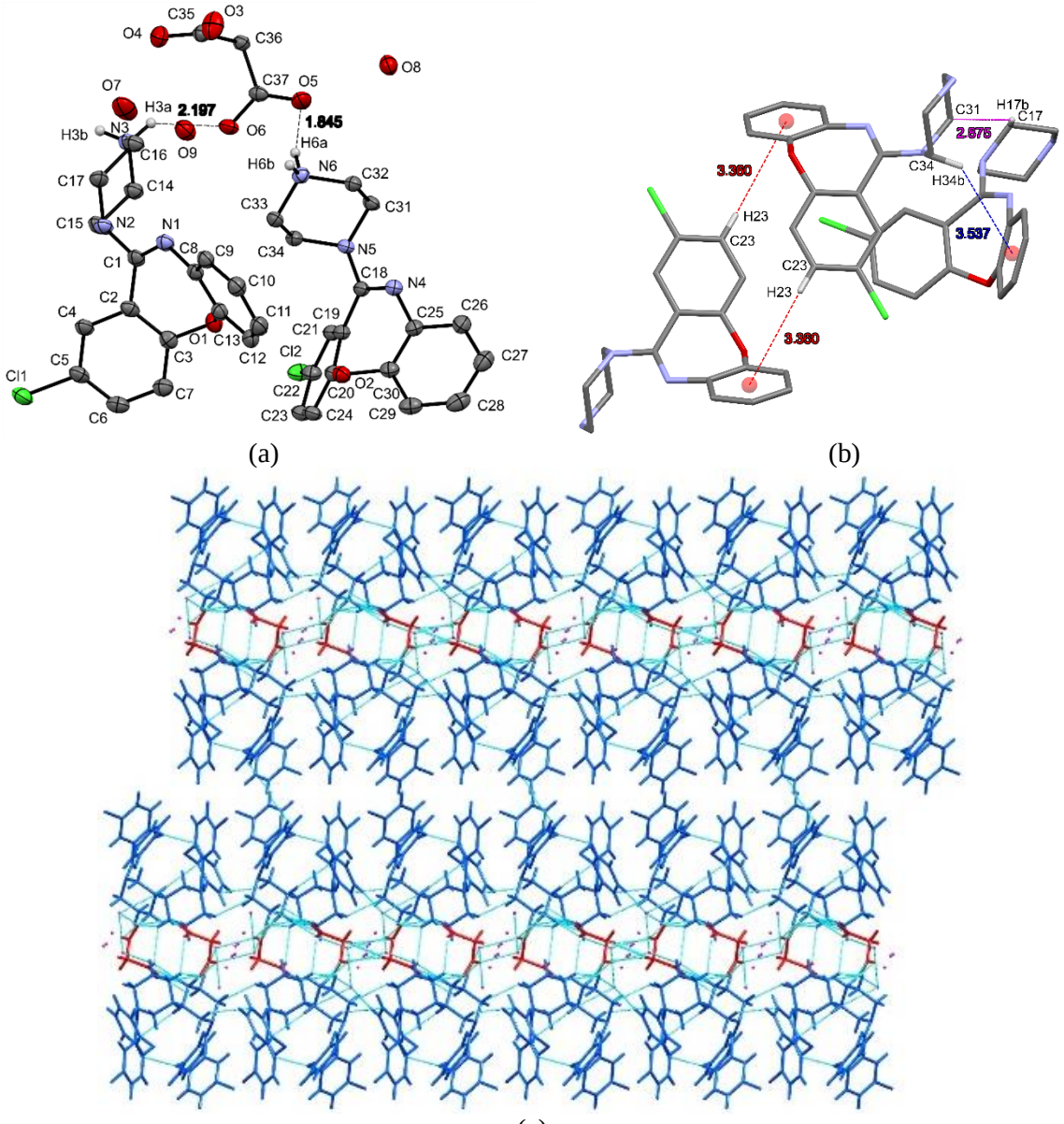

Figure 2.7: (a) Asymmetric unit of AMX: Malonic acid salt. (b) Intra layer interaction of AMX. (c) Layers of AMX and Malonic acid water channel in crystal packing along 'b' axis.

Table 2.4: Hydrogen bond geometry parameters in salts of AMX.

Salts	Interactions	D–H (Å)	H···A (Å)	D···A (Å)	D–H···A (˚)	Symmetry code
AMX: D(-)Tartaric acid (1:1)	N3–H3A…O5	0.91	2.31	2.857(6)	119	4-x, -½+y, 1-z
	N3–H3A…O7	0.91	2.10	2.938(6)	153	4-x, -½+y, 1-z
	N6–H6B…O8	0.91	1.78	2.680(5)	172	4-x, -½+y, 1-z
	C16–H16B…O7	0.99	2.50	3.264(6)	134	4-x, -½+y, 1-z
	N3–H3B…O3	0.91	1.81	2.670(5)	157	1+x, y, z
	O6–H6C…N4	0.84	2.61	3.313(5)	142	3-x, ½+y, 1-z
	C31–H31A…O6	0.99	2.51	3.192(6)	126	3-x, -½+y, 1-z

	C32–H32A…O3	0.99	2.46	3.362(5)	152	3-x, -½+y, 1-z
	N6–H6A…O4	0.91	1.81	2.682(6)	160	x, y, z
	C15–H15B…O8	0.99	2.27	3.154(6)	148	x, y, z
	C31–H31B…O4	0.99	2.54	3.241(8)	127	x, y, z
	O5–H5A…O3	0.84	2.05	2.571(5)	119	x, y, z
	O6–H6C…O7	0.84	2.20	2.665(5)	115	x, y, z
	C10–Cl1… π	1.744	3.754(3)	4.005(6)	85.20(18)	1+x, 1+y, z
	C10–Cl1…π	1.744	3.573(3)	5.169(5)	151.12(15)	1+x, 1+y, z
	C27–Cl2…π	1.742	3.757(3)	3.981(6)	84.29(18)	x, -1+y, z
	C27–Cl2…π	1.742	3.534(3)	5.123(6)	150.48(15)	x, -1+y, z
	C17–H17B…C4	0.99	2.716	3.497	136.06	1+x, y, z
	C34–H34A…C21	0.99	2.727	3.572	143.51	2+x, 1+y, z
AMX: Fumaric acid (1:1)	N3–H3A···O6	0.91	1.81	2.703(1)	166	-1+x, 1+y, -1+z
	N3–H3B···O5	0.91	1.93	2.821(1)	165	1-x, -y, 1-z
	O4–H4A···O8	0.84	1.79	2.623(1)	173	1-x, -y, 1-z
	N6–H6A···O7	0.91	1.82	2.717(1)	167	1-x, -y, 1-z
	N6–H6B···O10	0.91	1.84	2.712(1)	160	1-x, -1-y, 1-z
	O9–H9A···O8	0.85	1.98	2.817(1)	166	-x, -1-y, 1-z
	O9–H9B···O6	0.85	1.95	2.804(1)	179	1-x, -1-y, 1-z
	O10–H10A···O9	0.85	1.91	2.756(1)	173	1-x, -1-y, 1-z
	O10–H10B···O7	0.85	1.91	2.747(1)	171	1-x, -1-y, 1-z
	C14–H14A···O3	0.99	2.47	3.193(1)	129	x, 1+y, -1+z
	C15–H15B···O1	0.99	2.58	3.142(1)	116	1-x, -y, -z
	C16–H16B···O3	0.99	2.57	3.531(1)	163	-x, -y, 1-z
	C31–H31B···O4	0.99	2.45	3.271(1)	140	-x, -y, 1-z
	C32–H32B···Cl1	0.99	2.74	3.543(1)	139	x, y, 1+z
	C9–H9···Cl1	0.95	2.836	3.752	162.39	x, y, 1+z
	C15–H15A···Cl2	0.99	2.928	3.752	141.28	x, y, z
	C37–H37···O4	0.95	2.42	2.755(1)	101	x, y, 1+z
	C17–H17B···π	0.99	3.324	3.999	127	x, y, 1+z
	C31–H31A···π	0.99	3.004	3.949	159.83	1-x, -y, 1-z
	C33–H33B…π	0.989	2.973	3.774	138.76	1-x, -y, 1-z
	C34–H34A···π	0.989	3.483	4.027	116.77	1-x, -y, 1-z
	C5–Cl1···π	1.733	3.484	4.966	142.02(4)	-x, -y, -z
	C22–Cl2···π	1.734	3.544	5.101	148.28(4)	1-x, -y, 1-z

AMX: Maleic acid (1:1)	N3–H3A···O3	0.89	2.55	2.910(2)	105	-x, -½+y, 3/2 -z
	N3–H3A···O3	0.89	1.89	2.767(2)	167	x, 3/2-y, -½+z
	N3–H3B···O4	0.89	1.91	2.793(2)	171	x, 3/2-y, ½+z
	O2–H5···O5	1.36(4)	1.07(4)	2.426(2)	170	x, 3/2-y, ½+z
	C14–H14A···O2	0.97	2.58	3.188(2)	121	x, 3/2-y, ½+z
	C15–H15A···O2	0.97	2.57	3.150(2)	118	x, 3/2-y, ½+z
	C15–H15B···O5	0.97	2.57	3.165(2)	120	x, 3/2-y, ½+z
	C19–H19···O3	0.93	2.37	3.269(2)	162	x, 5/2-y, -½+z
	C16–H16B···Cl1	0.97	2.86	3.538	128	x, 1+y, z
	C10–H10···π	0.93	2.77	3.632	155	1-x, -½+y, 3/2-z
AMX: Succinic acid (1:1)	N3–H3A···O5	0.89	1.86	2.734(3)	165	x, y, z
	N3–H3B···O13	0.89	2.09	2.888(3)	149	x, y, z
	N6–H6A···O14	0.89	1.84	2.701(3)	162	2-x, 1-y, 1-z
	N6–H6B···O12	0.89	1.83	2.699(3)	167	1-x, 1-y, 1-z
	N9–H9A···O18	0.89	1.82	2.681(3)	162	x, y, z
	N9–H9B···O9	0.89	1.83	2.709(3)	167	x, y, z
	N12–H12A···O8	0.89	1.86	2.732(3)	165	x, y, z
	N12–H12B···O19	0.89	2.10	2.907(3)	150	x, y, z
	O13–H13A···O15	0.85	1.94	2.779(3)	168	2-x, ½+y, ½-z
	O13–H13B···O12	0.85	1.99	2.749(2)	148	1+x, y, z
	O14–H14C···O20	0.85	1.93	2.731(3)	157	1-x, ½+y, ½-z
	O15–H15C···O7	0.85	1.98	2.816(3)	167	x, y, z
	O15–H15D···O21	0.85	2.00	2.837(3)	170	1+x, y, z
	O16–H16C···O17	0.85	1.99	2.830(3)	170	x, y, z
	O16–H16D···O6	0.85	1.97	2.818(3)	172	x, y, z
	O17–H17C···O8	0.85	1.95	2.794(3)	170	x, y, z
	O17–H17D···O10	0.85	2.02	2.853(3)	167	x, y, z
	O18–H18A···O22	0.85	1.89	2.697(3)	159	1-x, -½+y, ½-z
	O19–H19A···O9	0.85	1.97	2.739(3)	150	x, y, z
	O19–H19B···O16	0.85	1.98	2.808(3)	164	1-x, -½+y, ½-z
	O20–H20A···O11	0.85	1.93	2.779(3)	177	x, y, z
	O20–H20B···O19	0.85	2.11	2.954(3)	173	x, y, z
	O21–H21A···O5	0.85	1.96	2.786(3)	164	-1+x, y, z
	O21–H21B···O11	0.85	2.04	2.860(3)	163	x, y, z
	O22–H22A···O10	0.85	1.93	2.771(3)	171	x, y, z

	O22–H22B···O13	0.85	2.08	2.926(3)	175	-1+x, y, z
	C17–H17A···N1	0.97	2.31	2.685(3)	102	x, y, z
	C31–H31A···O4	0.97	2.57	3.377(3)	141	x, y, z
	C34–H34A···O11	0.97	2.58	3.511(3)	160	1-x, 1-y, 1-z
	C34–H34B···N4	0.97	2.35	2.704(3)	101	x, y, z
	C51–H51A···O10	0.97	2.57	3.510(3)	162	x, y, z
	C51–H51B···N7	0.97	2.34	2.692(3)	101	x, y, z
	C65–H65A···O1	0.97	2.60	3.426(3)	144	x, ½-y, ½+z
	C68–H68B···N10	0.97	2.31	2.688(3)	102	x, y, z
	C15–H15A···π	0.97	2.90	3.791(3)	154	2-x, 1-y, -z
	C16–H16B···π	0.969	2.76	3.630(2)	150	2-x, 1-y, -z
	C33–H33A···π	0.971	2.76	3.575(2)	142	2-x, 1-y, 1-z
	C50–H50A···π	0.971	2.81	3.615(2)	141	x, ½-y, -½+z
	C66–H66B···π	0.969	2.90	3.788(3)	152	x, ½-y, ½+z
	C67–H67A···π	0.971	2.72	3.591(2)	150	x, ½-y, ½+z
	C5–Cl1···π	1.738	3.2829(11)	4.878(3)	151.09(8)	x, 3/2-y, -½+z
	C22–Cl2···π	1.737	3.2602(11)	4.833(3)	148.97(8)	x, ½-y, ½+z
	C39–Cl3···π	1.739	3.2835(11)	4.858(2)	149.09(8)	1-x, -½+y, ½-z
	C56–Cl4···π	1.732	3.2804(11)	4.866(3)	150.78(8)	1-x, -½+y, ½-z
AMX: Malonic acid (1:1)	N3–H3A···O4	0.89	2.50	3.109(3)	126	1-x, ½+y, 3/2-z
	N3–H3A···O6	0.89	2.20	2.883(3)	133	1-x, ½+y, 3/2-z
	N3–H3B···O3	0.89	1.86	2.737(3)	166	x, 1+y, z
	N6–H6A···O5	0.89	1.85	2.717(3)	163	1-x, -y, 1-z
	N6–H6A···O6	0.89	2.56	3.289(2)	139	1-x, -y, 1-z
	N6–H6B···O3	0.89	2.49	3.122(3)	128	x, ½-y, -½+z
	N6–H6B···O4	0.89	1.87	2.753(3)	171	x, ½-y, -½+z
	O8–H8A···O9	0.85	2.33	2.897(3)	125	1-x, 1-y, 1-z
	O8–H8B···O4	0.85	2.51	2.946(3)	112	1-x, 1-y, 1-z
	O9–H9A···O6	0.85	2.00	2.837(3)	169	1-x, 1-y, 1-z
	O9–H9B···O8	0.85	2.07	2.897(3)	165	1-x, 1-y, 1-z
	O9–H9B···O7	0.85	1.93	2.737(11)	158	1-x, 1-y, 1-z
	C10–H10···O9	0.93	2.56	3.486(3)	176	x, -1+y, z
	C12–H12···O2	0.93	2.53	3.238(3)	133	x, ½-y, ½+z
	C32–H32A···O3	0.97	2.57	3.066(3)	112	x, ½-y, -½+z
	C32–H32B···O8	0.97	2.573	3.509(3)	162	1-x, 1-y, 1-z

	C32–H32B···O7	0.97	2.575	3.424(13)	146	1-x, 1-y, 1-z
	C33–H33B···π	0.97	3.176	4.009	145	x, ½-y, -½+z
	C34–H34B···π	0.97	3.537	4.202	128	x, y, z
	C23–H23···π	0.93	3.360	4.223	155	2-x, 1-y, 1-z
	C5–Cl1···π	1.747	3.769	4.716(3)	112	x, y, z

Overlay of calculated patterns from the single crystals on the experimental powder XRD patterns confirm the homogeneousness and purity of newly formed salts of AMX with D (-) tartaric acid, fumaric acid, maleic acid, succinic acid and malonic acid (Figure 2.8). The comparison of simulated PXRD patterns of the salts from the single crystal and the experimental PXRD data indicated that the hydrated salts (3, 6 and 8) have different PXRD pattern compared to the crude material, while the anhydrous salts (2 and 5) found by single-crystal X-ray diffraction matched with that of the crude material.

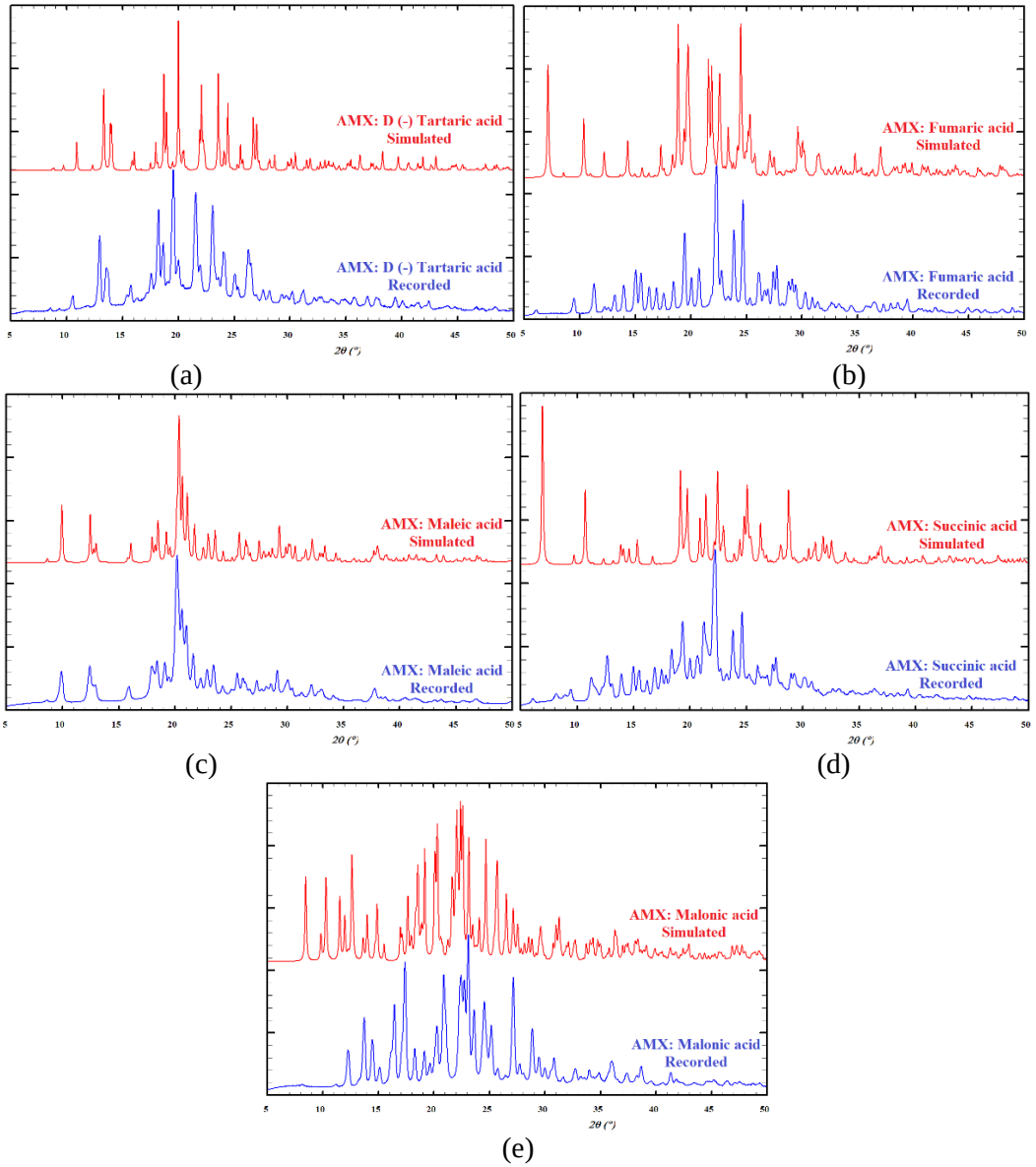

Figure 2.8: Comparisons of PXRD patterns recorded from powdered samples and simulated from single-crystal X-ray diffraction data.

2.3.4 Hirshfeld Analysis

We have determined Hirshfeld surfaces of the AMX salts from SCXRD data. It shows the hydrogen bonding is strictly directional, and it holds the AMX and coformer molecules via N–H···O hydrogen bonding, as shown in Figure 2.9. We have determined fingerprint plots for all salts and seen the interaction between all atoms versus each atom inside and outside of the Hirshfeld surface, which indicates the intensity of each type of interaction in Figure 2.11. We have analysed the percentage interactions between all the participating atoms inside and outside of Hirshfeld surface. We have found that the hydrogen atom is most interacting atom amongst C, H, N, O, Cl atoms as shown in Figure 2.10. This study supports the structural aspects of SCXRD data of all the salts of AMX.

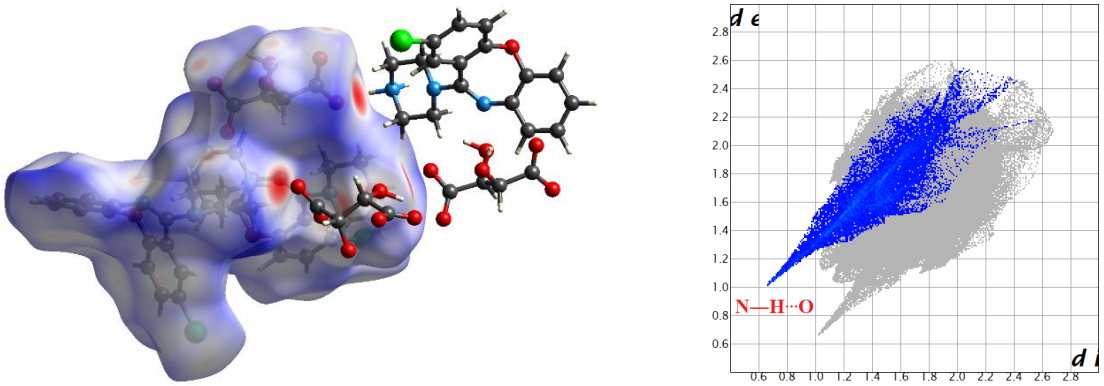

(a)

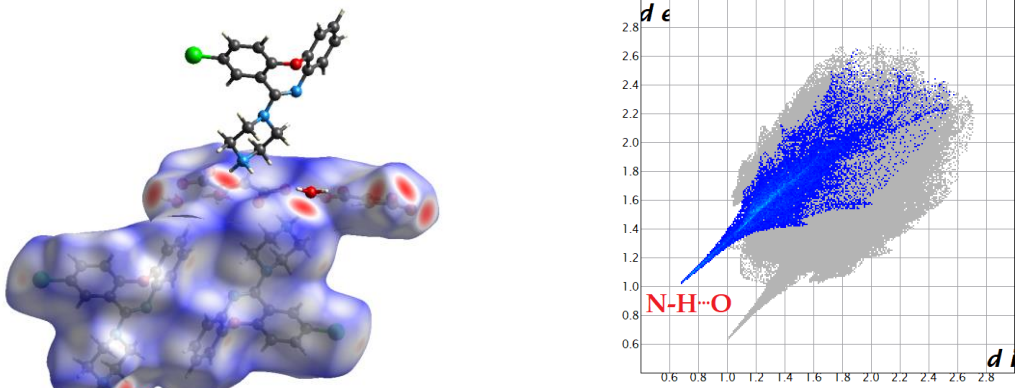

(b)

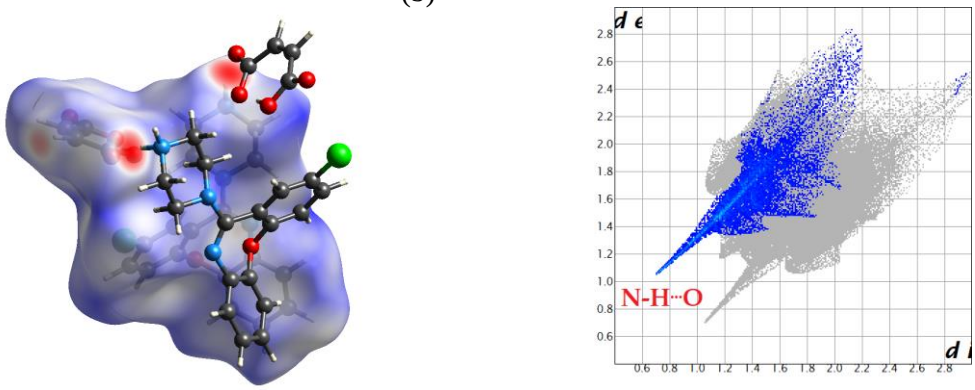

(c)

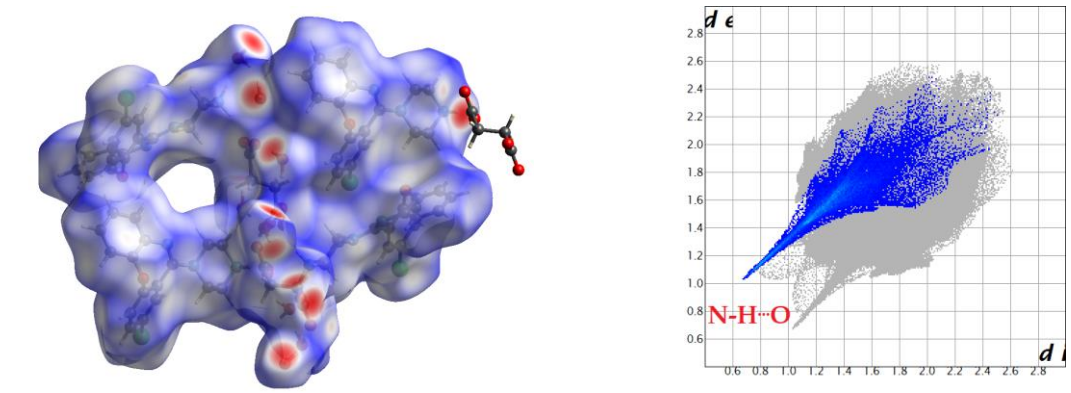

(d)

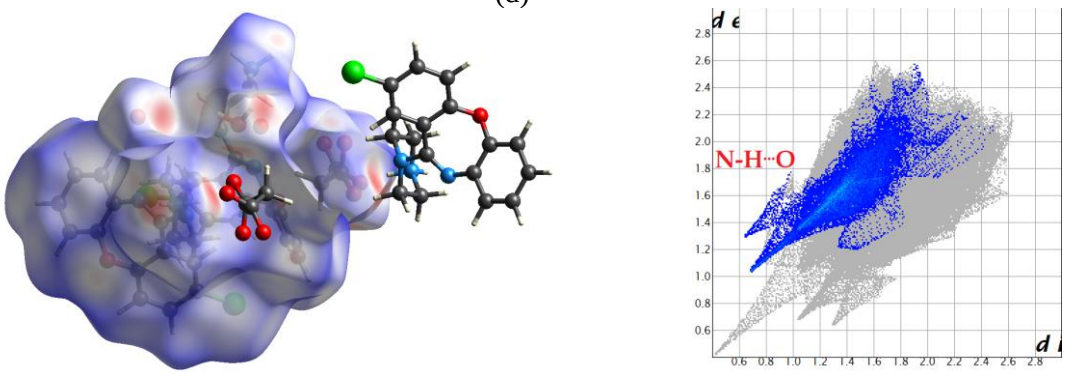

(e)

Figure 2.9: Hirshfeld surfaces and fingerprint plot of (a) AMX: D (-) tartaric acid; (b) AMX: Fumaric acid; (c) AMX: Maleic acid; (d) AMX: Succinic acid and (e) AMX: Malonic acid.

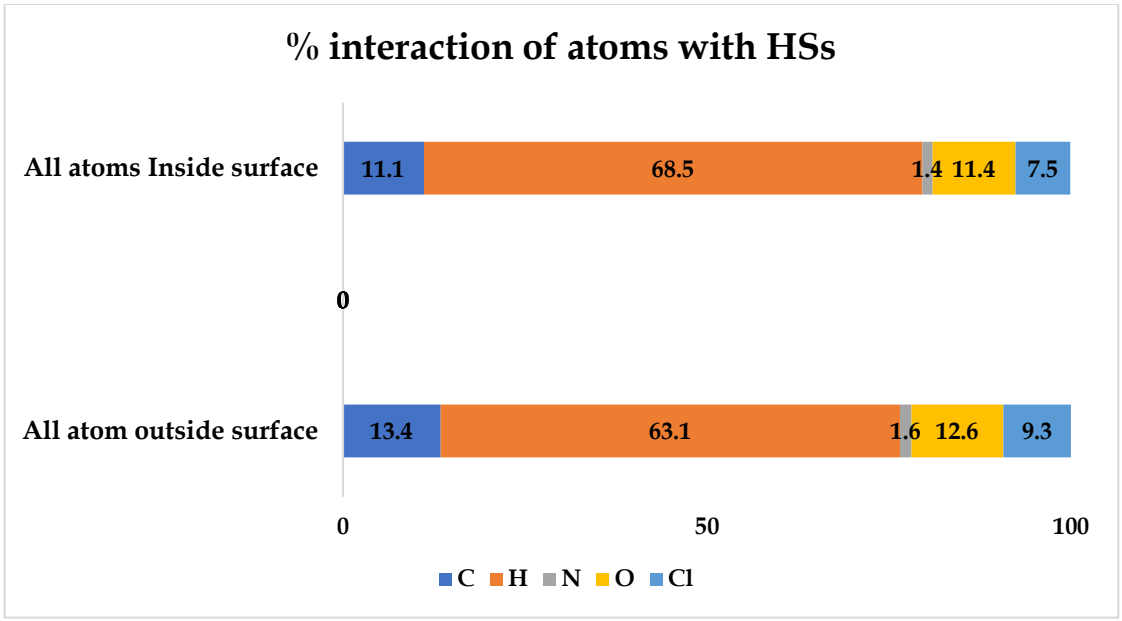

Figure 2.10: Percentage interactions diagrams of AMX: D (-) tartaric acid salt (% interaction diagrams for other AMX salts has been given in Figure S2.16 on page 13 – 14 in supporting file in attached DVD)

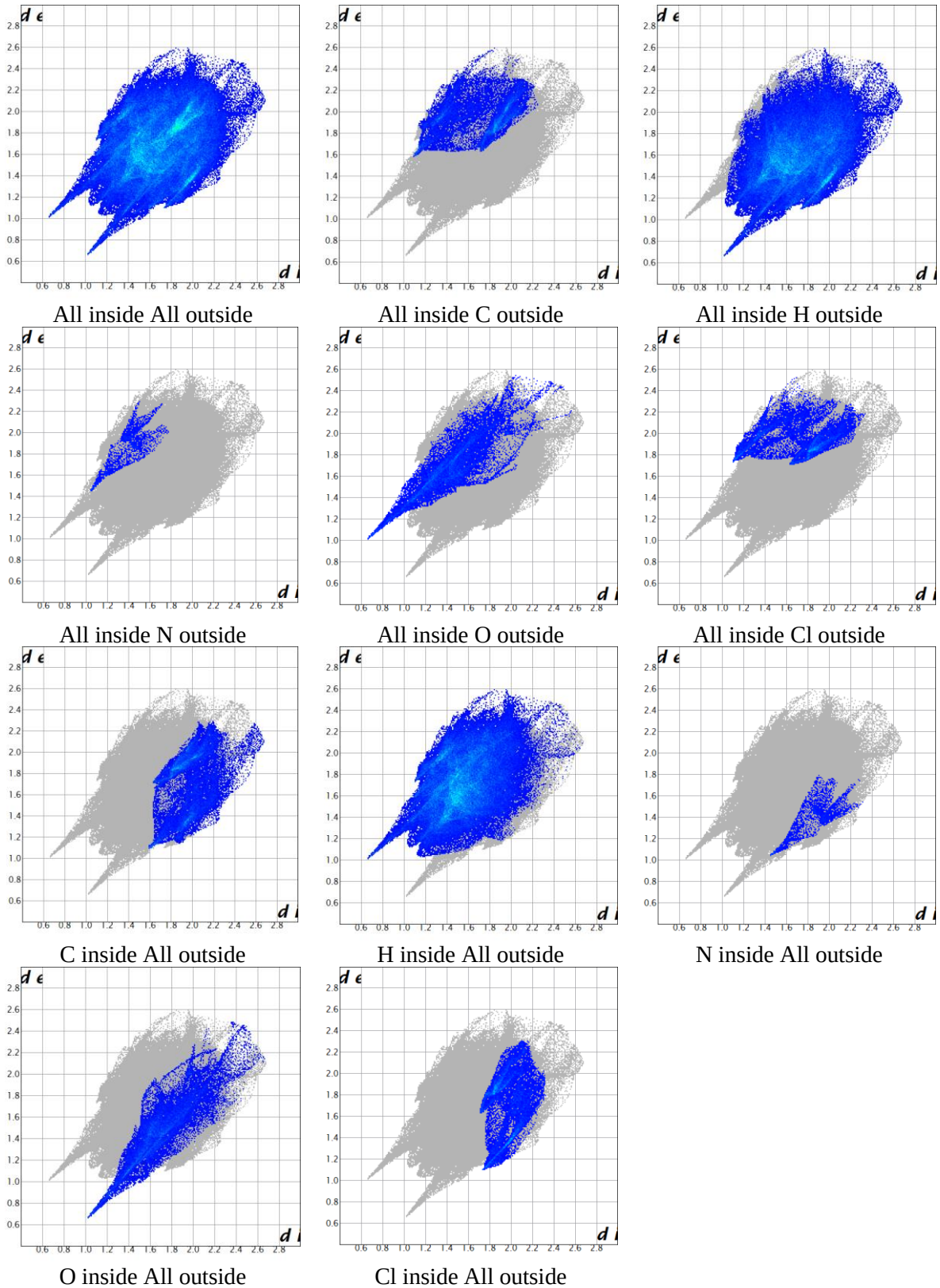

Figure 2.11: Fingerprint plots of AMX: D (-) tartaric acid salt (fingerprint plots for other salts Figure S2.11 – S2.15 on page 8 – 12 has been provide in supporting file in attached DVD).

2.3.5 Partition Coefficient

We have determined the partition coefficient for AMX and its newly developed salts in the phosphate buffer solution at pH 7 and n-octanol. Log P was found 1.45 for AMX. All the salts of AMX showed lower $log_{10}P$ value and lowest was found -0.17 for AMX: adipic acid salt as shown in Table 2.5. This decline in the partition coefficient value signifies the more hydrophilic nature of the AMX salts than pure AMX.

Table 2.5: partition coefficient of AMX and its salts.

Name	$log_{10}P$
AMX	1.45
AMX: D(-)Tartaric acid	0.55
AMX: D(+)Tartaric acid	0.72
AMX: Fumaric acid	0.25
AMX: Maleic acid	0.44
AMX: Succinic acid	1.01
AMX: Citric acid	0.74
AMX: Malonic acid	0.85
AMX: L (-) Malic acid	0.78
AMX: Adipic acid	-0.17

2.3.6 Solubility Study

AMX (a BCS class II drug) has poor water solubility (0.171 mg / mL).[112] Hence it limits the pharmacokinetic and pharmacodynamic parameters of API, which affect intrinsic dissolution rate and bioavailability. Enhancement of solubility with the help of crystal engineering of AMX with acids has been observed. Solubility experiment of AMX and its salts were performed in phosphate buffer solution at pH 7 and 37 ˚C to determine the aqueous solubility. The solubility of each salt is measured after 24 h by plotting a calibration curve using UV-visible spectroscopy. Related experimental details, calibration curves and UV-Vis spectra are provided as a supporting information [Figure S2.17 – S2.26 on page 14 – 17] in the enclosed DVD). The solubility of AMX and its salts has been displayed in Table 2.6. The water solubility of AMX has increased by 4.1 to 194.5 times for its salts. The highest solubility is observed in L (-) Malic acid salt of AMX (64.19 mg/mL) and the lowest in citrate salt of AMX (1.36 mg/mL).

2.3.7 Intrinsic Dissolution Rate Analysis

The IDR experiment was performed on the pellet of AMX and newly formed AMX salts. The IDR was determined for AMX and all salts and listed in Table 2.7. IDR of AMX was found 0.016 mg min^{-1} cm^{-1} and the highest was seen in AMX: L (-) malic acid salt (4.651 mg min^{-1} cm^{-1}). The results indicated that the salts of AMX have significant enrichment in intrinsic dissolution rate from 13.1 to 283.2 times compared to the parent drug. Therefore, AMX salts could potentially be used instead of the

parent drug for future formulations. This salt was found to be stable in ambient air. Thus, the pallet of this compound could be made easily for IDR analysis. This data indicates that this salt will reach the bloodstream faster than pure AMX and act much faster than pure AMX.

Table 2.6: Solubility of AMX and its salts.

Name	Solubility (mg/mL)
AMX	0.33
AMX: D (-) tartaric acid	15.84
AMX: D (+) tartaric acid	16.54
AMX: Fumaric acid	17.19
AMX: Maleic acid	13.02
AMX: Succinic acid	16.63
AMX: Citric acid	1.36
AMX: Malonic acid	17.51
AMX: L (-) Malic acid	64.19
AMX: Adipic acid	16.66

Table 2.7: Intrinsic dissolution rate of AMX and all salts in PBS7.

Name	IDR ($mg.min^{-1}.cm^{-1}$)
AMX	0.016
AMX: D (-) tartaric acid	0.214
AMX: D (+) tartaric acid	0.980
AMX: Fumaric acid	0.999
AMX: Maleic acid	0.375
AMX: Succinic acid	4.456
AMX: Citric acid	0.681
AMX: Malonic acid	3.525
AMX: L (-) Malic acid	4.651
AMX: Adipic acid	0.994

2.4 Conclusion

We have developed nine novel salts of amoxapine by rational use of the ΔpK_a rule of 3. We have found five single crystals of AMX salt with D (-) tartaric acid, fumaric acid, maleic acid, succinic acid and malonic acid with solved structure by single-crystal XRD. AMX: D (-) tartaric acid crystallize in chiral space group $P2_1$ whereas all other salts crystallize in nonchiral $P\bar{1}$ and $P2_1/c$ space groups. In the crystal structure of salts, the proton of the corresponding acid is transferred to the nitrogen of the piperazine ring in AMX by ionic $N^+–H\cdots O^-$ hydrogen bond. The crystal structures of these five salts have common features in the packing of ions and solvents. AMX: fumaric acid salt and AMX: succinic

acid salt has an alternate arrangement of AMX^+ layer and acid-water channel due to antiparallel arrangement of AMX^+ in the same layer providing binding sites for the respective carboxylate anion or water molecule to form strong hydrogen bonds. Therefore, these salts have a lower melting point than other salts as AMX: fumaric acid salt has a melting point of 127.2 ˚C which is higher than AMX: succinic acid (95.8 ˚C) AMX layer is following more regularity in AMX: fumaric acid salt. It can also be differentiated by melting enthalpies; AMX: fumaric acid salt has less melting enthalpy 13.9 J/g than AMX: succinic acid salt (23.4 J/g). In the case of AMX: D (-) tartaric acid salt, AMX: maleic acid salt and AMX: malonic acid salt, single crystals have different patterns. A parallel arrangement of AMX molecule holds acid layer on one side by hydrogen bonding and another side one layer of AMX bonded by Van der Waal's forces which further connected to acid layer. So, two layers of AMX are present in between the acid layer and these are less well arranged than the previous two crystals and have higher melting points and melting enthalpy. AMX: maleic acid salt has the lowest solubility of 13.02 mg/mL of these five salts, but others have higher solubility. AMX: D (-) tartaric acid and AMX: maleic acid salts are anhydrous, but the other three are hydrated. This may be attributed to the higher solubility of these three AMX: fumaric acid salt, AMX: succinic acid salt and AMX: malonic acid salt. Hirshfeld surface study helps to validate the crystal structure and its interactions with other molecules. It shows the percentage share of each type of interaction and indicates the hydrogen bonding is more prominent in the crystal packing. The partition coefficient was determined to check the hydrophilic nature of the newly formed salts, and all salts are more hydrophilic than AMX. Solubility and IDR experiments were performed in phosphate buffer solution at pH 7 and 37 ˚C for AMX and pure API salts. We have found many folds increment in solubility (i.e., 4.1 to 194.5 times) and IDR (i.e., 13.1 to 283.2 times). We have improved the solubility and IDR of AMX by the cocrystallization method, and these new salts can be used as an alternative to pure drug.

Chapter 3

Cocrystals of Doxepin with Improved Solubility for Enhanced Pharmaceutical Applicability

Chapter 3

3.1 Introduction

Doxepin (DOX; 3-(dibenz[b,e]oxepin-11(6H)-ylidene)-N,N-dimethyl-1-propanamine, monohydrochloride; Figure 3.1) is a tricyclic antidepressant which FDA approved in 1969 to treat the major depressive disorder. Further, it was agreed to treat insomnia and anxiety and topically have been authorized to manage skin pruritus due to its multiple receptors targeting. It shows antagonist effects on alpha-adrenergic, muscarinic, and histaminic receptors.[113–116] DOX has proven its efficacy as an analgesic in treating neuropathic pain[117,118] and as a prophylactic agent against migraines[119,120] but not approved yet for the treatment of neuropathic pain and migraines.

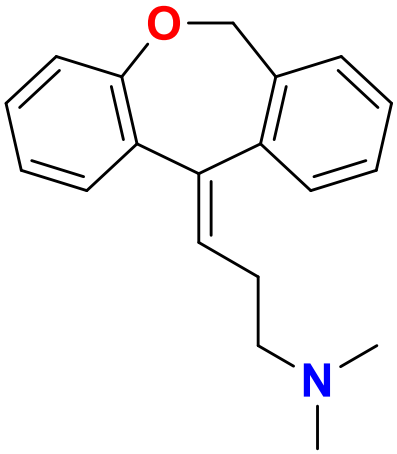

Figure 3.1: Chemical structure of Doxepin.

Depression seems to result from a chemical imbalance and a lack of neurotransmitters in the brain. DOX, a tricyclic antidepressant drug; works by increasing the neurotransmitter's serotonin and norepinephrine concentration in the brain. DOX shows antagonistic action in the central nervous system and blocks the histamine (H_1), adrenergic (α_1), and muscarinic receptors. It extends the availability of these neurotransmitters within the synaptic cleft and enhances their neurotransmission by avoiding their reuptake back into the presynaptic terminal.[121,122] DOX is administered orally and absorbed through the gastro intestinal tract with 30 % bioavailability, and peak plasma concentration reaches within two hours. It bounds to the plasma protein about 80%, and it metabolizes in the liver by cytochrome enzymes

and produces active metabolite N-desmethyldoxepin by hydroxylation.[123,124] DOX is found in the liquid phase at room temperature and has low water solubility and intrinsic dissolution rate (IDR).

This chapter will demonstrate the development of novel salts of DOX in the solid phase with organic acids with higher aqueous solubility and IDR. These salts have been characterized by powder X-ray diffraction (PXRD) and differential scanning calorimetry (DSC). These salts have been studied using the procedure described in Chapter 2.

3.2 Experimental Section

3.2.1 Materials

Doxepin hydrochloride (98% purity), Terephthalic acid (98% purity) and 4-nitrobenzoic acid (98% purity) were purchased from Sigma Aldrich. Oxalic acid dihydrate (99% purity) was obtained from Merck Specialties Pvt. Ltd. Di-sodium hydrogen phosphate anhydrous (99% purity) and potassium dihydrogen phosphate anhydrous (99% purity) were bought from Hi-media laboratories Pvt. Ltd. Analytical grade solvents methanol (99.9% purity) and ethanol (99.9% purity) were obtained from Merck and Spectrochem Pvt. Ltd.

3.2.2 Purification of DOX and Characterization

As DOX is sold as its hydrochloride salt, we first extracted pure DOX by treating it with 0.1 N NaOH solution. We took doxepin hydrochloride in a beaker, added 0.1 N NaOH, and stirred for 2 h. Then, pure DOX was extracted with dichloromethane in a separating funnel. We have separated the organic layer, and the solvent was evaporated by rotatory evaporator apparatus to extract liquid DOX.

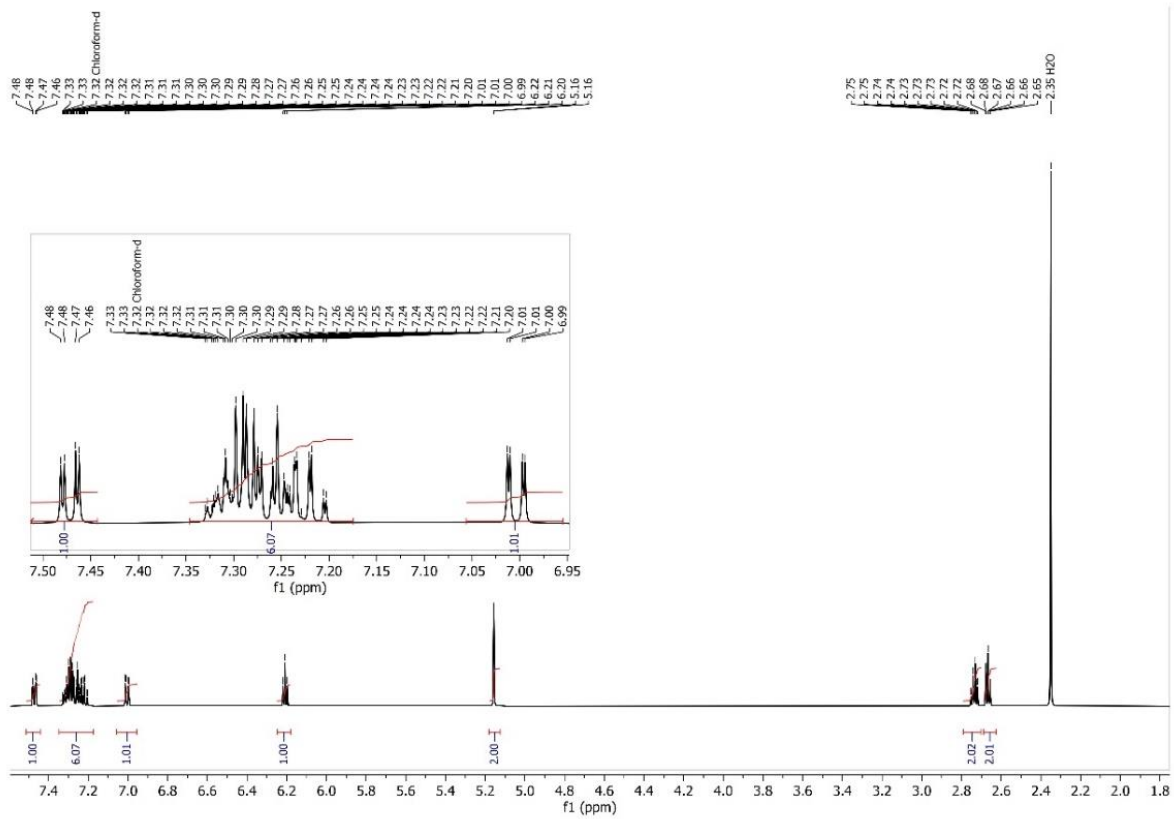

(a)

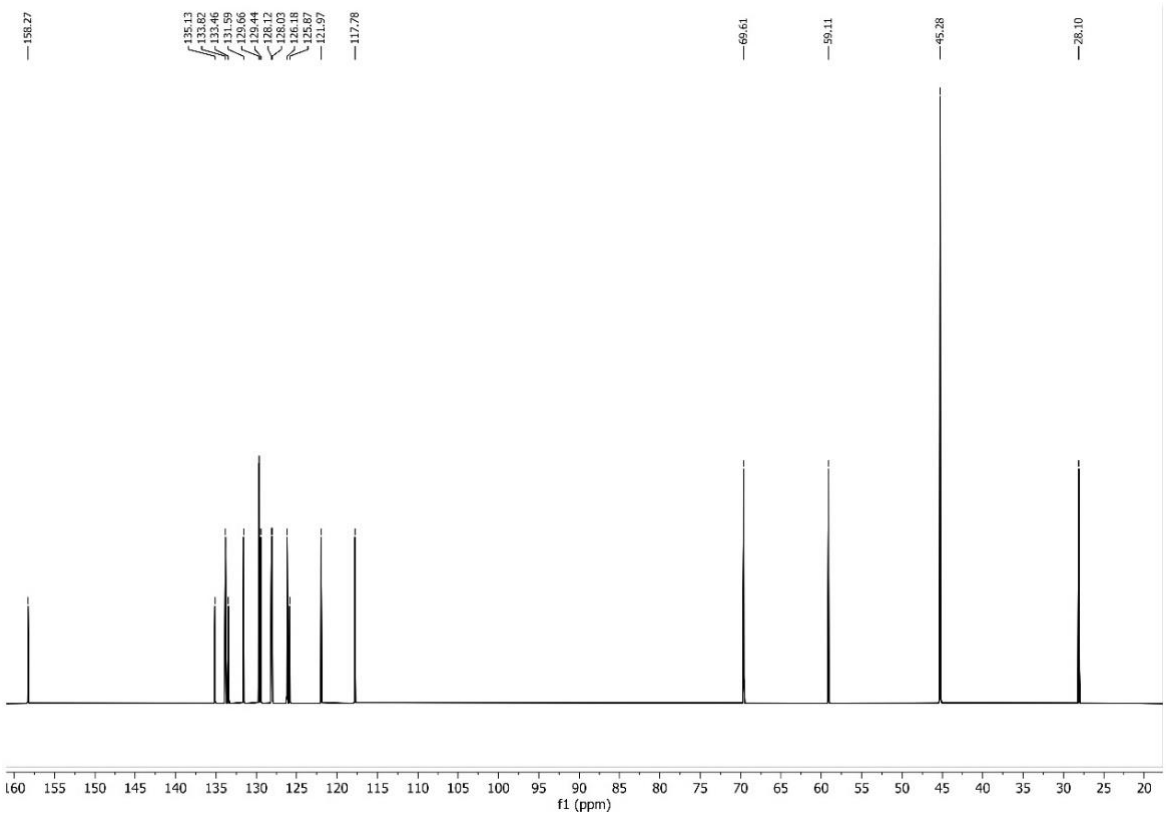

(b)

Figure 3.2: (a) Proton NMR spectra of pure DOX; (b) ^{13}C NMR spectra of pure DOX.

The compound dried under a high vacuum for 2 h to obtain a highly viscous liquid compound (pure DOX). We have characterized it by ^{1}H and ^{13}C NMR spectroscopy in $CDCl_3$ solvent using Bruker Avance III 400 MHz NMR (Figure 3.2 (a) for ^{1}H NMR and (b) for ^{13}C NMR).

3.2.3 Method for cocrystal formation

The cocrystals of DOX were developed using dissolution and subsequent solvent evaporation methods. We have taken liquid DOX and a cocrystal former [one among oxalic acid dihydrate (1:1), terephthalic acid (1:1) and 4-nitrobenzoic acid (1:2)] in a 250 mL round bottom flask and added ethanol to dissolve the mixture. These solutions were stirred for 2 h, and the solvent was evaporated using a rotary evaporator. A high vacuum was applied on these samples for 2 h to obtain a free-flowing powder from the salt. We have tried with many coformers to obtain solid salts, but we could only get the solid form from these three coformers.

3.2.4 Powder X-ray Diffraction (PXRD)

PXRD data were recorded on a Rigaku Ultima IV powder X-ray diffractometer using parallel beam geometry equipped with Cu K_α source, 2.5° primary and secondary Soller slits, 5° in-plane divergence slit with 10 mm height limit slit, sample rotation stage (120 RPM) attachment and DTex Ultra detector. The data were collected over 2θ range 5°–50° with a scanning speed of 2° per minute with 0.02° steps.

3.2.5 Differential Scanning Calorimetry Analysis

The melting points and melting enthalpies of the DOX and salts were recorded on the Perkin-Elmer DSC-8000 instrument. All the samples (2-5 mg) were heated at a rate of 5 ˚C/min in sealed aluminum pans without the hole. The melting points, the fusion enthalpies, DSC traces of DOX and the developed salts have been reported in the Table 3.2 and the DSC traces are available in the supporting information [Figure S3.1 – S3.4 on page no. 18-19] file in the enclosed DVD.

3.2.6 Single Crystal X-ray Diffraction (SCXRD)

SCXRD experiments of DOX: oxalic acid and DOX: terephthalic acid hydrate single crystal were performed on a Bruker AXS KAPPA APEX-II CCD diffractometer (Monochromatic Mo Kα radiation). Unit cell determination, data collection at 100K and 120 K respectively and data reduction were made using the Bruker APEX-III package.[125] SCXRD experiment of DOX: terephthalic acid and DOX: 4-nitrobrnzoic acid single crystals were performed on Rigaku XtaLABmini X-ray diffractometer equipped with Mercury CCD detector with graphite monochromatic Mo-Kα radiation (λ = 0.71073 Å) at 100.0 (2) K using ω scans. The data were reduced using CrysAlisPro 41_64.93a software.[126] The crystal structures were solved using Olex^2 package[99] equipped with XT[100] and were further refined using XL.[101] Crystal packing and interaction diagrams were created using Mercury software.[102] The details of the single-crystal X-ray diffraction data collection, structure solution and refinement are given in Table 3.3. Single crystals of DOX: oxalic acid was made by slow evaporation from a solution of ethanol at 4 ^{o}C in the refrigerator. Single crystals of DOX: terephthalic acid hydrate salt was obtained from water: ethanol (1:1) mixture solution at 4 ^{o}C in the fridge. Single crystal of DOX: terephthalic acid salt was synthesized by dissolving the compound in DMSO and stirred at 70 ^{o}C, then cool at room temperature and left for slow evaporation at room temperature. DOX and 4-nitrobenzoic acid single crystal was made by slow evaporation from a solution in water: ethanol (1:1) mixture at 4 ^{o}C in the refrigerator. Good quality single crystals were obtained within 10-15 days.

3.2.7 Hirshfeld Surface Analysis

Hirshfeld surfaces and 2D fingerprint plots of the single crystal data of DOX salts were generated using Crystal Explorer 17.5 package as described in detail in Chapter 2, section 2.2.6.[103–105]

3.2.8 Determination of Partition Coefficient

Partition coefficients of DOX and it's all salts were determined by the slow stirring method following the same procedure described in Chapter 2, section 2.2.8.[106]

3.2.9 Solubility Analysis

The saturation solution of the compounds determined the solubility of DOX and its salts. The calibration curves were drawn between absorbance *vs*. concentration for the pure drug DOX and all the salts by known concentrations solutions using a UV-Vis spectrophotometer. We had taken 50 mg of the compound (pure DOX or the salt) in 5 mL of a vial, and 2 mL of PBS7 was added with a magnetic bead. These vials were stirred at 1500 rpm at 37 ^{o}C for 24h to achieve saturation solubility. These solutions were centrifuged at 10000 RPM. We had then withdrawn the supernatant solution and diluted

that up to 1000 times (10000 times for DOX: oxalic acid) with PBS7 to determine the concentration of DOX using UV−VIS spectroscopy.[127] Solubility of DOX and all the salts were determined by multiplication of concentrations with dilution factor. All the UV-VIS spectra are given in the supporting information [Figure S 3.10 – S3.13 on page number 24 – 25] document in the enclosed DVD.

3.2.10 Intrinsic Dissolution Rate

Intrinsic dissolution rates of newly formed salts of DOX were determined using USP certified Lab India 8000+ Dissolution Tester using the method described in Chapter 2, Section 2.2.9.[109]

3.3 Results & Discussion

Doxepin (pK_a = 8.96) was expected to form salts with organic acids having pK_a ranging from 1.27 to 4.82, which are not so strong to cause harm to DOX and the cells. According to the ΔpK_a rule of 3,[50,110,111] salt formation occurs at least three units and more of pK_a[111] difference. This concept is reflected in the case of DOX (Table 3.1). Salt formation is detected in the case of the following acids, which are used as coformers.

Table 3.1: pKa and ΔpK_a values of DOX and coformers used in this study.

Name	pK_a	ΔpK_a
Doxepin	8.96	
Oxalic acid	1.27, 4.28	7.69, 4.68
Terephthalic acid	3.51, 4.82	5.45, 4.14
4-Nitrobenzoic acid	3.41	5.55

3.3.1 Synthesis of Cocrystals

The solvent evaporation method was used to synthesize the salts of the liquid drug DOX. We have used several coformers (2-Nitrobenzoic acid, 3-hydroxybenzoic acid, 3-Nitrobenzoic acid, 4-Hydroxybenzoic acid, 4-Nitrobenzoic acid, Acetic acid, Adipic acid, Anthranilic acid, Benzoic acid, Citric acid, DL-Tartaric acid, Formic acid, Fumaric acid, Glutaric acid, Glycine, Glycolic acid, Isophthalic acid, L-Asparagine Monohydrate, L-Aspartic acid, L-Tyrosine, L-Malic acid, Malonic acid, Mandelic acid, Oxalic acid dehydrate, Pimelic acid, Sorbic acid, Succinic acid and Terephthalic acid) in different stoichiometric ratio to form a solid phase salt of DOX. But there were three new solid crystalline phases of DOX found with oxalic acid (1:1), terephthalic acid (1:1) and 4-nitrobenzoic acid (1:2) and were identified by PXRD. These novel salts were also characterized by DSC analysis.

3.3.2 Powder X-ray Diffraction (PXRD)

We characterized new salts of DOX by comparing PXRD patterns of new salts by their starting materials, as shown in Figure 3.3. It is evident from these PXRD patterns that the salts formed by the solvent evaporation method resulted in a new crystalline solid phase compared to the DOX and the corresponding organic acid used in the experiment. DOX is an amorphous phase, whereas all the developed new salts are crystalline, as seen in Figure 3.3. It indicates the formation of new solid phases.

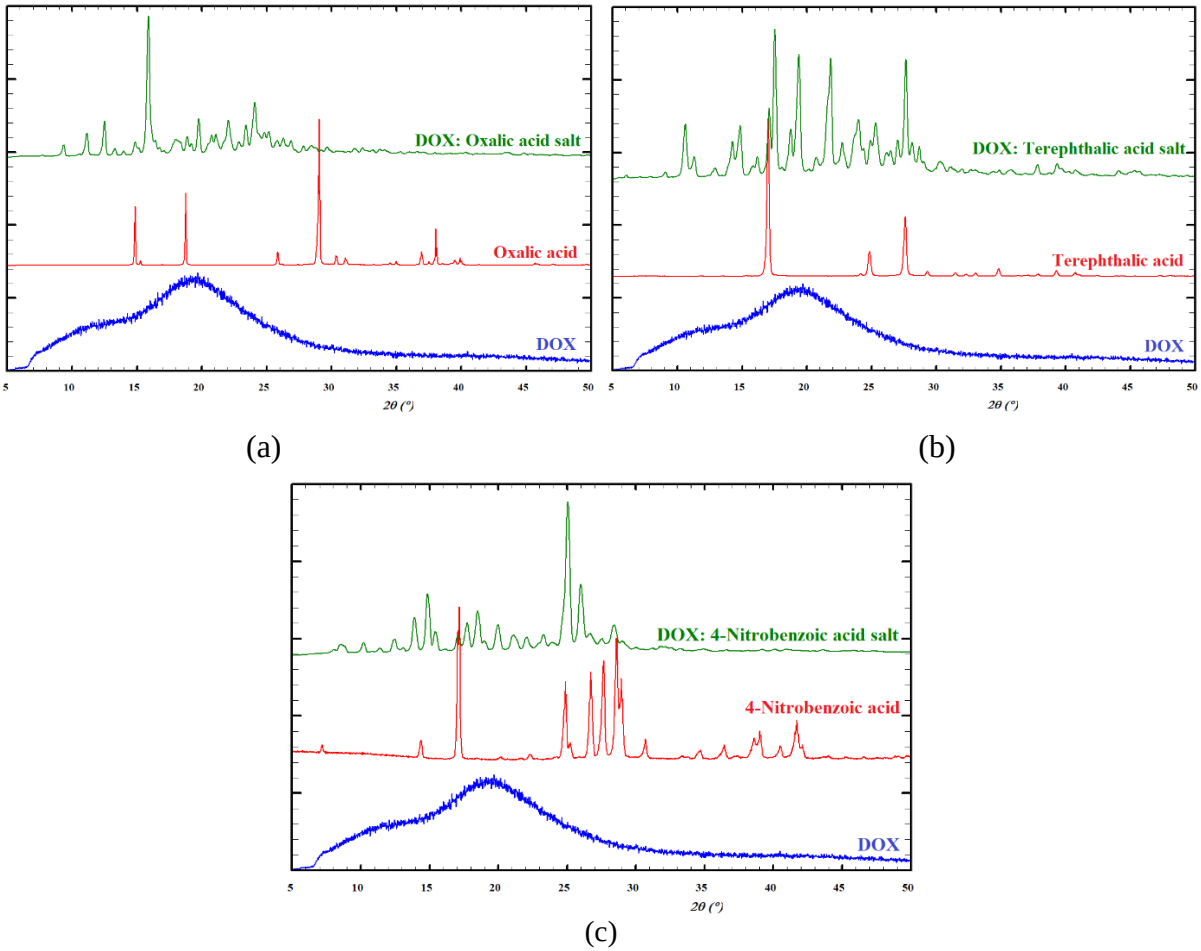

Figure 3.3: PXRD patterns of salts of DOX in comparison with DOX and coformers.

3.3.3 Thermal Analysis

DSC thermogram of DOX shows that this is liquid at room temperature. The melting point of DOX is -27.7 ˚C, and the freezing point is -74.24 ˚C found. These DSC data on these solid phases show that the compounds have different melting points concerning the parent drug, confirming new solid phases' development. The melting enthalpy of cocrystals was different from DOX. The highest melting point was found for DOX: terephthalic acid salt (203.7 ˚C), and the lowest was found for DOX: 4-nitrobenzoic acid salt (132.1 ˚C), which indicates DOX: terephthalic acid salt is the most stable solid phase.

Table 3.2: Melting points and melting enthalpies of DOX and their salts.

Name	Melting Point of DOX/Coformer (ºC)	Melting Point of Salt of DOX (ºC)	Melting enthalpies (J/g)
DOX	-27.7		1.03
DOX: Oxalic Acid	101	180.7	39.0
DOX: terephthalic acid	300	203.7	93.7
DOX: 4-Nitrobenzoic acid	237	132.1	55.7

3.3.4 Single Crystal X-ray Diffraction Analysis

We have grown single crystals of DOX salts and recorded single-crystal X-ray diffraction data. We have tabulated in Table 3.3 crystallographic parameters of four salts of DOX (DOX: oxalic acid; DOX: terephthalic acid hydrate; DOX: terephthalic acid and DOX: 4-nitrobenzoic acid). The salt formation was confirmed through single-crystal X-ray structural analysis. These single-crystal data reveal that the salt formation occurs by proton transfer from acidic coformer molecule to tertiary nitrogen of DOX molecule and interacted by the N–H···O hydrogen bonding. We have found the hydrate of a terephthalic acid salt of DOX in DMSO solvent.

3.3.4.1 DOX: Oxalic acid salt

In the asymmetric unit of DOX: oxalic acid salt, two molecules of DOX, one molecule of deprotonated oxalic acid and one molecule of protonated oxalic acid are present. This salt is crystallized in a triclinic lattice with $P\ \bar{1}$ space group. The acidic proton of one oxalic acid is transferred to the tertiary nitrogen atom of DOX and form N1–H1···O8 (1.905 Å) and N2–H2···O6 (1.909 Å) strong hydrogen bond. This acidic molecule is further connected to other oxalic acid molecules through O4–H4A···O7 (1.666 Å) and O10–H10···O9 (1.677 Å) hydrogen bonding shown in Figure 3.4a and formed DOX: oxalic acid salt. In crystal packing, DOX molecule forms a layer of drug molecule by week hydrogen and van der Waals' interactions, which interact both sides by the layer of the oxalic acid channel by strong and weak hydrogen bonding as displayed along the 'b' axis in Figure 3.4c. DOX molecules in the layer are connected by C–H···π bonds as shown in Figure 3.4b, and all hydrogen bond interaction and C–H···π interactions are listed in Table 3.4.

3.3.4.2 DOX: Terephthalic acid hydrate salt

The asymmetric unit of DOX: terephthalic acid hydrate salt has one molecule of DOX, half molecule of terephthalic acid and one water molecule. This is crystallized in monoclinic lattice with the $P2_1/c$ space group. The proton of terephthalic acid is transferred to the tertiary nitrogen atom of DOX and forms N1–H1···O3 (1.597 Å) strong hydrogen bond. This acidic molecule is further connected to a water molecule by O4–H4D···O2 (2.021 Å) hydrogen bonding as shown in Figure 3.5a and formed hydrated salt. In crystal packing, DOX molecule forming a layer of drug molecule by week hydrogen and Van der Waals' interactions which are interacted both sides by the layer of terephthalic acid water channel by strong and weak hydrogen bonding as displayed along the 'b' axis in Figure 3.5c. DOX molecules in the layer connected by C–H···π bonds as shown in Figure 3.5b and all hydrogen bond interaction and C–H···π interactions are listed in Table 3.4.

Table 3.3: Crystallographic data of DOX salts.

Data/Salt	DOX: Oxalic acid	DOX: Terephthalic acid hydrate	DOX: Terephthalic acid	DOX: 4-Nitrobenzoic acid
Empirical formula	$2(C_{19}H_{22}NO)^{+}$ $(C_2O_4)^{2-}$ $(C_2H_2O_4)$	$(C_{19}H_{22}NO)^{+}$ $(C_4H_2O_2)^{-}$ (H_2O)	$(C_{19}H_{22}NO)^{+}$ $(C_8H_5O_4)^{-}$	$(C_{19}H_{22}NO)^{+}$ $(C_7H_4NO_4)^{-}$ $(C_7H_5NO_4)$
CCDC number	2119630	2095674	2095675	2095676
Formula weight	738.81	380.45	445.49	613.61
Crystal system	Triclinic	Monoclinic	Triclinic	Monoclinic
Space group	$P\ \bar{1}$	$P2_1/c$	$P\ \bar{1}$	$P2_1/n$
a(Å)	11.324(6)	8.4636(16)	7.938(3)	13.8793(7)
b(Å)	12.419(7)	22.025(4)	9.400(4)	13.7947(6)
c(Å)	14.590(9)	11.371(2)	14.999(6)	15.4865(7)
α(°)	107.519(15)	90	89.318(10)	90
β(°)	99.386(18)	105.16(2)	84.792(9)	95.276(4)
γ(°)	100.183(17)	90	88.338(9)	90
V(Å^3)	1874.1(18)	2045.8(7)	1114.1(7)	2952.5(2)
Z	2	4	2	4
ρ_{calc}(g/cm^{-3})	1.309	1.235	1.328	1.380
Temperature (K)	100.0(2)	100.00(10)	296.0(2)	100.0(2)
μ/ mm^{-1}	0.093	0.084	0.091	0.102
$2\theta_{min,\ max}$ ()	3.542 to 50	4.986 to 50.108	2.726 to 57.972	5.082 to 65.572
F (000)	784.0	812.0	472.0	1288.0
$h_{min,max}$; $k_{min,max}$; $l_{min,max}$	-13, 13; -10, 14; -17, 17	-10, 10; -26, 26; -10, 13	-10, 10; -11, 12; -20, 18	-21, 11; -17, 19; -16, 23
Total no. of reflections	11532	14481	12725	17058
R_{int}	0.1480	0.1115	0.0318	0.0536
No. of unique reflections	6605	3611	5281	9756
R_1 [I>2σ(I)]	0.0880	0.0833	0.0457	0.1418
wR2 (all data)	0.1981	0.2739	0.1142	0.4611
GooF on F^2	0.930	1.009	1.051	1.440
$\Delta\rho_{max,min}$/eÅ^{-3}	0.49/-0.34	0.69/-0.31	0.28/-0.24	1.08/-0.57

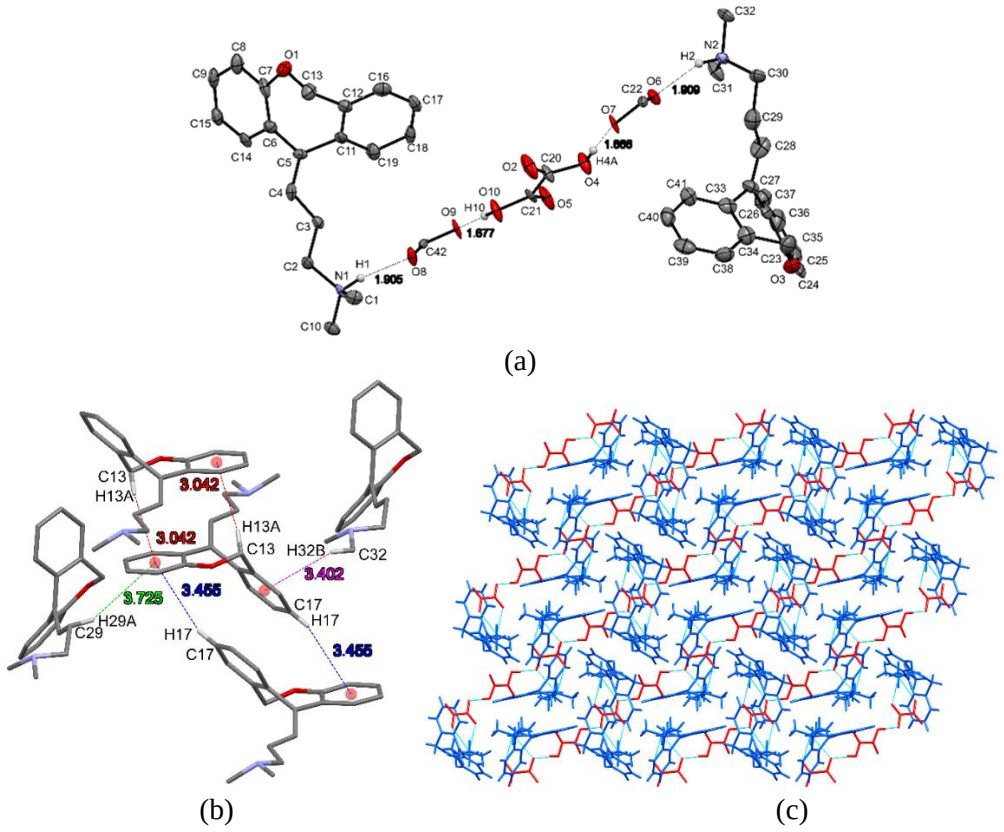

Figure 3.4: (a) Asymmetric unit of DOX: oxalic acid salt; (b) Intermolecular interaction between DOX molecules in a layer of DOX; (c) Crystal packing diagram of DOX: oxalic acid salt along 'b' axis.

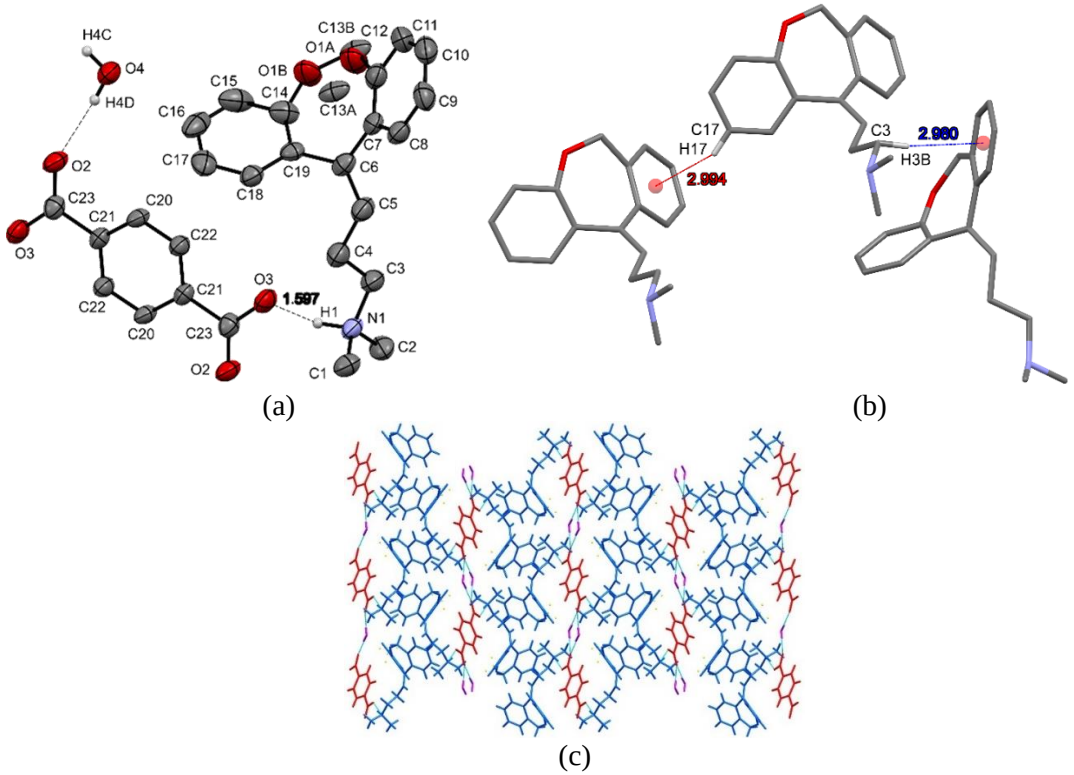

Figure 3.5: (a) Asymmetric unit of DOX: terephthalic acid hydrate salt; (b) Intermolecular interaction between DOX molecules in a layer of DOX; (c) Crystal packing diagram of DOX: terephthalic acid hydrate salt along 'b' axis.

3.3.4.3 DOX: Terephthalic acid salt

The asymmetric unit of DOX: terephthalic acid salt has one DOX molecule and one terephthalic acid in Figure 3.6a. This salt is crystallized in triclinic lattice and $P\ \bar{1}$ space group. The carboxylic acid of terephthalic acid donated one proton to the tertiary nitrogen of DOX molecule and hydrogen-bonded by N1–H1···O2 (1.816 Å) and other proton are shared by to terephthalic acid molecules O5–H3···O2 (2.50 Å) and O5–H3···O3 (1.31 Å) which is connected by hydrogen bonds as per the Figure 3.6a and the Table 3.4. Alternative layers of DOX molecule and terephthalic acid molecule formed by hydrogen bonding as shown in Figure 3.6c. DOX molecule interacted with another DOX molecule by weak hydrogen bonds and van der Waals' forces which provides stability to the salt as shown in Figure 3.6b. All hydrogen and C–H···π bonding are given in Table 3.4.

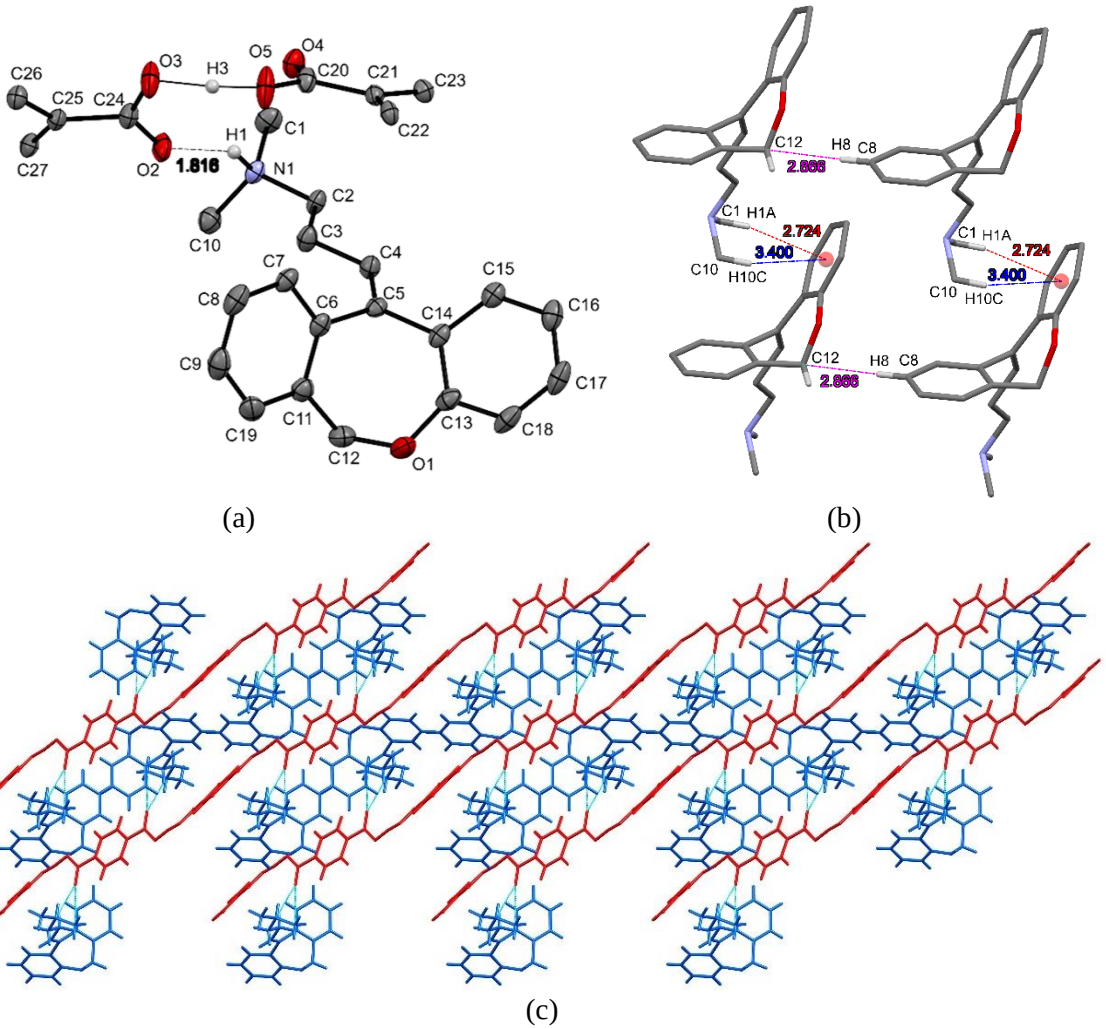

Figure 3.6: (a) Asymmetric unit of DOX: terephthalic acid salt; (b) Intermolecular interaction between DOX molecule in DOX layer; (c) Crystal packing diagram of DOX: terephthalic acid salt along 'b' axis.

3.3.4.4 DOX: 4-Nitrobenzoic acid salt

One DOX molecule and two molecules of 4-nitrobenzoic acid are present in the asymmetric unit of DOX: 4-nitrobenzoic acid salt, as shown in Figure 3.7a. The whole DOX molecule is disordered and

displayed in two parts. This salt is crystallized in monoclinic lattice and $P2_1/n$ space group. The acidic proton of one 4-nitrobenzoic acid molecule is transferred to the DOX nitrogen atom and connected via N–H···O strong hydrogen bonding, whereas the second molecule of 4-nitrobenzoic acid is attached to the first molecule of 4-nitrobenzoic acid by O–H···O hydrogen bond and form DOX: 4-nitrobenzoic acid salt as per Figure 3.7a. In crystal packing, acidic molecules are present between the DOX molecules and interact by strong and weak hydrogen bonding, as displayed in Figure 3.7c. DOX molecules are interacted by the hydrogen bonds and Van der Waals' forces, as shown in Figure 3.7b. These hydrogen bonds and weak bonds are tabulated in Table 3.4.

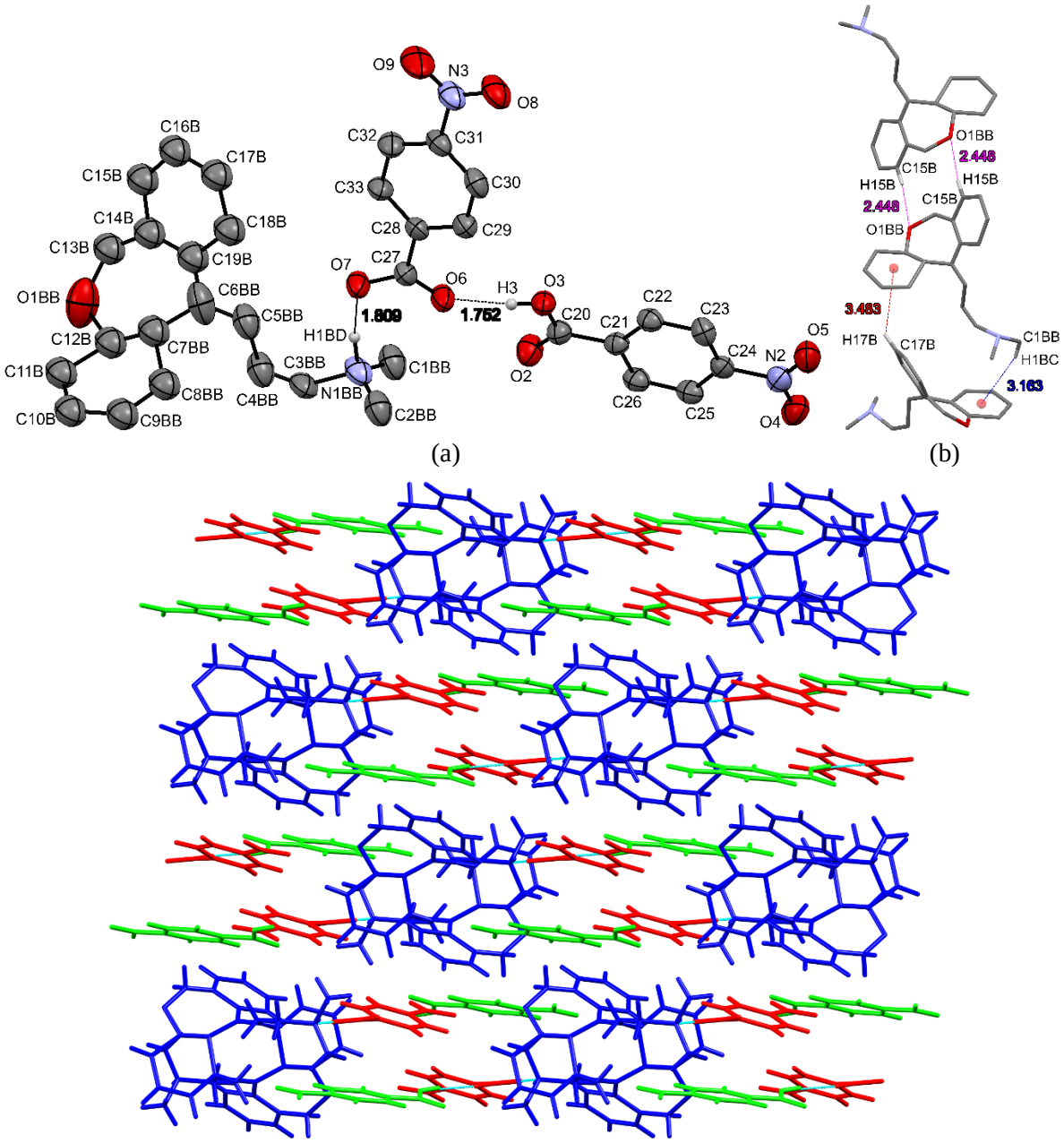

Figure 3.7: (a) Asymmetric unit of DOX: 4-nitrobenzoic acid salt; (b) Intermolecular interaction between DOX molecules within a DOX layer; (c) Crystal packing diagram of DOX: 4-nitrobenzoic acid salt along 'b' axis.

Table 3.4: Hydrogen bond geometry parameters in salts of DOX and C–H···π bonds.

Salts	Interactions	D–H (Å)	H···A (Å)	D···A (Å)	D–H···A (°)	Symmetry code
DOX: Terephthalic acid hydrate (2:1)	N1–H1···O3	1.01(5)	1.60(5)	2.587(5)	166(4)	1-x, 1-y, 1-z
	O4–H4C···O2	0.85	2.02	2.866(5)	177	-x, 1-y, -z
	O4–H4D···O2	0.85	2.02	2.867(5)	174	x, y, z
	C1–H1B···O4	0.96	2.50	3.371(6)	151	1+x, y, 1+z
	C2–H2B···O4	0.96	2.53	2.390(6)	149	1+x, y, 1+z
	C4–H4A···O3	0.97	2.60	3.237(6)	123	1-x, 1-y, 1-z
	C13A–H13D···O2	0.97	2.50	3.174(8)	127	x, y, z
	C3–H3B···π	0.97	2.98	3.918(5)	163	x, ½-y, ½+z
	C17–H17···π	0.93	2.99	3.702(5)	134	1+x, y, z
DOX: Terephthalic acid (2:1)	N1–H1···O2	0.98	1.82	2.686(2)	146	-1+x, y, z
	N1–H1···O4	0.98	2.47	3.030(2)	116	-1+x, y, z
	O5–H3···O2	1.14(3)	2.50(3)	3.296(2)	126(2)	x, y, z
	O5–H3···O3	1.14(3)	1.31(3)	2.449(2)	171(3)	x, y, z
	C1–H1B···O4	0.96	2.49	3.127(2)	124	-1+x, y, z
	C1–H1A···π	0.96	2.72	3.660(2)	165	x, -1+y, z
	C10–H10A···π	0.96	2.75	3.549(2)	141	x, -1+y, z
	C22–H22…π	0.93	2.76	3.530(2)	141	x, y, z
DOX: 4-nitrobenzoic acid (1:2)	N1AA–H1AD···O7	0.98	1.71	2.678(9)	170	1-x, 1-y, 1-z
	O3–H3···O6	0.82	1.75	2.568(3)	173	x, 1+y, z
	C10A–H10A···O9	0.93	2.51	3.403(12)	161	-½+x, 3/2-y, ½+z
	C5AA–H5AA···O9	0.93	2.38	3.261(12)	158	x, y, z
	N2–O5···π	1.219	3.712(3)	3.657(3)	77.93(18)	1-x, 2-y, 2-z
	C3AA–H3AB···π	0.97	2.73	3.419(9)	128	½-x, ½+y, 3/2-z
	C3AA–H3AB···π	0.97	2.80	3.510(10)	131	½-x, ½+y, 3/2-z

We have compared the simulated powder X-ray pattern from SCXRD data with the recorded PXRD data to compare the structure with the compound, as shown in Figure 3.8. The experimental powder X-ray diffraction pattern of DOX: oxalic acid salt matched with the simulated pattern of the salt (Figure 3.8a), which indicates the formation of 1:1 salt of DOX with oxalic acid. In the case of DOX: terephthalic acid salt, the recorded pattern matched with the simulated simple salt but not with the salt monohydrate (Figure 3.8b), which indicates the formation of a 1:1 salt of DOX: terephthalic acid by the solvent evaporation method. The experimental PXRD pattern of DOX: 4-nitrobenzoic acid powder

pattern matched with the simulated pattern of 2:1 salt of DOX (Figure 3.8c) and confirmed salt formation by the solvent evaporation method.

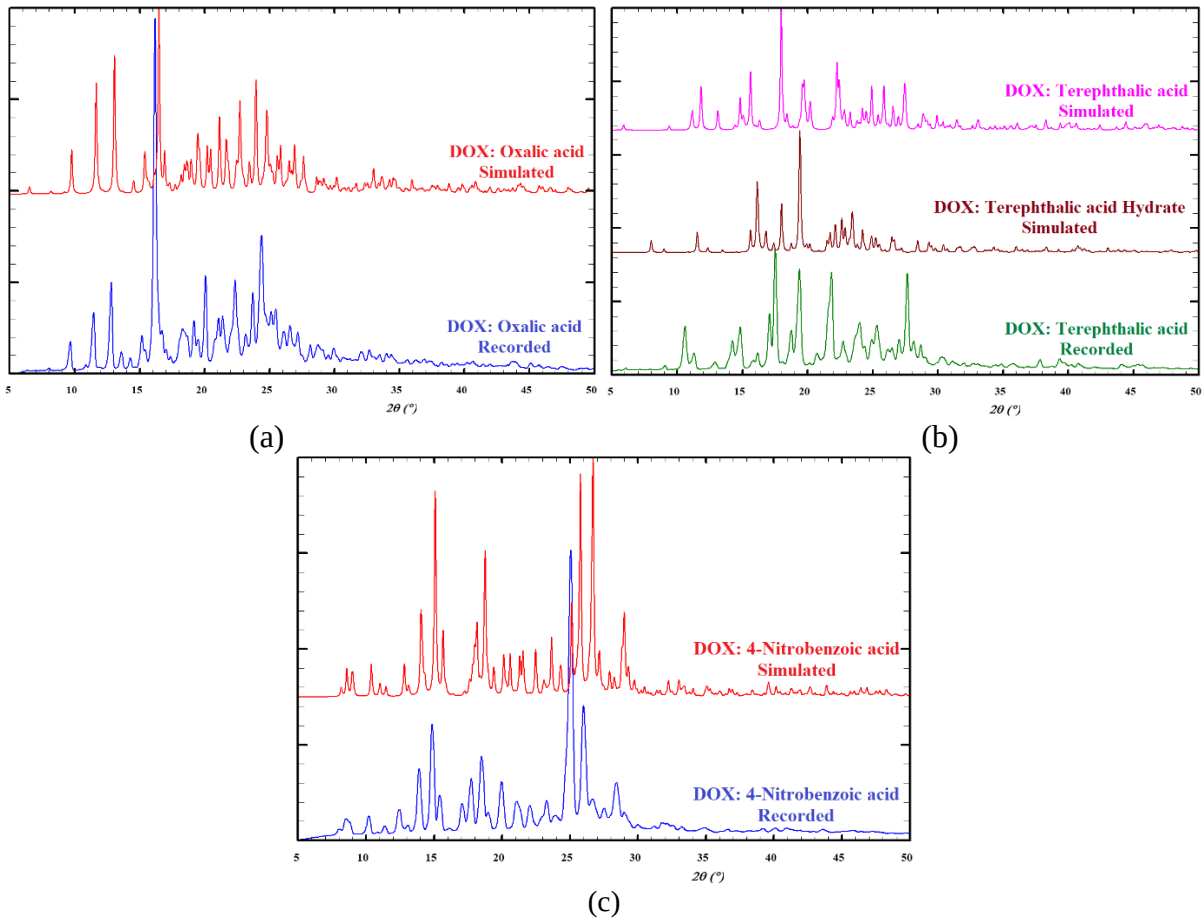

Figure 3.8: Comparisons of PXRD patterns recorded from powdered samples and simulated from single-crystal X-ray diffraction data.

3.3.5 Hirshfeld Surface Analysis

We have generated Hirshfeld surfaces of the salts of DOX by SCXRD data. We have seen the interactive surfaces in the Hirshfeld diagram by red in color in Figure 3.9. The strong interactions are observed by the red Hirshfeld surface and sharp peak in the fingerprint plot. The acidic proton of the corresponding acid molecules is transferred to the Nitrogen atom of DOX and form hydrogen bonding. We have calculated the percentage share of all the interactions inside and outside the Hirshfeld surface. These are detailed in the supporting information [Figure S 3.5 – S3.9 on page number 19 – 23] file in the enclosed DVD. The maximum was found for the week interactions like hydrogen bond and Van der Waals' forces.

3.3.6 Partition Coefficient

The partition coefficient of DOX and all salts are determined and presented in Table 3.5. $log_{10}P$ value of DOX is found 0.78, which is higher than all the salts, which indicates the hydrophilic nature of the DOX salts. This parameter supports the improved aqueous solubility of new composites. Highest $log_{10}P$ value is found for DOX: oxalic acid salt, and lowest is found for DOX: terephthalic acid salt. These results show that these salts will be rapidly soluble in oral drug delivery compared to pure DOX.

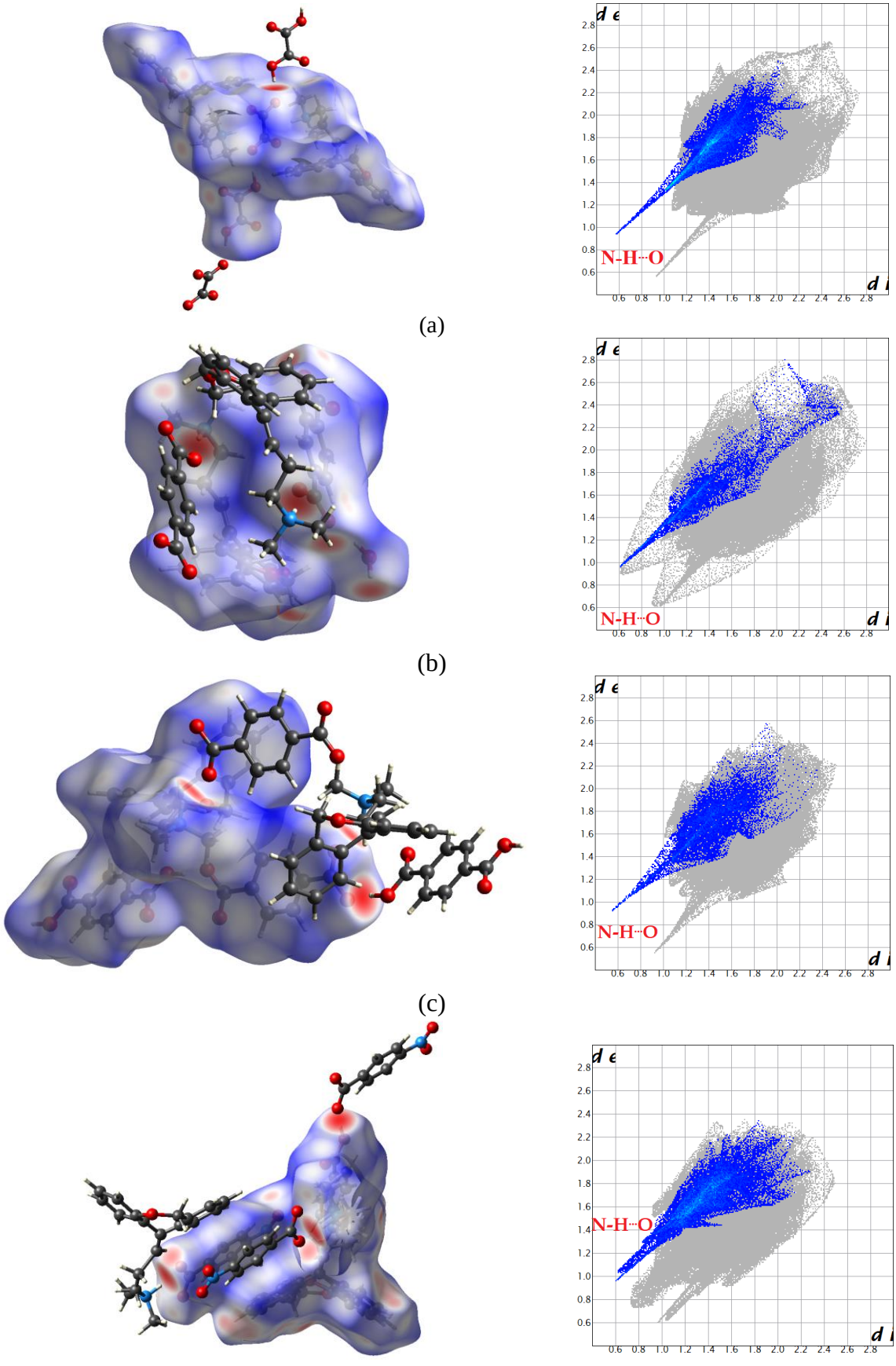

Figure 3.9: Hirshfeld surface and fingerprint plot of (a) DOX: oxalic acid salt; (b) DOX: terephthalic acid salt; (c) DOX: terephthalic acid hydrate salt; (d) DOX: 4-nitrobenzoic acid salt.

Table 3.5 Partition coefficient of DOX and its salts.

Name	$log_{10}P$
DOX	0.78
DOX: Oxalic acid	0.37
DOX: Terephthalic acid	-0.65
DOX: 4-Nitrobenzoic acid	-0.52

3.3.7 Solubility Studies

The water solubility of the DOX and newly developed salts was determined in PBS7 at 37 ˚C and given in Table 3.6. Related calibration curves and UV-Vis spectra are provided as a supporting information [Figure S3.10 – S3.13 on page 24 – 25] in the enclosed DVD. The saturation solubility of the salts was found better than pure DOX, which was improved by 1.2 to 11.2 times. Maximum water solubility was seen for DOX: Oxalic acid salt (16.758 mg/ mL) and minimum for DOX: 4-Nitrobenzoic acid salt (1.82 mg/ mL). This improved solubility may result from alternate layering of the DOX and conformer channel in crystal packing. DOX: oxalic acid salt shows maximum saturation solubility because protonated oxalic acid provides extra space in the crystal packing of salt, making it easy to solubilize in water.

Table 3.6: Solubility of DOX and its salts.

Name	Solubility mg / mL
DOX	1.49
DOX: Oxalic acid	16.75
DOX: Terephthalic acid	2.38
DOX: 4-Nitrobenzoic acid	1.82

3.3.8 Intrinsic Dissolution Rate Analysis

DOX is liquid at room temperature, so IDR determination is not possible for this. Still, its newly developed salts are solid phase material, so IDR analysis was performed for the salts of DOX in PBS7 by the LABINDIA dissolution test apparatus. The IDR of salts was tabulated in Table 3.7 and found maximum for DOX: oxalic acid salt (0.58 $mg.min^{-1}.cm^{-1}$) and minimum for DOX: terephthalic acid salt (0.24 $mg.min^{-1}.cm^{-1}$). We have plotted time vs. % dissolution of salts and found that complete dissolution occurs for DOX: oxalic acid salt 1.5 h, DOX: terephthalic acid salt in 8h and DOX: 4-nitrobenzoic acid salt in 4h in Figure 3.10. Hence, these salts of DOX are the better choice for formulation. These were found to be more stable in ambient air and not sensitive to moisture. Therefore, the pallets of these salts could be made easily for IDR analysis.

Table 3.7: Intrinsic dissolution rate of salts of DOX in PBS7.

Name	IDR ($mg.min^{-1}.cm^{-1}$)
DOX: Oxalic acid	0.58
DOX: Terephthalic acid	0.24
DOX: 4-Nitrobenzoic acid	0.41

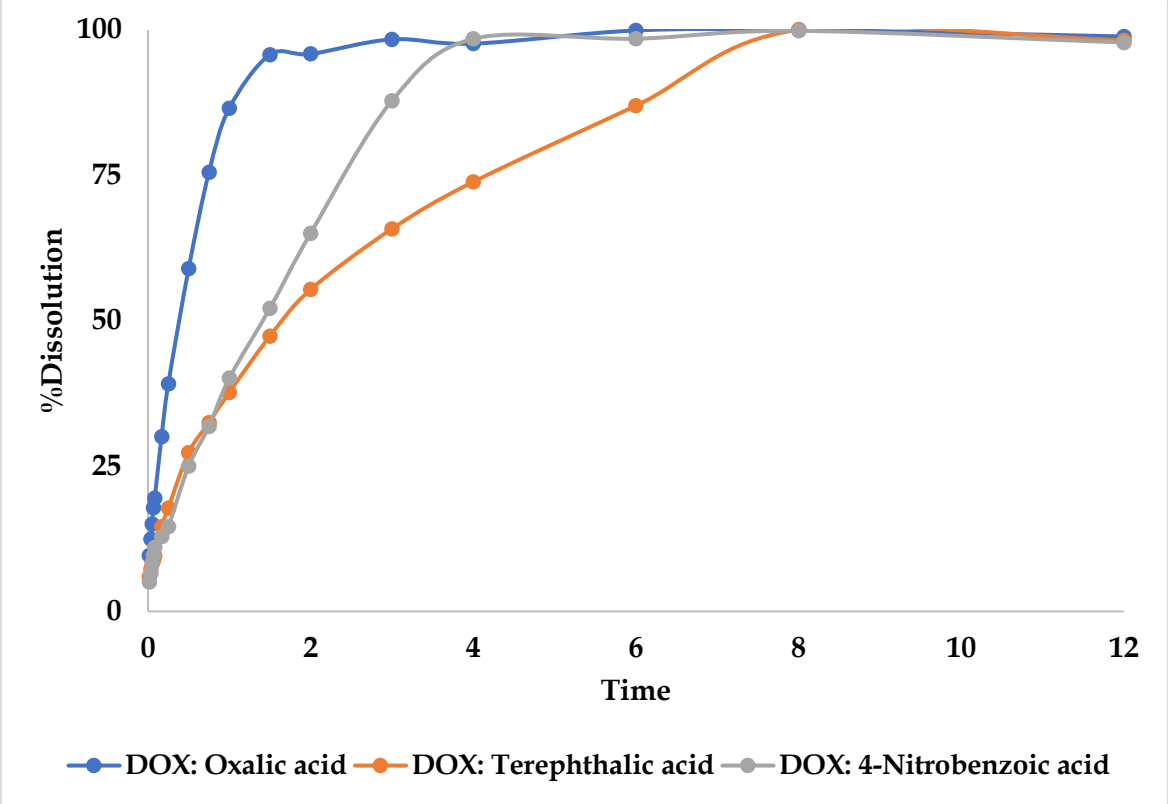

Figure 3.10: Time vs. % Dissolution plot of salts of DOX.

3.4 Conclusion

Solid salts of liquid drug DOX were synthesized using the Δpk_a rule of three and crystal engineering. We have successfully synthesized the salts of DOX with oxalic acid, terephthalic acid and 4-nitrobenzoic acid by solvent evaporation method and characterized by PXRD and DSC. We have studied structural analysis with the help of SCXRD, and we found single crystals of DOX: oxalic acid, DOX: terephthalic acid and DOX: 4-nitrobenzoic acid. Salts are formed by transferring acidic protons to tertiary nitrogen of DOX and forming a hydrogen bond. These salts formed an alternate layered structure of DOX and coformer molecules and interacted by hydrogen bond and van der Waals' forces in crystal packing. We determined the salts' Hirshfeld surface and fingerprint plots. We found the strong directional interaction between DOX and acid molecules by hydrogen bonding between N–H…O and O–H…O. The maximum share of interaction was found by week bindings like week hydrogen bonds and van der Walls' bonds. These salts are more hydrophilic than pure DOX by the determination of partition coefficient. We have found improved water solubility for all the salts of DOX, and it increased up to 11.2 times. IDR of new solid salts was determined in PBS7 and found maximum for DOX: oxalic acid. These salts are more stable than pure drug DOX and solid at room temperature, so easy to handle for making formulations.

Chapter 4

Cocrystals of Zaleplon with Improved Solubility for Enhanced Pharmaceutical Applicability

Chapter 4

4.1 Introduction

Insomnia is a disorder, which makes it difficult for some human beings to fall asleep, continue to have a prolonged sleep, makes people wake up earlier than others and doesn't allow them to get back to sleep again. This type of disturbed sleep often causes fatigue when we wake up. Insomnia may reduce our energy level and affect our mood and may affect our general health, performance at the workplace, and may have an adverse effect on the quality of our life. The occurrence of insomnia in human beings increases with age and is commonly seen in the elderly population.[128] More than half of the older people complain about the disappointment with sleep quality, like prolonged time to initiate sleep, interrupted sleep etc., at night.[129,130] Insomnia results in sleeping in the daytime, lethargy, poor daytime functioning etc.[128,131] People who have insomnia start to increase the use of the hypnotic drug with age to overcome insomnia.[132] Insomnia in the geriatric population is a consequence of various factors like physical, psychological, and social life.[133,134] Most of them are prescribed hypnotic drugs to improve the quality of sleep.[135,136]

Zaleplon (N-[3-(3-cyanopyrazolo[1,5-a]pyrimidin-7-yl)phenyl]-N-ethylacetamide; ZLP, Figure 4.1) is a sedative-hypnotic drug that is mainly used for insomnia.[137] It comes under pyrazolopyrimidine chemical classification witch is non-benzodiazepine hypnotic. ZLP acts as an agonist for the benzodiazepine α1 subunit receptor on the brain's $GABA_A$ receptor and binds selectively on the α1 subunit.[138] ZLP is absorbed orally up to 30% and is eliminated quickly because of its plasma half-life of 1 hour only.[139] ZLP is extensively metabolized by aldehyde oxidase and CYP3A4 enzymes, and it produces inactive metabolites.[140,141] ZLP is a BCS class II drug which has off white color, powder form with very low water solubility (0.16 mg / mL).[142]

The formulation of poorly water-soluble drugs has been a most challenging mission for the pharma industry. Improving water solubility and dissolution rate can enhance the bioavailability of such API and other impacts on therapeutic effectiveness and patient compliance.[143] Poor water solubility becomes a limiting step for ZLP in absorption, IDR, and bioavailability. The cocrystallization technique is the most important method to modify the solubility, IDR, and bioavailability in a highly economical

way.[144] This technique introduces another component in the drug's crystal lattice without changing the pharmacological effects and improves physiochemical properties.[145]

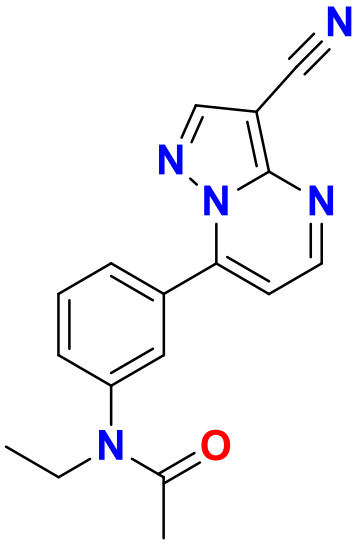

Figure 4.1: Chemical structure of zaleplon.

We have designed new cocrystals of zaleplon to enhance the solubility and IDR using simple biologically acceptable organic acids. The theme of this chapter is to demonstrate the synthesis of four cocrystals of ZLP using the solvent evaporation method. We would like to highlight their spectroscopic, thermal, and structural characterization using DSC, powder, and single-crystal X-ray diffraction methods. We have constructed Hirshfeld surfaces of these cocrystals to see the surface interactions of ZLP with surrounding molecules in the solid-state. We have determined their saturation solubility, IDR, and partition coefficient to establish the enhancement of solubility and dissolution rate in PBS7.

4.2 Experimental Section

4.2.1 Materials

Zaleplon (99% pure) was purchased from Precise Chemipharma Pvt. Ltd. Fumaric acid (99% purity) was got from Sisco Research Laboratories Pvt. Ltd. Oxalic acid dihydrate (99% purity) was bought from Merck Specialities Pvt. Ltd. Malonic acid (99% purity) was purchased from Himedia Laboratories Pvt. Ltd. Terephthalic acid (98% purity) was obtained from Sigma Aldrich. Di-sodium hydrogen phosphate anhydrous (99% purity) and potassium dihydrogen phosphate anhydrous (99% purity) were bought from Hi-media laboratories Pvt. Ltd. Analytical grade solvents methanol (99.9% purity) and ethanol (99.9% purity) were obtained from Merck and Spectrochem Pvt. Ltd.

4.2.2 Method for cocrystal formation

The cocrystals of ZLP were developed using the solvent evaporation method. A 2:1 molar mixture of the ZLP and a cocrystal former [one among fumaric acid, oxalic acid dihydrate and malonic acid] was taken in a 100 mL round bottom flask and added 15 mL ethyl acetate for fumaric acid and malonic acid, whereas 15 mL of ethanol added for oxalic acid dihydrate. These solutions were stirred for 4 h. Afterward, the solvent was evaporated using a rotary evaporator. ZLP and terephthalic acid

were taken in 2:1 stoichiometric ratio in a 100 mL round bottom flask, and water was added. This solution was refluxed for 4 h, and then water was evaporated by a rotary evaporator. A high vacuum was applied on these samples for 2 h to obtain a free-flowing powder.

4.2.3 Powder X-ray Diffraction (PXRD)

PXRD data were recorded on a Rigaku Ultima IV powder X-ray diffractometer using parallel beam geometry equipped with Cu K_α source, 2.5° primary and secondary soller slits, 5° in-plane divergence slit with 10 mm height limit slit, sample rotation stage (120 RPM) attachment and DTex Ultra detector. The data were collected over 2θ range 5°–50° with a scanning speed of 2° per minute with 0.02° steps.

4.2.4 Differential Scanning Calorimetry Analysis

The melting points and melting enthalpies of the ZLP and cocrystals were recorded on the Perkin-Elmer DSC-8000 instrument. All the samples (2-5 mg) were heated at a rate of 5 ˚C/min in sealed aluminum pans without the hole. The melting points, the fusion enthalpies, DSC traces of ZLP and the developed cocrystals have been reported in supporting information file (Figure S4.1 – S4.5 on page 26 – 27 in DVD attached).

4.2.5 Single Crystal X-ray Diffraction (SCXRD)

SCXRD experiments ZLP: fumaric acid, ZLP: malonic acid and ZLP: terephthalic acid were performed on a Bruker AXS KAPPA APEX-II CCD diffractometer (Monochromatic Mo Kα radiation). Unit cell determination, data collection (at room temperature), and data reduction were made using the Bruker APEX-III package.[125] SCXRD experiment of ZLP: oxalic acid was performed on Rigaku XtaLABmini X-ray diffractometer equipped with Mercury CCD detector with graphite monochromatic Mo-Kα radiation (λ = 0.71073 Å) at 100.0 (2) K using ω scans. The data were reduced using CrysAlisPro 41_64.93a software.[126] The crystal structures were solved using Olex^2 package[99] equipped with XT[100] and were further refined using XL.[101] Crystal packing and interaction diagrams were created using Mercury.[102] The details of the single-crystal X-ray diffraction data collection, structure solution and refinement are given in Table 4.3. Single crystals of ZLP: fumaric acid and ZLP: malonic acid cocrystals were obtained from ethyl acetate solution at 4 ˚C in the refrigerator. Single crystal of ZLP: terephthalic acid cocrystal was synthesized by dissolving the compound in water at 4 ˚C in the fridge. ZLP and Oxalic acid single crystal was made by slow evaporation from a solution in ethanol at low temperature in the refrigerator. Good quality single crystals were obtained within ten days.

4.2.6 Hirshfeld Surface Analysis

Hirshfeld surfaces and 2D fingerprint plots on the single crystal data of ZLP cocrystals were generated using Crystal Explorer 17.5 package as described in detail in Chapter 2, section 2.2.6.[103–105]

4.2.7 Determination of Partition Coefficient

Partition coefficients of ZLP and its all cocrystals were determined by the slow stirring method following the same procedure described in Chapter 2, section 2.2.8.[106]

4.2.8 Solubility Analysis

The saturation solution of the compounds determined the solubility of ZLP and all newly formed cocrystals. Firstly, calibration curves were drawn between absorbance *vs*. concentration for the drug ZLP and all the cocrystals by different known concentrations solutions using a UV-Vis spectrophotometer. 50 mg of compounds were taken in 5 mL of a vial, and 2 mL of PBS7 was added with a magnetic bead. These vials were stirred at 1500 rpm, 37 °C for 24h to determine saturation solubility. These solutions were centrifuged at 10000 RPM. We took supernatant solution and diluted it up to 10000 times with PBS7 to determine concentrations using UV−VIS spectroscopy.[127] Solubility of ZLP/cocrystals was calculated by multiplying these concentrations with dilution factor.

4.2.9 Intrinsic Dissolution Rate

Intrinsic dissolution rates were determined using USP certified Lab India 8000+ Dissolution Tester described in Chapter 2, Section 2.2.9.[109]

4.3 Results & Discussion

Zaleplon (pK_a = 0.3) is likely to form cocrystals with GRAS organic acids having pK_a ranging from 1.27 to 5.69. According to the ΔpK_a rule of 3,[50,110,111] when ΔpK_a of <1 means it creates a neutral cocrystal. This concept is also observed in the case of ZLP (Table 4.1). Cocrystal formation is detected in the case of all acids which are used as coformer.

Table 4.1: pKa and ΔpK_a values of ZLP and coformers used in this study.

Name	pK_a	ΔpK_a
Zaleplon	0.3	
Fumaric acid	3.03, 4.44	-2.73, -4.14
Terephthalic acid	3.51; 4.82	-3.21, -4.52
Oxalic acid	1.27; 4.28	-0.97, -3.98
Malonic acid	2.83. 5.69	-2.53, -5.39

4.3.1 Synthesis of Cocrystals

We have used several coformers (Succinic acid, Trimesic acid, Asparagine monohydrate, Fumaric acid, L-Tyrosine, Maleic acid, Terephthalic acid, Oxalic acid dihydrate, Malonic acid, Nicotinamide, Pimelic acid, Mandelic acid, L (-) Malic acid, Glutaric acid, DL-Tartaric acid, Citric acid, L (+) Ascorbic acid, Sorbic acid) to form cocrystals of ZLP. Still, most of them were ended with a physical mixture. There were only four new crystalline phases of ZLP with fumaric acid, terephthalic acid, oxalic acid and malonic acid were synthesized by solvent evaporation method and were identified by PXRD. These novel cocrystals were also characterized by DSC analysis. All these new complexes of ZLP indicated proper cocrystal formation and hydrogen bonding with hydrogen bond acceptor.

4.3.2 Powder X-ray Diffraction

New cocrystals of ZLP were prepared and their PXRD pattern is shown in Figure 4.2. It is evident from these PXRD patterns that the cocrystals formed by the solvent evaporation method resulted in a

new crystalline phase compared to the ZLP and the corresponding organic acid used in the experiment. These PXRD patterns also indicate that the new cocrystals were crystalline.

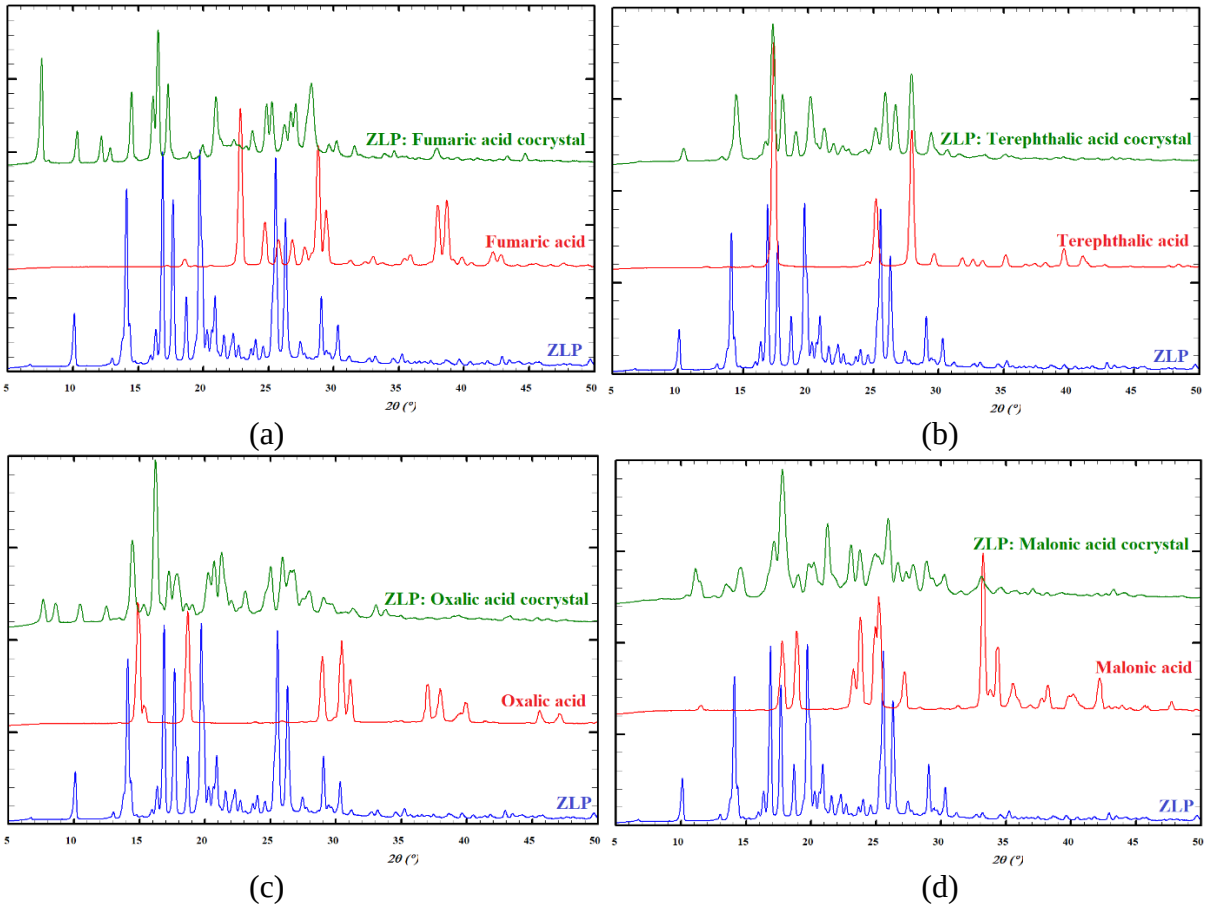

Figure 4.2: PXRD patterns of cocrystals of ZLP in comparison with LFX and coformers.

4.3.3 Thermal Analysis

The results of DSC thermograms for ZLP and all the cocrystals are provided in Table 4.2. These data on these phases show that the complexes have different melting/decomposition temperatures with respect to the parent drug, which further confirmed the development of new solid phases. The melting enthalpy of cocrystals was different from ZLP. The highest melting point was found for ZLP: terephthalic acid cocrystal. The lowest was found for ZLP: Malonic acid cocrystal, indicating ZLP: terephthalic acid cocrystal is the most stable solid phase.

Table 4.2: Melting points and melting enthalpies of ZLP and their cocrystals

Name	Melting Point of ZLP/Coformer (ºC)	Melting Point of ZLP Cocrystals (ºC)	Melting enthalpies (J/g)
ZLP	187		102.7
ZLP: Fumaric acid	287	163	72.8
ZLP: Terephthalic acid	300	186	81.1
ZLP: Oxalic acid	101	171	11.0
ZLP: Malonic acid	136	118	45.0

4.3.4 Single Crystal X-ray Analysis

We have grown four single crystals of ZLP with fumaric acid, terephthalic acid, oxalic acid and malonic acid. Structural parameters of these cocrystals are given in following Table 4.3. The cocrystal formation was confirmed through single crystal structural analysis. These single crystals reveal that cocrystal formation occurs by hydrogen bonding without transferring acidic proton to the drug molecule. These cocrystals are formed by O–H···O hydrogen bonding.

4.3.4.1 ZLP: Fumaric acid cocrystal

The asymmetric unit of ZLP: fumaric acid cocrystal has one molecule of ZLP and half molecule of fumaric acid. This is crystallized in monoclinic lattice with the $P2_1/c$ space group. The carboxylic acid of fumaric acid is connected to the carbonyl group of ZLP by O2–H2···O1 (1.722 Å) strong hydrogen bond shown in Figure 4.3a and formed a cocrystal. In the crystal packing, the ZLP molecule has been found to form a layer of drug molecule arranged anti-parallel by week hydrogen and van der Waals' interactions. This molecular sheet is interconnected on both sides by the layers of fumaric acid by strong and weak hydrogen bonding along the 'b' axis, as shown in Figure 4.3c. Two ZLP molecules are connected by C5–H5···O1 (2.680 Å) hydrogen bond, as shown in Figure 4.3b. All the hydrogen bonds present in this cocrystal are listed in Table 4.4.

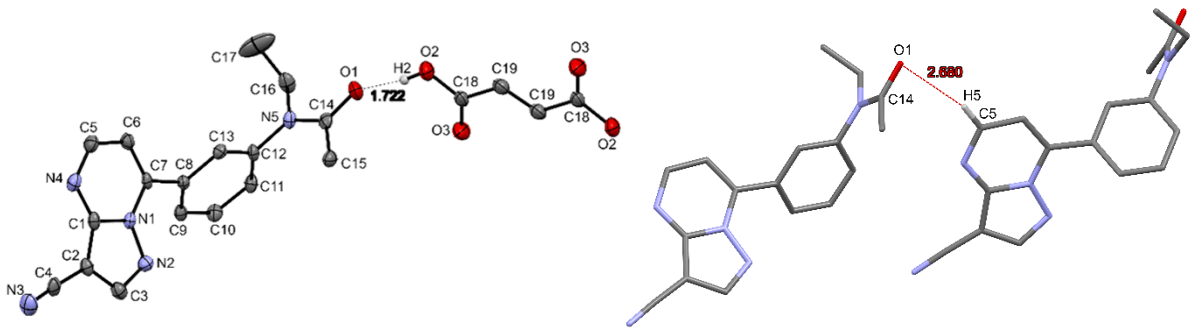

(a) (b)

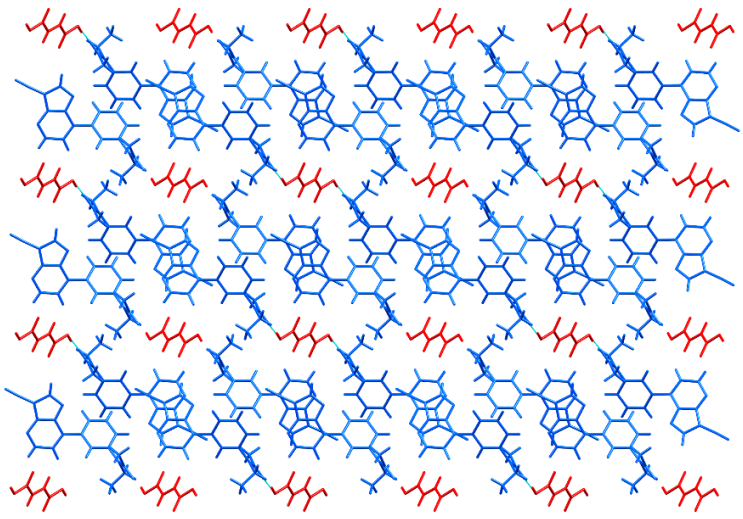

(c)

Figure 4.3: (a) Asymmetric unit of ZLP: fumaric acid salt; (b) Intermolecular interaction between ZLP molecules in a layer of ZLP; (c) Crystal packing diagram of ZLP: fumaric acid salt along 'b' axis.

Table 4.3: Crystallographic data of the cocrystals of zaleplon.

Data/Salt	**ZLP: Fumaric acid**	**ZLP: Terephthalic acid**	**ZLP: Oxalic acid**	**ZLP: Malonic acid**
Empirical formula	$(C_{17}H_{15}N_5O)$ $(C_2H_2O_2)$	$(C_{17}H_{15}N_5O)$ $(C_4H_3O_2)$ (H_2O)	$(C_{17}H_{15}N_5O)$ $0.5(C_2H_2O_4)$	$(C_{17}H_{15}N_5O)$ $0.5(C_3H_4O_4)$
CCDC number	2076774	2076775	2076776	2076777
Formula weight	363.38	406.42	350.36	357.37
Crystal system	Monoclinic	Triclinic	Monoclinic	Monoclinic
Space group	$P2_1/c$	$P\bar{1}$	$P2_1/c$	$C2/c$
a(Å)	12.200(9)	7.5409(2)	11.6224(15)	20.067(7)
b(Å)	7.190(5)	10.6961(3)	7.0816(9)	8.369(3)
c(Å)	20.566(15)	13.6463(4)	20.6760(18)	21.178(9)
α(°)	90	71.3720(10)	90	90
β(°)	91.938(17)	88.8010(10)	99.352(9)	101.624(18)
γ(°)	90	71.6030(10)	90	90
V(Å^3)	1803(2)	985.80(5)	1679.1(3)	3484(2)
Z	4	2	4	8
ρ_{calc}(g/cm^{-3})	1.339	1.369	1.386	1.363
Temperature (K)	100.0(2)	296.0(2)	100.0(2)	296.0(2)
μ/ mm^{-1}	0.094	0.098	0.098	0.096
$2\theta_{min,\ max}$ (°)	3.34 to 50.18	4.25 to 50.048	6.09 to 65.606	5.104 to 53.836
F (000)	760.0	426.0	732.0	1496.0
$h_{min,max}$; $k_{min,max}$; $l_{min,max}$	-14, 14; -8, 6; -24, 24	-8, 8; -12, 12; -16, 16	-17, 13; -10, 10; -31, 30	-24, 24; -10, 8; -13, 26
Total no. of reflections	10272	11050	19673	9005
R_{int}	0.0747	0.0192	0.0962	0.0447
No. of unique reflections	3200	3454	5877	3622
R_1 [I>2σ(I)]	0.0537	0.0501	0.0892	0.0520
wR2 (all data)	0.1339	0.1410	0.3053	0.1263
GooF on F^2	0.990	1.047	1.005	0.954
$\Delta\rho_{max,min}$/eÅ^{-3}	0.23/-0.28	0.51/-0.34	0.45/-0.32	0.21/-0.20

4.3.4.2. ZLP: Terephthalic acid cocrystal

The asymmetric unit of ZLP: terephthalic acid cocrystal has one molecule of ZLP, half molecule of terephthalic acid and one water molecule, as shown in Figure 4.4a. This was found to crystallize in triclinic lattice with $P\ \bar{1}$ space group. The carboxylic acid of terephthalic acid is hydrogen-bonded to water molecule O3–H3a···O2 (1.81 Å), which is further connected to the carbonyl group of ZLP molecule O2–H2a···O1 (2.00 Å) with hydrogen bond and the cocrystal is formed. ZLP molecules and terephthalic acid water channels formed alternative layers in crystal packing by (C–H···N and C–H···π) strong and weak hydrogen bonds, which provides stability to the cocrystal. All hydrogen bonding is given in Table 4.4.

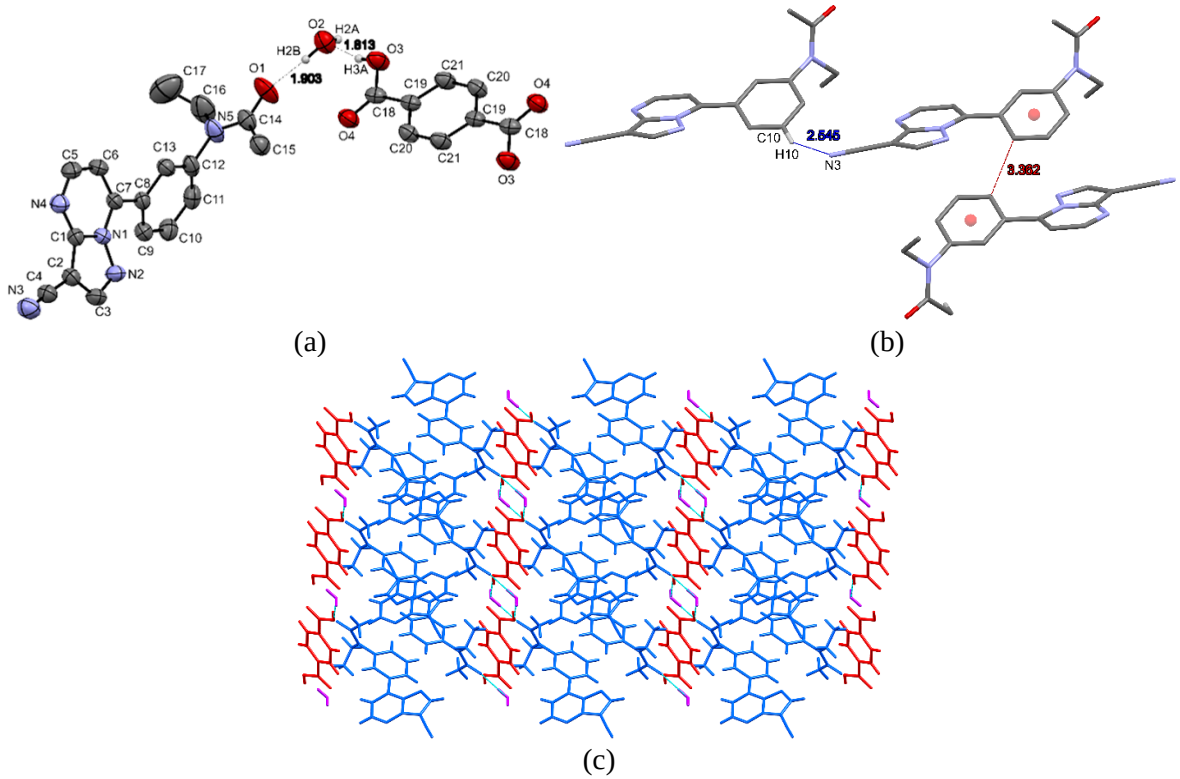

Figure 4.4: (a) Asymmetric unit of ZLP: terephthalic acid salt; (b) Intermolecular interaction between ZLP molecules in a layer of ZLP; (c) Crystal packing diagram of ZLP: terephthalic acid salt along 'b' axis.

4.3.4.3. ZLP: Oxalic acid cocrystal

One ZLP molecule and half molecule of oxalic acid are present in the asymmetric unit of ZLP: oxalic acid cocrystal, as shown in Figure 4.5a. The oxalic acid molecule is disordered and displayed in two parts. This cocrystal is crystallized in monoclinic lattice and $P2_1/c$ space group. Carboxylic group of oxalic acid is connected to the carbonyl oxygen of ZLP molecule via O2B–H2B···O3 (1.706 Å) strong hydrogen bonding to form ZLP: oxalic acid cocrystal. ZLP and oxalic acid formed alternate layers in crystal packing (Figure 4.5c). ZLP molecules interacted by (C–H···O, C–H···N and C–H···C) strong and weak hydrogen bonds with van der Waals' forces in a layer of ZLP (Figure 4.5b). These hydrogen bonds are tabulated in Table 4.4.

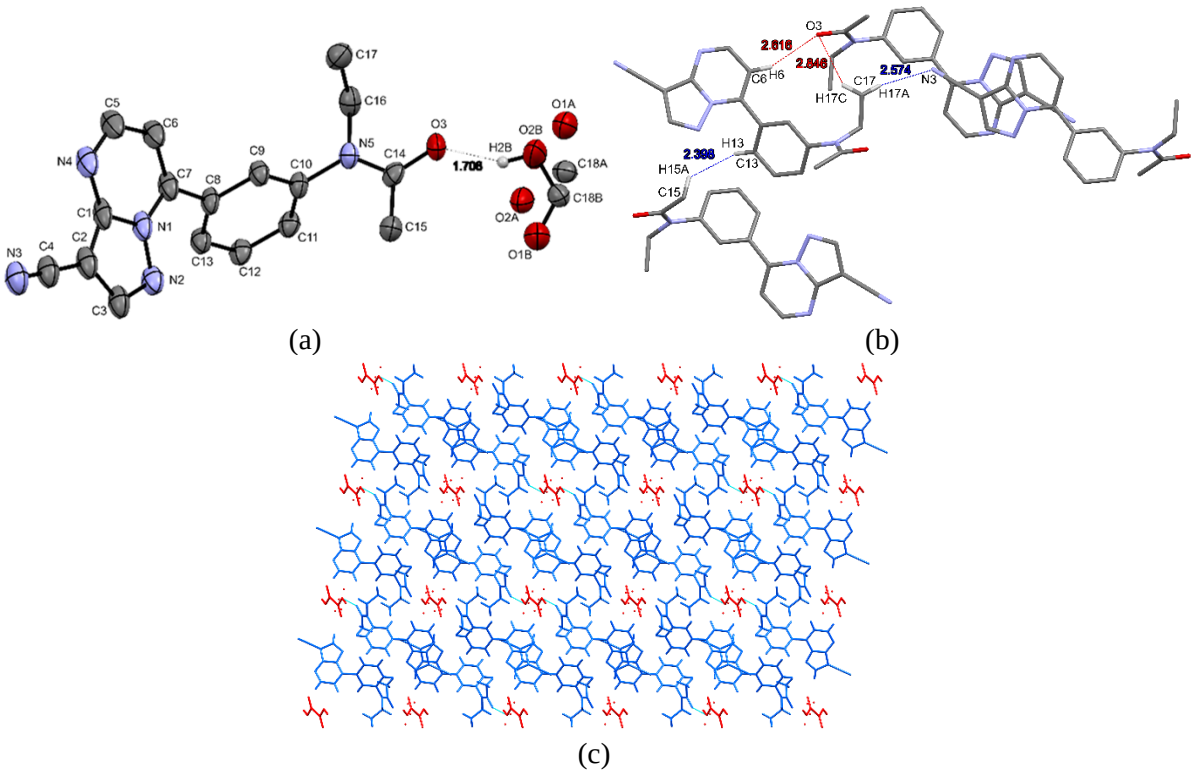

Figure 4.5: (a) Asymmetric unit of ZLP: oxalic acid salt; (b) Intermolecular interaction between ZLP molecules in a layer of ZLP; (c) Crystal packing diagram of ZLP: oxalic acid salt along 'b' axis.

4.3.4.4 ZLP: Malonic acid cocrystal

This cocrystal contains one ZLP molecule and half malonic acid molecule in the asymmetric unit of ZLP: malonic acid cocrystal, as displayed in Figure 4.6a. This ZLP cocrystal is cocrystallized with malonic acid in a monoclinic lattice with a *C*2/c space group. This cocrystal is formed by hydrogen bonding O2–H2···O1 (1.783 Å) between carboxylic acid of malonic acid and the carbonyl group of ZLP molecules. In crystal packing, ZLP and malonic acid are connected in V shape due to the bent structure of malonic acid and formed layers of ZLP molecules and malonic acid channel (Figure 4.6c). ZLP molecules are connected by C–H···N and C–H···O hydrogen bonds and van der Waals' forces in a layer as depicted in Figure 4.6b. All the hydrogen bonds with symmetry elements are listed in Table 4.4.

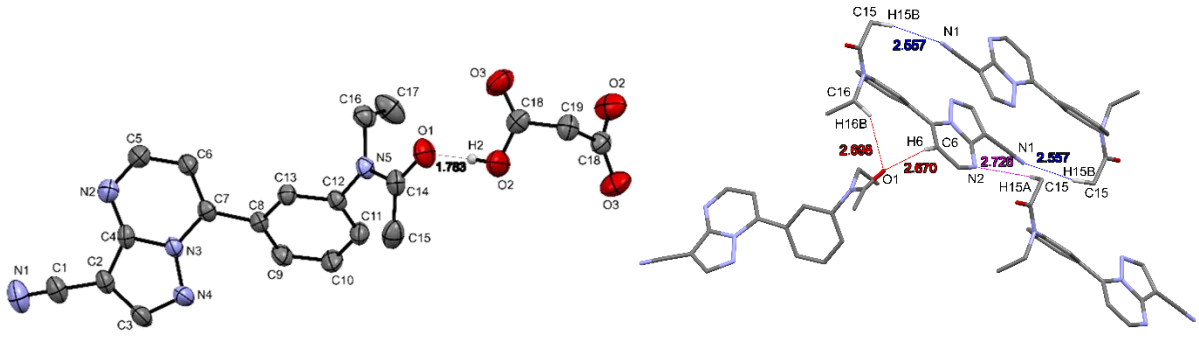

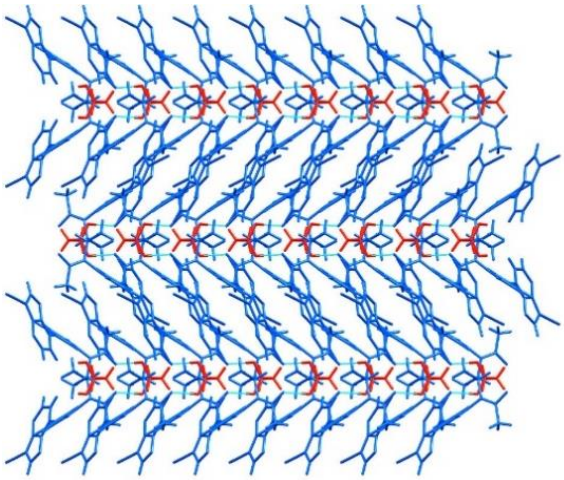

(c)

Figure 4.6: (a) Asymmetric unit of ZLP: malonic acid salt; (b) Intermolecular interaction between ZLP molecules in a layer of ZLP; (c) Crystal packing diagram of ZLP: malonic acid salt along 'a' axis.

We have compared the simulated PXRD pattern from single-crystal X-ray diffraction data to the experimentally recorded PXRD pattern, as shown in Figure 4.7. The simulated PXRD patterns matched with the recorded PXRD pattern of ZLP: fumaric acid, ZLP: oxalic acid and ZLP: malonic acid cocrystals. The simulated PXRD pattern of ZLP: terephthalic acid is different from the recorded one because a single crystal has a water molecule in the crystal lattice.

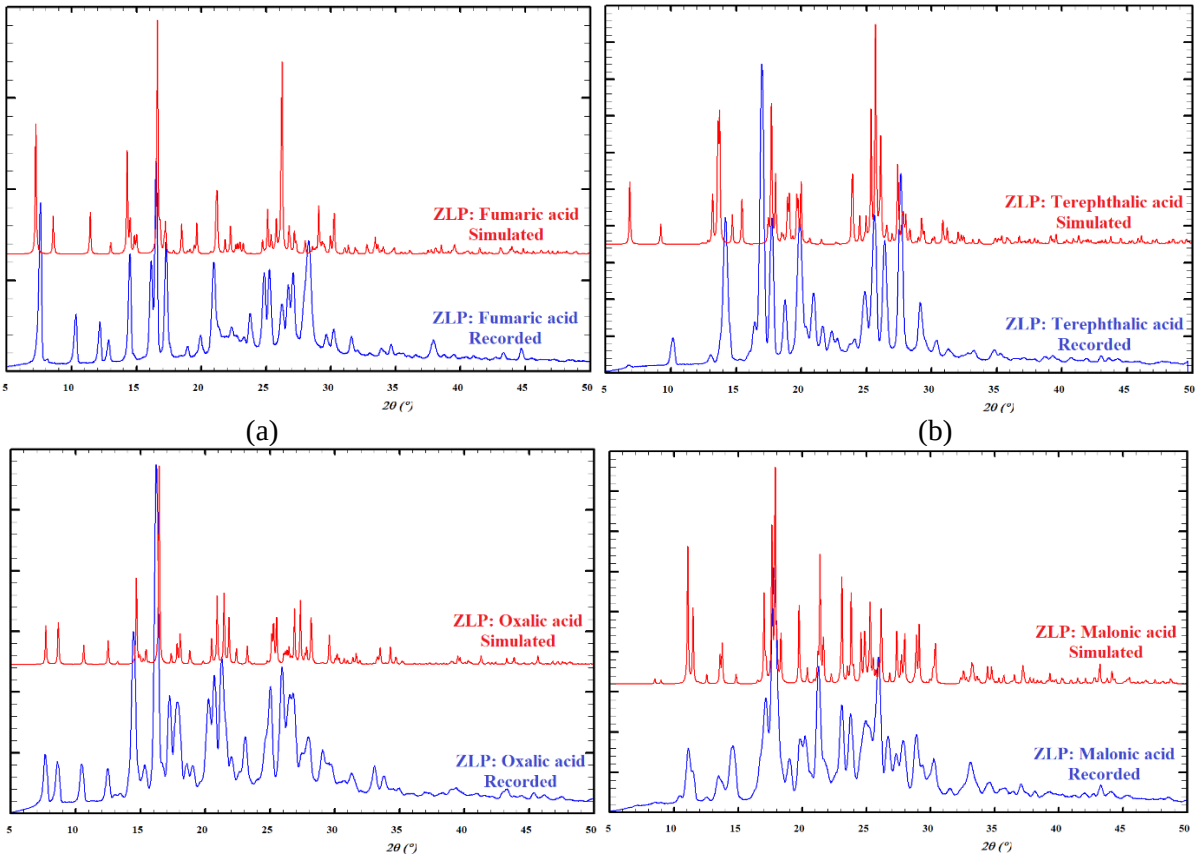

Figure 4.7: Comparisons of PXRD patterns recorded from powdered samples and simulated from single-crystal X-ray diffraction data.

Table 4.4. Hydrogen bond geometry parameters in ZLP cocrystals.

Salts	Interactions	D–H (Å)	H···A (Å)	D···A (Å)	D–H···A (°)	Symmetry code
ZLP: Fumaric acid	O2–H2···O1	0.84	1.72	2.556(4)	172	x, y, z
	C3–H3···O3	0.95	2.39	3.156(4)	137	1-x, y-½, 3/2-z
	C6–H6···O2	0.95	2.56	3.359(4)	142	2-x, y-½, 3/2-z
	C9–H9···N2	0.95	2.57	2.950(4)	104	x, y, z
	C16–H16B···O1	0.99	2.28	2.670(4)	102	x, y, z
ZLP: Terephthalic acid	O2–H2A···O1	0.82(4)	2.00(4)	2.815(3)	176(4)	1-x, 2-y, -z
	O2–H2B···O1	0.89(4)	1.90(4)	2.770(3)	164(4)	1+x, y, z
	O3–H3A···O2	0.82	1.81	2.611(3)	164	x, y, z
	C5–H5···O3	0.93	2.57	3.386(3)	147	2-x, 1-y, -z
	C6–H6···O4	0.93	2.52	3.436(3)	170	x, y, z
	C9–H9···N2	0.93	2.34	2.880(3)	117	x, y, z
	C10–H10···N3	0.93	2.55	3.376(4)	149	-1+x, 1+y, z
	C16–H16A···O1	0.97	2.33	7.736(4)	104	x, y, z
ZLP: Oxalic acid	O2B–H2B···O3	0.84	1.71	2.487(6)	153	-x, -½+y, ½-z
	C3–H3···O1B	0.95	2.16	3.099(6)	169	1+x, y, z
	C17–H17A···N3	0.98	2.57	3.441(5)	147	-1+x, ½-y, -½+z
ZLP: Malonic acid	O2–H2···O1	0.82	1.78	2.586(3)	166	3/2-x, ½+y, 3/2-z
	C3–H3···O2	0.93	2.59	3.375(3)	143	x, 1-y, -½+z
	C9–H9···N4	0.93	2.54	2.975(3)	109	x, y, z
	C13–H13···O3	0.93	2.34	3.258(3)	169	x, y, z
	C15–H15B···N1	0.96	2.56	3.441(4)	153	1-x,1-y,1-z
	C16–H16A···O1	0.96	2.33	2.719(3)	103	x, y, z

4.3.5 Hirshfeld Surface Analysis

Hirshfeld surfaces (HSs) are generated from the single-crystal structures to analyze the surface interactions between ZLP and surrounding molecules, as shown in Figure 4.8. The Carbonyl group of ZLP offers a strong hydrogen bond with the carboxylic acid of fumaric acid, oxalic acid and malonic acid (Figure 4.8a, 4.8c, 4.8d). In contrast, terephthalic acid is connected through one water molecule (Figure 4.8b). These interactions of corresponding acid molecules with ZLP molecules are shown in red color in the constructed Hirshfeld surface of ZLP molecules. This interaction is strong and directional, which is evident in the fingerprint plots of these cocrystals showing sharp peaks (all fingerprint plots for all four cocrystals are displayed in Supporting file Figure S4.6 – S4.9 on page 28 - 31 with enclosed DVD. Mostly the HSs interactions are present through hydrogen atoms inside and outside of HSs, which shows the highest interaction percentage in surface interaction (Figure S4.10 on

page 31 – 32 in Supporting file with enclosed DVD), which support the presence of O–H···O, C–H···O, C–H···N and C–H···C strong and weak hydrogen bonds in crystal packing.

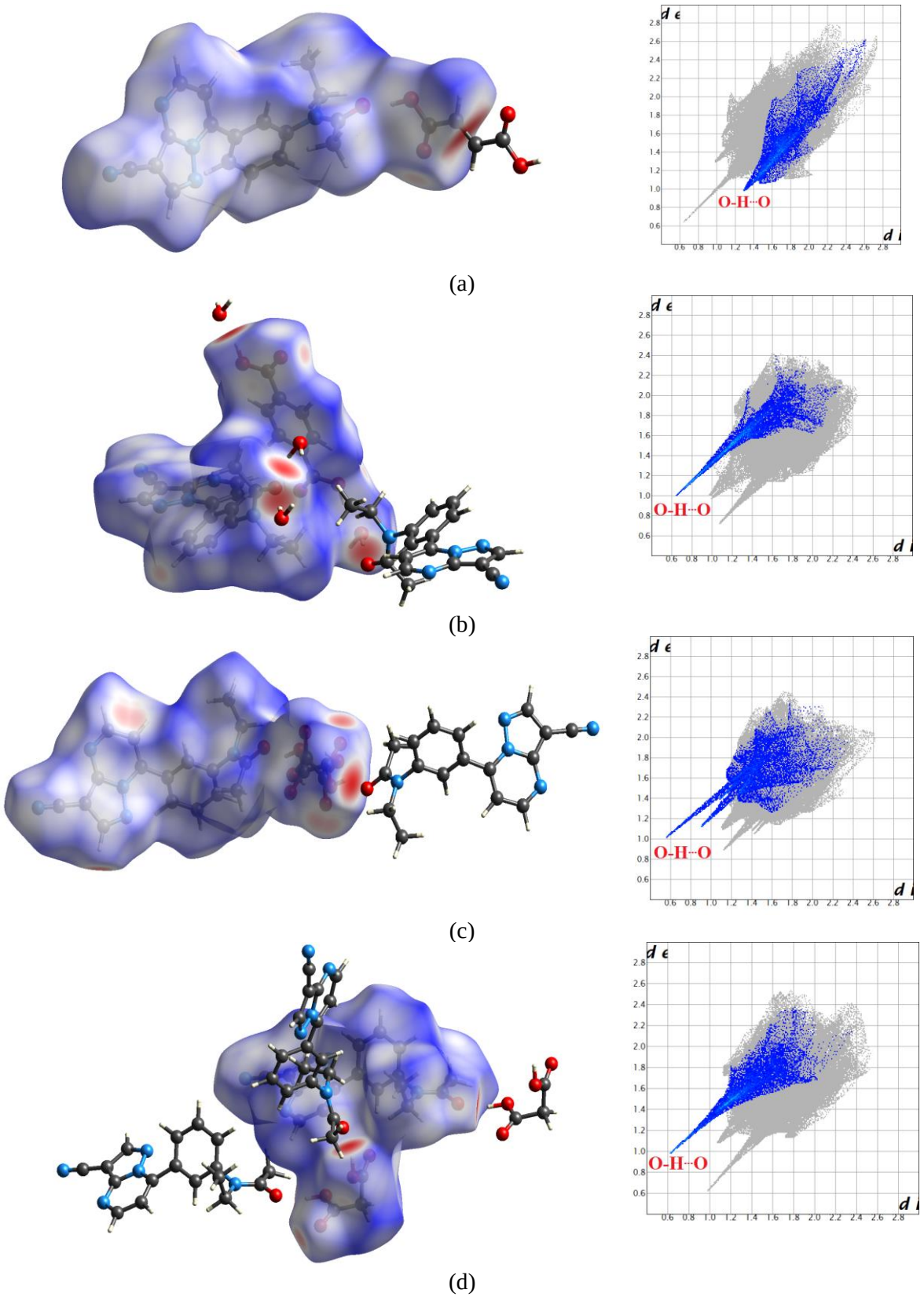

(a)

(b)

(c)

(d)

Figure 4.8. Hirshfeld surfaces and fingerprint plot of (a) ZLP: Fumaric acid cocrystal; (b) ZLP: Terephthalic acid cocrystal; (c) ZLP: Oxalic acid cocrystal, and (d) ZLP: Malonic acid cocrystal.

4.3.6 Partition Coefficient

The partition coefficient of ZLP and all cocrystals are determined and listed in Table 4.5. The $log_{10}P$ value of ZLP is found 1.01, which is higher than all the cocrystals, which indicates the hydrophilic nature of ZLP cocrystals. This value supports the higher solubility of new cocrystals. The highest $log_{10}P$ value is found for ZLP: oxalic acid cocrystal, and the lowest is found for ZLP: terephthalic acid cocrystal. These results show that these cocrystals would dissolve faster in oral drug delivery in comparison to pure ZLP.

Table 4.5 Partition coefficient of ZLP and its cocrystals.

Name	$log_{10}P$
ZLP	1.01
ZLP: Fumaric acid	0.58
ZLP: Terephthalic acid	0.27
ZLP: Oxalic acid	0.92
ZLP: Malonic acid	0.89

4.3.7. Solubility Studies

The new compounds' water saturation solubility and ZLP were determined in phosphate buffer solution at pH 7 and 37 ˚C (listed in Table 4.6). Associated calibration curves and UV-Vis spectra are provided as a supporting information [Figure S4.11 – S4.15 on page 33 – 35] in the enclosed DVD. The saturation solubility of the cocrystals of ZLP was found to be greater than pure drug ZLP, which is improved by 2.8 to 18.8 times. Maximum water solubility was seen for ZLP: malonic acid cocrystal (8.24 mg/ mL), and the minimum was seen for ZLP: terephthalic acid cocrystal (1.23 mg/ mL). This improved solubility may result from alternate layers of ZLP and conformer formed in the crystal packing of the cocrystals.

Table 4.6: Solubility of ZLP and its cocrystals.

Name	Solubility (mg / mL)
ZLP	0.44
ZLP: Fumaric acid	7.48
ZLP: Terephthalic acid	1.23
ZLP: Oxalic acid	3.58
ZLP: Malonic acid	8.24

4.3.8. Intrinsic Dissolution Rate Analysis

IDR analyses were done for ZLP and newly formed cocrystals in PBS7 at 37 ^{o}C. The IDR increased for all cocrystals and has been found 1.09 to 4.41 times faster dissolution rate. Therefore, these cocrystals of ZLP could be used in place of the ZLP for future formulations. These were found to be more stable in ambient air and not sensitive to moisture. Therefore, the pallets of these salts could

be made easily for IDR analysis. The intrinsic dissolution rate for the parent drug and the cocrystals is given in Table 4.7. ZLP: fumaric acid cocrystal has maximum IDR 0.123 mg $min^{-1}cm^{-2}$ which is highest than ZLP 0.028 mg $min^{-1}cm^{-2}$.

Table 4.7: IDR of ZLP and its cocrystals.

Name	IDR (mg / mL / cm^{-1})
ZLP	0.028
ZLP: Fumaric acid	0.123
ZLP: Terephthalic acid	0.036
ZLP: Oxalic acid	0.049
ZLP: Malonic acid	0.030

4.4 Conclusion

Zaleplon (ZLP) is a hypnotic drug used in the treatment of insomnia. It has low water solubility, which is why this suffers from a low intrinsic dissolution rate (IDR) and lower bioavailability. We have developed new cocrystals of zaleplon with naturally occurring and biologically safe organic acid molecules by a solvent evaporation method, which was successfully characterized by PXRD and DSC. We have demonstrated the formation of a novel crystalline phase, and the single-crystal X-ray diffraction analysis of these cocrystals confirmed the composition. Cocrystals of ZLP with various acids have been found to have strong hydrogen bonds between ZLP, acid and water molecules, and the Hirshfeld study supported these interactions. Crystal packing of these cocrystals has shown the formation of alternate layers of ZLP and acid/acid-water channel, which may be the reason for improved physicochemical characters of new cocrystals. These novel cocrystals are more hydrophilic than ZLP as per partition coefficient and indicated up to 19 times enhancement in solubility in PBS7 at 37 ^{o}C. The intrinsic dissolution rate study establishes that these cocrystals have significantly higher dissolution rates compared to the parent drug. These cocrystals are the better alternative to pure drug ZLP with improved solubility and IDR to treat insomnia. These cocrystals may be further taken up for an *in-vivo* biological study on mice, and subsequently, the human trial may be conducted in the future.

PART-II

Antibiotic Drugs

Chapter 5

Salts of Ofloxacin with Improved Solubility for Enhanced Pharmaceutical Applicability: In-vitro Biological Studies

Chapter 5

5.1 Introduction

Ofloxacin (OFX) is a synthetic, broad-spectrum antibiotic of the second-generation fluoroquinolone class of antibiotic drugs.[146] OFX is a racemic mixture of 50% of (*S*)-9-fluoro-2,3-dihydro-3-methyl-10-(4-methylpiperazin-1-yl)-7-oxo-7H-pyrido[1,2,3-de]-1,4-benzoxazine-6-carboxylicacid (commonly known as levofloxacin) and 50% of its *R* isomer, (as shown in Figure 5.1).[147] It targets inhibition of the bacterial enzyme DNA gyrase and DNA topoisomerase IV.[148,149] Crystal structures of OFX was reported in the literature.[150] It contains one carboxylic group with the pK_a value of 5.97 and one basic site piperazine ring with pK_a 9.28 as listed in Table 5.1.[151] OFX is used against both gram-positive and gram-negative bacteria effectively.[152] In general, fluoroquinolones are extensively used to treat and prevent various infectious diseases like nongonococcal urethritis,[153] cervicitis,[154] chronic bronchitis,[155] atypical pneumonia,[156] tuberculosis,[157] leprosy,[158] pelvic inflammatory diseases,[159] chlamydia,[160] gonorrhoea[161] etc. Some of the fluoroquinolone antibiotics are known to cause serious side effects that may be irreversible. High or extended use of OFX causes serious side effects, including tendon problems, nerve damage, serious mood or behavior fluctuations, low blood sugar, headache, hunger, irritations, numbness, tingling, burning pain, confusion, agitation, paranoia, thoughts of suicide and sudden pain. In rare cases, OFX may damage the aorta, which could lead to dangerous bleeding or death.[162–164]

The poor solubility, low intrinsic dissolution rate (IDR), poor thermal stability, and fast moisture intake property of API influence the therapeutic efficacy of pharmaceuticals and their market value.[165,166] OFX is one such drug that is poorly soluble in water (3.4 mg/ mL) and has very low IDR ($0.19\ mg\ min^{-1}\ cm^{-2}$) in phosphate buffer solution at pH = 7 in pellet form. Consequently, numerous attempts have been made to improve the aqueous solubility and dissolution rate of such drugs. The early attempts included the complexation of the drug with water-soluble substances such as cyclodextrins,

emulsions, micelle formation, solid dispersions, solid-state alteration and pharmaceutical salts and cocrystallization.[167,168]

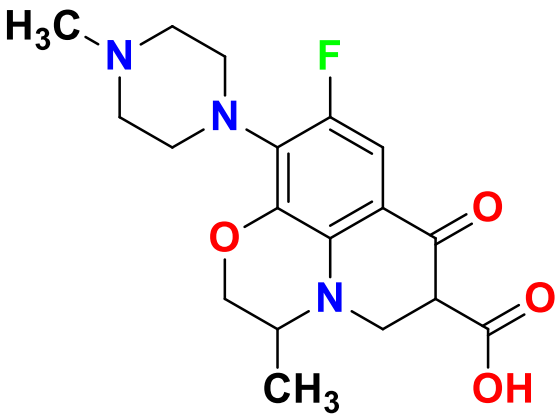

Figure 5.1: Chemical Structure of Ofloxacin.

Recently, pharmaceutical cocrystals received immense importance because they have been found to modify the solubility and bioavailability of the APIs.[169] The inherent change in physicochemical properties due to the introduction of another component into the crystal lattice and the existence of supramolecular synthons affords many potential applications of cocrystals.

We have used gram-negative bacteria *E. Coli* (anaerobic, coliform) and *S. Typhimurium* (facultative aerobic, flagellate) for our studies on the salts of OFX in this manuscript. *E. Coli* usually are found in the lower intestine of warm-blooded organisms like healthy humans and animals. Most varieties of *E. Coli* are commensal in humans and are harmless or help in digestion. But a few strains, such as *E. Coli* O157:H7, are pathogenic and can cause severe abdominal cramps, bloody diarrhea and vomiting.[170] *S. Typhimurium* causes salmonellosis in humans and food animals. This is characterized by fever, acute intestinal inflammation, and diarrhea after 24 h of infection.[171] In this chapter, we have studied the minimum inhibitory concentration (MIC) of our novel salts of OFX on these two bacteria.

We have made an effort to enhance the solubility, IDR, and MIC of various solid forms of OFX using simple organic biologically acceptable acids. Herein, we report the synthesis of five new salts of OFX using solvent drop assisted grinding method, their characterization using PXRD and differential scanning calorimetry (DSC) methods. We have determined the partition coefficient to detect the nature of the salt towards the water. Their saturation solubility determination and IDR analysis to establish the enhancement of solubility and rate of dissolution in phosphate buffer solution at pH 7 and MIC to analyze its potency on bacteria.

5.2 Experimental Section

5.2.1 Materials

Ofloxacin (99% pure), adipic acid (99.5% purity) and pimelic acid (98% purity) were purchased from Sigma-Aldrich Co. Citric acid (99.7% purity), L-malic acid (99.5% purity), malonic acid (99% purity), Di-sodium hydrogen phosphate anhydrous (99% purity) and potassium dihydrogen phosphate anhydrous (99% purity) were bought from Hi-media laboratories Pvt. Ltd. Methanol (99.9% purity)

was procured from Merck, Millipore Corporation. Luria Bertani (LB) broth was purchased from Himedia Laboratories Pvt. Ltd., India and Brain Heart Infusion (BHI) broth was obtained from Sigma Aldrich, U.S.A.

5.2.2 Solvent Drop Grinding Method

The salts of OFX were synthesized by the solvent drop-assisted grinding method. An equimolar mixture of the OFX and the cocrystal former (one among citric acid, malonic acid, L-malic acid, pimelic acid, and adipic acid) was taken by accurate weighing, and 50-100 μL of methanol was added to the mixture using a micropipette. The slurry was ground in agate mortar and pestle till the solvent was evaporated to leave a dry powder. This process was repeated six to eight times till a new single-phase was obtained. Powder X-ray diffraction data were recorded after every step of grinding with solvent drop till a new single-phase (identified by the disappearance of the peaks of the ingredients and appearance of new peaks) was confirmed. The new phase of these salts was determined and characterized by the PXRD and DSC methods. We have set up crystallization assembly by dissolving these salts in different solvents in different combinations, but we could not grow a suitable single crystal to determine its structure by SCXRD.

5.2.3 Powder X-ray Diffraction

PXRD data were recorded on a Rigaku Ultima IV X-ray diffractometer using parallel beam geometry equipped with a Cu K_α radiation, 2.5° primary and secondary solar slits, 5° in-plane divergence slit with 10 mm height limit slit, with sample rotation stage (120 rpm) attachment and DTex Ultra detector. The data were collected over 2θ range 5° – 50° in 2θ with a scanning speed of 2° per minute with 0.02° steps.

5.2.4 Thermal Analysis

Perkin-Elmer DSC-8000 determined the melting points and melting enthalpy of the OFX and its complexes. All the samples (2-5 mg) were heated at 5° C/min heating rate in sealed aluminum pans (Table 3). The DSC traces are reported in the DSC thermograms in supporting information (Figure S5.1 – S5.6 on page 36 – 37) document in the enclosed DVD.

5.2.5 Partition Coefficient

Partition coefficients of OFX and its salts were determined by the slow stirring method. In a conical flask, 10 mL of PBS7 and 10 mL n-octanol were added, and 10 mg of the OFX and its salts were added to the corresponding flask. Each conical flask was stirred at a slow rate (300 RPM) for 24h. A separating funnel separated both phases. These phases were diluted 100 times by corresponding solvents, and the absorbance was determined by UV-Vis spectrophotometry.[106] Concentration of OFX in each phase was calculated by fitting this value in calibration curve, and partition coefficient (P) was calculated using the following formula and hence the value of $log_{10}P$ was calculated.

$$\mathrm{P} = \frac{Concentration\ of\ drug\ in\ octanol}{Concentration\ of\ drug\ in\ PBS7}$$

5.2.6 Solubility Analysis

The use of a UV-VIS spectrophotometer determined the solubility of OFX and its salts. We have drawn the calibration curves between absorption versus known concentrations of the OFX and newly formed salts in PBS7 at their respective λ_{max}. We prepared saturated solutions of pure OFX and all OFX salts by stirring (1500 rpm for 24 h) an excessive amount of the compound in 2 mL of phosphate buffer solution at pH 7 in 5 mL sealed vials at 37 °C. These solutions were then centrifuged at 10000 rpm for 15 min, and the supernatant solution was diluted 10000 times using phosphate buffer solution at pH 7. The absorbance of the diluted solution was measured at respective λ_{max} of salts, and the concentration of the OFX and salts were determined using the calibration curves. The solubility was calculated by multiplying the concentration with the dilution factor.

5.2.7 Determination of Intrinsic Dissolution Rate

Intrinsic dissolution experiments were carried out on a USP-certified Lab India 8000+ Dissolution tester. 100 mg of the solid (drug/salt) was taken in the intrinsic attachment and compressed to a 3.288 cm^2 pellet using a hydraulic KBr press at a pressure of 2 ton/$inch^2$ for two minutes. The pellet was compressed to provide a flat surface. Then, the pellet was dipped into 1 L of PBS7 warmed at 37 °C, with the paddle rotating at 75 rpm. At a regular interval, 5mL portions of the dissolution medium were withdrawn and replaced by an equal volume of fresh medium to maintain a constant volume. The amount of drug dissolved in each time interval was calculated using the calibration curve. The linear region of the dissolution profile was used to determine the IDR of the compounds. The same was done for up to 120 minutes. The samples collected after each interval was diluted 10 times with PBS7 for UV-Vis spectroscopy study. The solutions were filtered through a 0.25 μm syringe filter before UV-Vis spectroscopic analysis. The drug concentration at each interval was calculated using a calibration curve and plotted against time.[172] The linear region of the dissolution profile was used to determine the intrinsic dissolution rate (IDR) of the OFX and its salts.[106]

5.2.8 Minimum Inhibitory Concentration

Salt of OFX and OFX was dissolved in sterile water at a concentration of 50 mg/L. These were then diluted to various concentrations at double their strength (DS-D). *Escherichia Coli* and *Salmonella Typhimurium* were grown in Luria Bertani (LB) broth overnight at 37 ˚C. The culture was then diluted in 0.85 % NaCl solution to a McFarland turbidity of 0.5 (equivalent to OD_{600} =0.132). This culture was further diluted at 1:50 in 10 mL of double-strength Brain Heart Infusion (BHI) broth (DS-B). Additionally, 100 μL each of DS-D and DS-B was added to a well in a 96-well plate. After 48 h of incubation at 37 ˚C, OD_{600} was measured using a plate reader (Bio-Rad, U.S.A.). The dilution at which the OD_{600} was observed to be comparable to blank, was taken as the MIC for the derivative.[173]

5.3 Results and Discussion

OFX salts are made with the GRAS coformers, which were selected based on the ΔpK_a [$(pK_a)_{base} - (pK_a)_{acid}$] rule of three. This rule rationalizes the selection of the molecules based on the difference in pK_a values. If $\Delta pK_a > 3$, it is expected that the base (drug molecule in the current experiment) will form

a salt with the co-former (acid), whereas if is $\Delta pK_a < 1$, cocrystal formation is expected and if $1 < \Delta pK_a < 3$, an intermediate location of the proton is envisaged.[49] The pK_a and ΔpK_a values of OFX and coformers used in this study are listed in Table 5.1.

Table 5.1: pK_a values of OFX and Coformer with Structures.

Name	pK_a	ΔpK_a
Ofloxacin	5.67 (carboxylic acid), 9.28 (>N-Me group)	
Citric acid	3.13, 4.76, 6.39	6.15, 4.52, 2.89
Malonic acid	2.83, 5.69	6.45, 3.59
L-Malic acid	3.40, 5.20	5.88, 4.08
Pimelic acid	4.51, 5.58	4.77, 3.70
Adipic acid	4.43, 5.41	4.85, 3.87

We have prepared five novel salts of OFX with a rational approach of ΔpK_a rule of three. Here, we took citric acid, malonic acid, L-malic acid, pimelic acid, and adipic acid to form salts with OFX in a 1:1 stoichiometric ratio. Their ΔpK_a values range from 2.89 to 6.45 (in Table 5.1), which means the probability of salt formation is higher than cocrystals. All the salts are prepared by solvent drop assisted grinding method, and a new solid phase is generated, characterized by following procedures like PXRD and DSC.

5.3.1 Powder and single-crystal X-ray Diffraction Analysis

The PXRD patterns of the new salts of OFX are provided in Figure 5.2. The comparison of PXRD patterns of OFX, the corresponding coformer and the salt thus formed are shown. It is evident from the PXRD patterns that new crystalline phases had been created by the solvent drop-assisted grinding method. These salts were significantly more soluble in water than the pure drug. Recrystallization of these salts for single-crystal X-ray diffraction analysis was attempted numerous times using water and a mixture of water-methanol, water-ethanol, water-acetone etc., as a solvent and using a slow evaporation process. Unfortunately, we were unable to grow any single crystal of these salts. All the crystallization experiments resulted in fine polycrystalline powder, which resembled (confirmed by PXRD) the crude product (before recrystallization) obtained after solvent drop grinding.

5.3.2 Thermal Analysis

The DSC thermograms of antibiotic drug OFX and their newly synthesized salts have been recorded and analyzed for new crystalline phases. These thermograms indicate these salts' entirely different melting points than the pure API (270 °C) and their corresponding acids, as shown in Table 5.2, which indicated that a new solid phase was formed during the grinding process. The melting points of OFX salts range from 114 °C (lowest for OFX-Pimelic acid salt) to 196 °C (highest for OFX-L-Malic acid salt), which are lower in melting/decomposition temperature than pure drug OFX (270 °C). Among these salts, OFX-Pimelic acid has the lowest melting enthalpy (39.42 J/g), whereas OFX-Citric acid salt (355.22 J/g) has the highest.

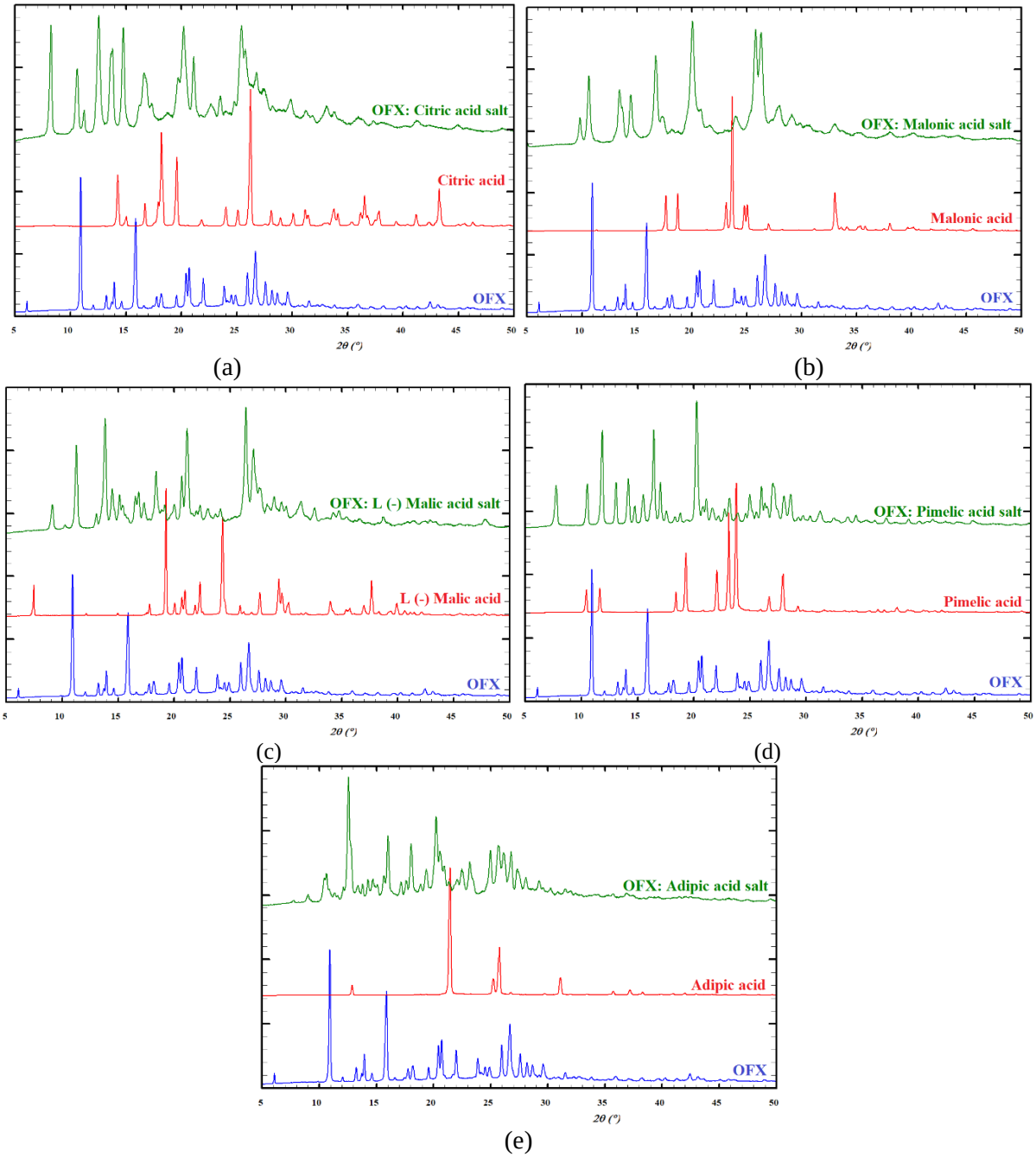

Figure 5.2: PXRD patterns of salts of OFX in comparison with LFX and coformers.

Table 5.2: Melting points and melting enthalpies of OFX and their salts.

Name of API and coformers	Melting Point of OFX and coformers (°C)	Melting Point of Salts of OFX (°C)	Melting enthalpy (J/g)
Ofloxacin	270	-	176.06
Citric acid	153	174	355.22
Malonic acid	135	154	51.42
L-Malic acid	131	196	159.21
Pimelic acid	106	114	39.42
Adipic acid	152	163	98.91

5.3.3 Partition Coefficient

We have determined the partition coefficient for OFX and all newly developed salts in PBS7 and n-octanol. We found all the salts have lower $log_{10}P$ value than pure drug OFX, which indicates the more hydrophilicity of the salts than the pure drug. OFX: citric acid salt has shown the highest negative $log_{10}P$ value -0.67, as shown in Table 5.3.

Table 5.3: Partition coefficient of OFX and all salts of OFX.

Name	$log_{10}P$
OFX	-0.51
OFX: Citric acid	-0.67
OFX: Malonic acid	-0.57
OFX: L-Malic acid	-0.57
OFX: Pimelic acid	-0.55

5.3.4 Solubility Studies

The solubility of OFX in phosphate buffer solution pH 7 at 37 ˚C was 3.44 mg / mL. Some physical and biological parameters like IDR and bioavailability are associated with solubility. This poor solubility restricts the pharmacokinetic and pharmacodynamic parameters of the antibiotic drug OFX. The solubility of OFX and its salts were measured after 24 h with continuous stirring in PBS7 at 37 ˚C with the excess amount of compound. The solubility of the salts was determined by drawing a calibration curve using the UV-visible spectrophotometric technique (Given in Supporting file in Figure S5.7 – S5.12 on page 38 – 39 with enclosed DVD). The saturation solubility of the OFX and its salts are listed in Table 5.4.

Table 5.4: Saturation Solubility Data of OFX and all salts in PBS7 at 37 ˚C.

Name	Solubility (mg/mL)
OFX	3.44
OFX: Citric acid	35.64
OFX: Malonic acid	44.53
OFX: L-Malic acid	65.84
OFX: Pimelic acid	53.57
OFX: Adipic acid	72.59

It is evident from Table 5.4 that the solubility of OFX has been altered by 10.4−21.1 times for its salts. The highest solubility is observed in adipic acid salt (72.59 mg/mL) and the lowest in citrate salt (35.64 mg/mL). These salts indicated a significant increase in solubility, and hence these salts were processed for IDR analysis and MIC determination.

5.3.5 Intrinsic Dissolution Rate Analysis

The IDR experiment was performed on these newly formed water-soluble salts in PBS7 at 37 ˚C. The results indicated that the salts of OFX with citric acid, malonic acid, L-malic acid, pimelic acid and adipic acid have enormous enrichment in intrinsic dissolution rate with is at least 21.1 times for pimelic acid salt (3.96 mg min^{-1} cm^{-1}) than the parent drug OFX (0.19 mg min^{-1} cm^{-1}). Therefore, these salts of

OFX could potentially be used in place of the parent drug for future formulations. These salts were found to be stable in ambient air and were not sensitive to moisture. Therefore, the pellet of these compounds could be made easily for IDR analysis. The intrinsic dissolution rate for the original drug and its salts are given in Table 5.5.

Table 5.5: IDR data of OFX and their salts at 37 ˚C in PBS7.

Name	IDR (j) (mg min^{-1} cm^{-2})
OFX	0.19
OFX: Citric acid	4.37
OFX: Malonic acid	8.04
OFX: L-Malic acid	4.56
OFX: Pimelic acid	3.96
OFX: Adipic acid	4.21

It is evident from Table 5.5 that IDR has improved 21.1 to 42.9 times for salts of OFX than pure drug OFX. This data indicates that these salts can be used for formulation in such a way that these salts will reach the bloodstream in a few seconds and can act on bacterial infection much faster than pure OFX. Highest IDR was achieved in malonic acid salt (8.04 mg min^{-1} cm^{-1}) of OFX. These salts have higher solubility and IDR with respect to pure drug; therefore, this salt could be a potent drug candidate for dispersal as a tablet formulation.

5.3.6 Minimum Inhibitory Concentration

MIC results are shown in Table 5.6. MIC data for *E. Coli* is slightly higher for all salts except pimelic acid salt of OFX (6.64×10^{-5} mmol / L) than OFX. So, this can be used in bacterial infection (because this is highly soluble as well).

Table 5.6: MIC data of OFX and its salts in *E. Coli* and *S. Typhimurium.*

Name	*E. Coli* (mmol / L)	*S. Typhimurium* (mmol / L)
OFX	8.30×10^{-5}	24.91×10^{-5}
OFX: Citric acid	15.33×10^{-5}	10.03×10^{-5}
OFX: Malonic acid	10.01×10^{-5}	19.35×10^{-5}
OFX: L-Malic acid	16.05×10^{-5}	18.11×10^{-5}
OFX: Pimelic acid	6.64×10^{-5}	15.54×10^{-5}
OFX: Adipic acid	19.64×10^{-5}	15.85×10^{-5}

OFX salts have shown significant MIC results in *S. Typhimurium,* which are listed in Table 5.6. OFX: Citrate (10.03×10^{-5} mmol / L) has emerged as the most potent drug candidate to inhibit bacterial colonies than pure OFX (24.91×10^{-5} mmol / L). Other salts have also shown improved MIC with higher solubility and IDR. Hence, these also can be used in the formulation to treat bacterial infection with a lower latency time of onset of action.

5.4 Conclusion

Cocrystallization of ofloxacin with natural organic acids by the solvent drop-assisted grinding method has resulted in new crystalline phases characterized by thermal and diffraction techniques. The

water solubility of the products was increased 21.1 to 42.9 times in phosphate buffer solution at pH 7. Paddle-type dissolution taster determined the intrinsic dissolution rate with UV-VIS spectrophotometry. The intrinsic dissolution rate study establishes that these salts have significantly higher dissolution rates than the parent drug. Therefore, we believe that these new salts will have better bioavailability for their antibacterial activity in cells and will be better candidates for treating bacterial infection than the parent drugs. These salts have been evaluated for minimum inhibitory concentration in *Escherichia Coli* (*E. Coli*) and *Salmonella Typhimurium* (*S. Typhimurium*) bacteria. MIC values were found to have significantly improved results along with better water solubility and IDR. These salts have great importance in the pharmaceutical industries in a highly water-soluble tablet form and offer a new formulation potential.

Chapter 6

Salts of Levofloxacin with Improved Solubility for Enhanced Pharmaceutical Applicability: Insights from structural and biological studies

Chapter 6

6.1 Introduction

Levofloxacin (*S*-9-fluoro-2,3-dihydro-3-methyl-10-(4-methylpiperazin-1-yl)-7-oxo-7H-pyrido[1,2,3-de]-1,4-benzoxazine-6-carboxylicacid;[174] LFX, Figure 6.1) is a synthetic broad-spectrum antibiotic belonging to the fluoroquinolone class of drug.[175] It targets to inhibit bacterial enzyme DNA gyrase and DNA topoisomerase IV.[176] Crystal structures of LFX[177] have been reported in the literature. It contains one carboxylic group with the pK_a = 6.0 (for the most acidic proton) as well as one basic site with pK_a 8.2 (for the most basic site).[178] LFX (*S* Isomer) shows 8-128 times higher pharmacological effect than *R*-isomer and 2 times higher activity than ofloxacin (OFX), the racemic mixture.[179]

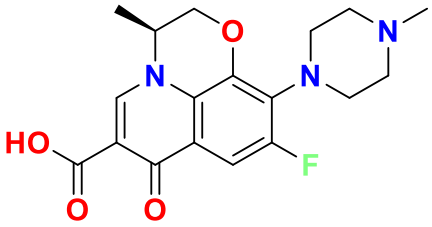

Figure 6.1: Chemical structure of Levofloxacin

Currently, the cocrystallization technique has been of great importance because it modifies the drug's physiochemical nature like stability, solubility, bioavailability, etc.[169,180–182] The crystal structures of the levofloxacin hemihydrate form and the less stable monohydrate form were first reported.[183] Besides these forms, the crystal structures of a levofloxacin tribromocadmium(II) salt and two organometallic complexes with Cu and Mg metals have been reported in the literature.[184,185] A recent study on various crystalline forms of LFX highlighted the formation of six salts of LFX with organic acids. The authors have used the crystal structure prediction methodologies to elucidate the structure of anhydrous LFX.[186] But, no efforts have been made till date to study the physical and biological properties (solubility, IDR and biological efficacy) of various cocrystals of LFX.

We aim to enhance further the solubility and IDR of solid forms (cocrystals) of Levofloxacin using simple biologically acceptable organic acids. Herein, we report the synthesis of a few salts of LFX using solvent drop grinding method and their characterization using powder X-ray diffraction and

thermal method. Their saturation solubility determination, intrinsic dissolution rate analysis and partition coefficient were studied to establish the enhancement of solubility and rate of dissolution in phosphate buffer solution at pH 7 (PBS7). We performed both *in-vivo* and *in-vitro* experiments to determine MIC, IC_{50}, pharmacokinetic profile and biodistribution pattern to evaluate the significance of the newly developed cocrystals.

6.2 Experimental Section

6.2.1 Materials

Levofloxacin (99% pure), Brain heart infusion (BHI) broth, adipic acid (99.5% purity), 3-nitrobenzoic acid (99% purity), mandelic acid (99% purity), pimelic acid (98% purity), *trans*-ferulic acid (99% purity), salicylic acid (99.8% purity) and sorbic acid (99% purity) were purchased from Sigma-Aldrich. L (-) malic acid (99.5% purity), disodium hydrogen phosphate anhydrous (99% purity), potassium dihydrogen phosphate anhydrous (99% purity) and Luria Bertani (LB) broth were obtained from Hi-media laboratories Pvt. Ltd. Maleic acid (99.5% purity) and succinic acid (99.5% purity) were procured from Sisco Research Laboratories Pvt. Ltd. D (-) tartaric acid (99% purity) was ordered from Spectrochem Pvt. Ltd. Analytical grade solvents methanol (99.9% purity) and ethanol (99.9% purity) were obtained from Merck and Spectrochem. N-octanol (99.5% purity) was purchased from CDH Pvt. Ltd.

6.2.2 Solvent Drop Grinding Method

The salts of LFX were developed using the solvent drop grinding method.[187] Equimolar mixture of the LFX and a cocrystal former [one among D (-) tartaric acid, maleic acid, succinic acid, salicylic acid, l (-) malic acid, *trans*-ferulic acid, pimelic acid, mandelic acid, 3-nitrobenzoic acid, adipic acid and sorbic acid] was ground with 50-100 μL of Methanol 99.9% in an agate mortar and pestle. The grinding was continued till a free-flowing powder was formed, and this procedure was repeated five to eight times to obtain a new single-phase crystalline powder material.

6.2.3 Powder X-ray Diffraction

PXRD data were recorded on a Rigaku Ultima IV powder X-ray diffractometer using parallel beam geometry equipped with Cu K_α source, 2.5° primary and secondary soller slits, 5° in-plane divergence slit with 10 mm height limit slit, sample rotation stage (120 RPM) attachment and DTex Ultra detector. The data were collected over 2θ range 5°–50° with a scanning speed of 2° per minute with 0.02° steps.

6.2.4 Thermal Analysis

The melting points and melting enthalpies of the LFX and salts were recorded on the Perkin-Elmer DSC-8000 instrument. All the samples (2-5 mg) were heated at a rate of 5° C/min in sealed aluminum pans without the hole. The melting points, the fusion enthalpies, and the DSC traces of LFX and the developed salts have been reported in supporting file in Figure S6.1 – S6.12 on page 40 – 45 in the enclosed DVD.

6.2.5 Single Crystal X-ray Diffraction (SCXRD)

SCXRD experiments were performed on a Bruker AXS KAPPA APEX-II CCD diffractometer (Monochromatic Mo Kα radiation) equipped with Oxford cryosystem 700 Plus. Unit cell determination, data collection (at 100K), and data reduction were made using the Bruker APEX-II package.[188] The crystal structures were solved using Olex^2 package[189] equipped with XT[101] and were further refined using XL.[100] Crystal packing and interaction diagrams were created using Mercury.[190] The details of the single-crystal X-ray diffraction data collection, structure solution and refinement are given in Table 6.2. LFX and D (-) tartaric acid crystals were made by slow evaporation from a 1:1 solution in Methanol and water. In the refrigerator, crystals of a maleic acid salt of LFX were obtained from Acetone: Methanol (1:1) mixture at 4 oC. LFX salt with pimelic acid was synthesized by dissolving the salt in a combination of Acetone: Methanol: Water (1:1:1), and the solution was kept at room temperature. LFX: 3-nitrobenzoic acid crystal was developed in phosphate buffer solution at pH 7 at 4 ^oC in refrigerator. Good quality single crystals were obtained within 15 days.

6.2.6 Hirshfeld Surface Analysis

Hirshfeld surfaces and 2D fingerprint plots on the single crystal data of LFX salts were generated using Crystal Explorer 17.5 package as described in detail in Chapter 2, section 2.2.6.[103–105]

6.2.7 Determination of Partition Coefficient

Partition coefficients of LFX and its all salts were determined by the slow stirring method following the same procedure described in Chapter 2, section 2.2.8.[106]

6.2.8 Solubility Analysis

A calibration curve was drawn for the pure drug LFX and all the salts between absorbance *vs.* concentration by solutions of known concentrations using UV-Vis spectrophotometer (Given in the supporting information file, Figure S6.18 – S6.29 on page 51 – 57 in the enclosed DVD). The solubility was determined by stirring all the salts and LFX in PBS7 at 37 ^oC, for 24h in different vials, as described in section 5.2.6.

6.2.9 Intrinsic Dissolution Rate

Intrinsic dissolution rates were determined using USP certified Lab India 8000+ Dissolution Tester described in Chapter 2, Section 2.2.9.[109]

6.2.10 Determination of Minimum Inhibitory Concentration (MIC)

The LFX and salts were dissolved in sterile water at a concentration of 0.001 mg/l. These LFX and salts were then diluted to various concentrations at double their strength (DS-D). *Escherichia coli* (from Invitrogen) or *Salmonella Typhimurium* (received from Dr. Mahak Sharma, IISER Mohali) were grown in Luria Bertani (LB) broth overnight at 37 °C. The culture was then diluted in 0.85 % NaCl solution to a McFarland turbidity of 0.5 (equivalent to OD_{600} =0.132). This was then further diluted at 1:50 in 10 mL of double-strength Brain Heart Infusion (BHI) broth (DS-B). Further, 100 µl each of DS-D and DS-B were added to a well in a 96-well plate. After 48 h of incubation at 37 °C, OD_{600} was

measured using a plate reader (Bio-Rad, U.S.A.). The dilution at which the OD_{600} was observed to be comparable to blank, was taken as the MIC for the derivative.[173]

6.2.11 Cells and animals used in the study

Caco-2, a human epithelial cell line used in this study, was obtained from American Type Culture Collection, ATCC. Cells were maintained in Dulbecco's Modified Eagle Medium (DMEM) medium containing 10 % fetal bovine serum (FBS) and incubated at 37 °C and 5 % CO_2. For *in-vivo* studies, Balb/c mice were used. All the animal handling and experimentation protocols were duly approved by the institutional animal ethics committee (IAEC) of the Indian Institute of Science Education and Research, Mohali (IISERM/SAFE/PRT/2018/002). All animal experiments were carried out in accordance with the guidelines of the Committee for Control and Supervision of Experiments on Animals (CPCSEA) (No. 1842/GO/ReBiBt/S/15/CPCSEA).

6.2.12 *In-vitro* Inhibitory Concentration (IC_{50}) Studies

Caco-2 cells (2.5×10^5) were plated in a 24-well plate and were infected with *S. Typhimurium* at a multiplicity of infection (MOI) of 50:1 for 30 min. Then, the bacteria were removed, and the extracellular bacteria were killed using 100 μg/mL gentamicin for 1 h. After 1 h, cells were incubated with media containing 20 μg/mL of gentamicin. After 6 h of infection, the salts (LFX: maleic acid and LFX: L-malic acid) and LFX were added to the infected cells at a concentration of 0.5 times their MIC or at MIC (1 X MIC). For LFX: succinic acid salt, we have used 0.25 and 0.5-times MIC, as no bacteria were enumerated beyond 0.5 X MIC. After 18 h of incubation, cells were washed twice with sterile phosphate buffer saline and were then lysed using 0.1 % TritonX-100 at 37 °C for 30 min. The bacteria were then plated on LB agar plates and enumerated. The cells that were not treated with any salts were taken as the maximum bacterial growth. The percent of the reduction in the total bacteria enumerated after treatment with salt was calculated for 0.5 X MIC and 1 X MIC (and 0.25 X and 0.5 X for LFX: succinic acid salt). These values were then plotted and the concentration where 50 % of the bacteria were killed was taken to be its IC_{50}.[191]

6.2.13 *In Vivo* Pharmacokinetic Studies

In vivo pharmacokinetic studies by oral route were performed on Balb/c mice (male, 19−25 g, 6−8 weeks old; n = 4). LFX and their maleic acid, succinic acid and L-malic acid salts were administered (equivalent to 10 mg/kg LFX) using an oral cannula. Blood samples (0.15 mL) were collected at each time 0, 5, 15, 30, 60, 90, 120 and 240 min from retro-orbital plexus. Plasma was separated using centrifugation at 10000 RPM. The supernatant was taken and Methanol (0.1 mL) was added to precipitate the plasma protein. The supernatant layer was mixed with the mobile phase (1 mL). All samples were filtered using a 0.22 μm nylon syringe filter. Calibration curves were drawn using a known concentration of LFX and salts (maleic acid, succinic acid and l-malic acid), and their contents were analyzed using RP-HPLC.[192] Pharmacokinetic parameters like area under the curve (AUC), the volume of distribution (V_d), biological half-life ($t_{1/2}$), elimination rate (K), and clearance (Cl) were determined

using one compartment based model oral drug delivery (1 CBM oral pharmacokinetic approach), employing MS office excel software.[193]

6.2.14 Biodistribution Study

Biodistribution studies were also performed on the Balb/c mice (Male, 19−25 g, 6−8 weeks old; n = 5). Drug/salts (LFX and their salts, 10 mg/kg of LFX) were administered analogously to the pharmacokinetic studies. Balb/c mice were sacrificed at every sampling time (30, 60, 120 and 240 min) by cervical dislocation. Heart, liver, kidney and brain were harvested and cleared of blood and other adhered materials using tissue paper. The organ was chopped and transferred into 1 mL PBS (pH = 7) and homogenized. Acetonitrile (0.5 mL) was added and centrifuged at 10000 RPM. The supernatant was taken and Methanol (0.5 mL) was added to precipitate the proteins. Samples were filtered using a 0.22 μm nylon membrane filter and analyzed employing RP-HPLC [194].

6.3 Results & Discussion

Levofloxacin (pK_a = 6.25) is likely to form salts with GRAS organic acids having pK_a ranging from 0.18 to 4.35. According to the ΔpK_a rule of 3,[50,110,111] when ΔpK_a is between 1 to 3 means, it may form salt/cocrystal, and when ΔpK_a is more than 3, it will form a salt. This concept is also observed in the case of LFX (Table 6.1). Salt formation is detected in the case of all acids which are used as coformer.

Table 6.1: pK_a and ΔpK_a values of LFX and Coformers.

Name of Co-former	pK_a	ΔpK_a
Levofloxacin	5.45 (carboxylic acid), 6.25 (>N-Me group)	
D (-) Tartaric Acid	2.89, 4.40	3.36, 1.85
Maleic acid	1.90, 6.07	4.35, 0.18
Succinic acid	4.20, 5.60	2.05, 0.65
Salicylic acid	2.97	3.28
L-Malic acid	3.40, 5.20	2.85, 1.05
Trans-ferulic acid	4.58	1.67
Pimelic acid	4.51, 5.58	1.74, 0.67
Mandelic acid	3.41	2.84
3-Nitrobenzoic Acid	3.47	2.78
Adipic acid	4.43, 5.41	1.82, 0.84
Sorbic acid	4.76	1.49

6.3.1 Synthesis of salts

Eleven new crystalline phases of LFX were synthesized by the solvent drop grinding method and were identified by PXRD. These novel salts were also characterized by PXRD and DSC analysis. All these complexes of LFX indicated proton transfer reaction (implying salt formation on the rational use of ΔpK_a rule of three).

6.3.2 Powder X-ray Diffraction Analysis

New salts of Levofloxacin were prepared and their PXRD patterns are shown in Figures 6.2A and B. It is evident from these PXRD patterns that new crystalline phases were formed by the solvent drop-assisted grinding LFX and the corresponding organic acid used in the experiment. The characteristic peaks for LFX and the corresponding organic acid were present initially, but those disappeared during repeated grinding of the mixture with dry Methanol. Recrystallization of these final products (new phases) resulted in single crystals, which indicated salt formation. These PXRD patterns also suggest that the new salts were crystalline.

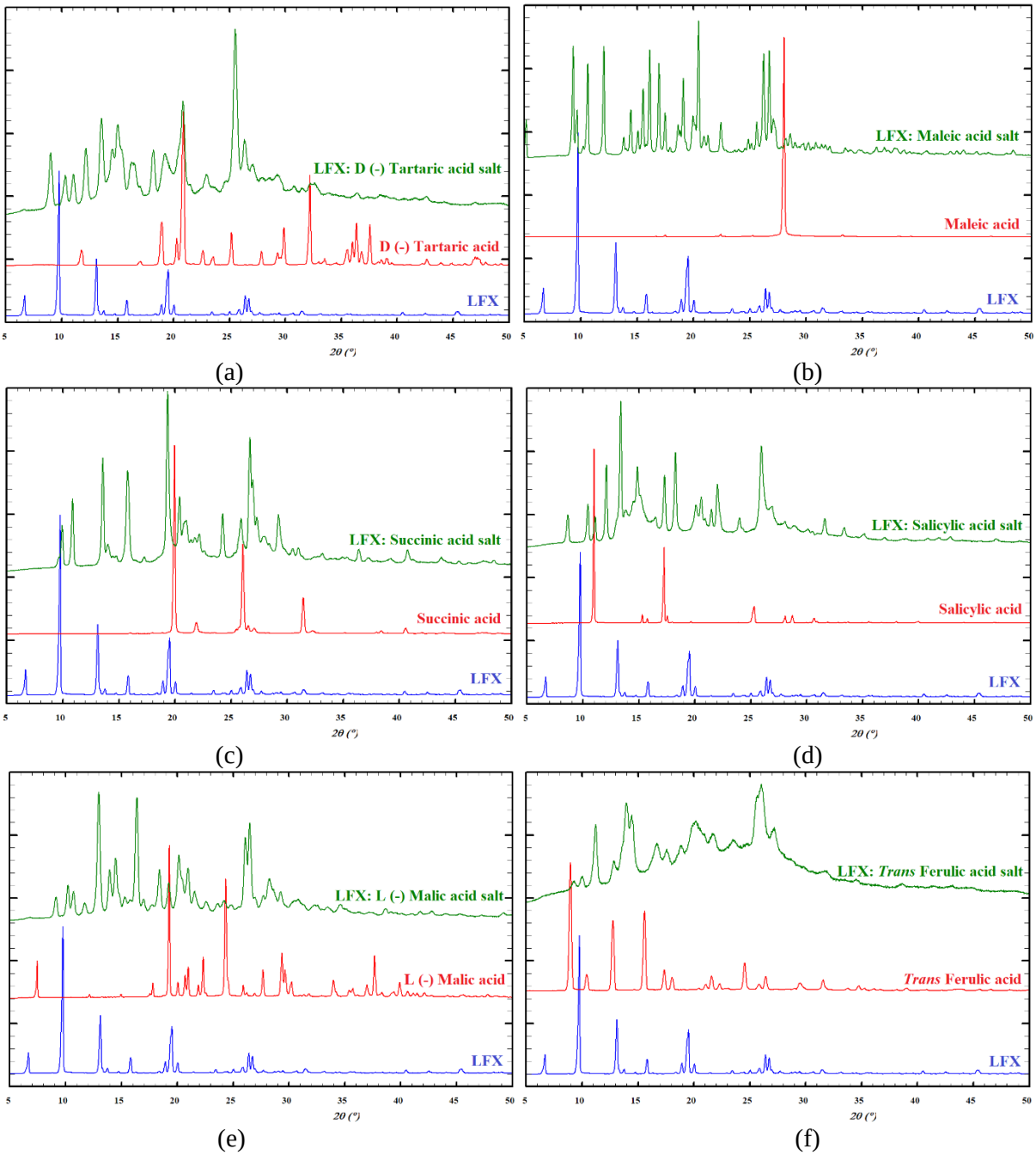

Figure 6.2A: PXRD patterns of salts of LFX in comparison with LFX and coformers.

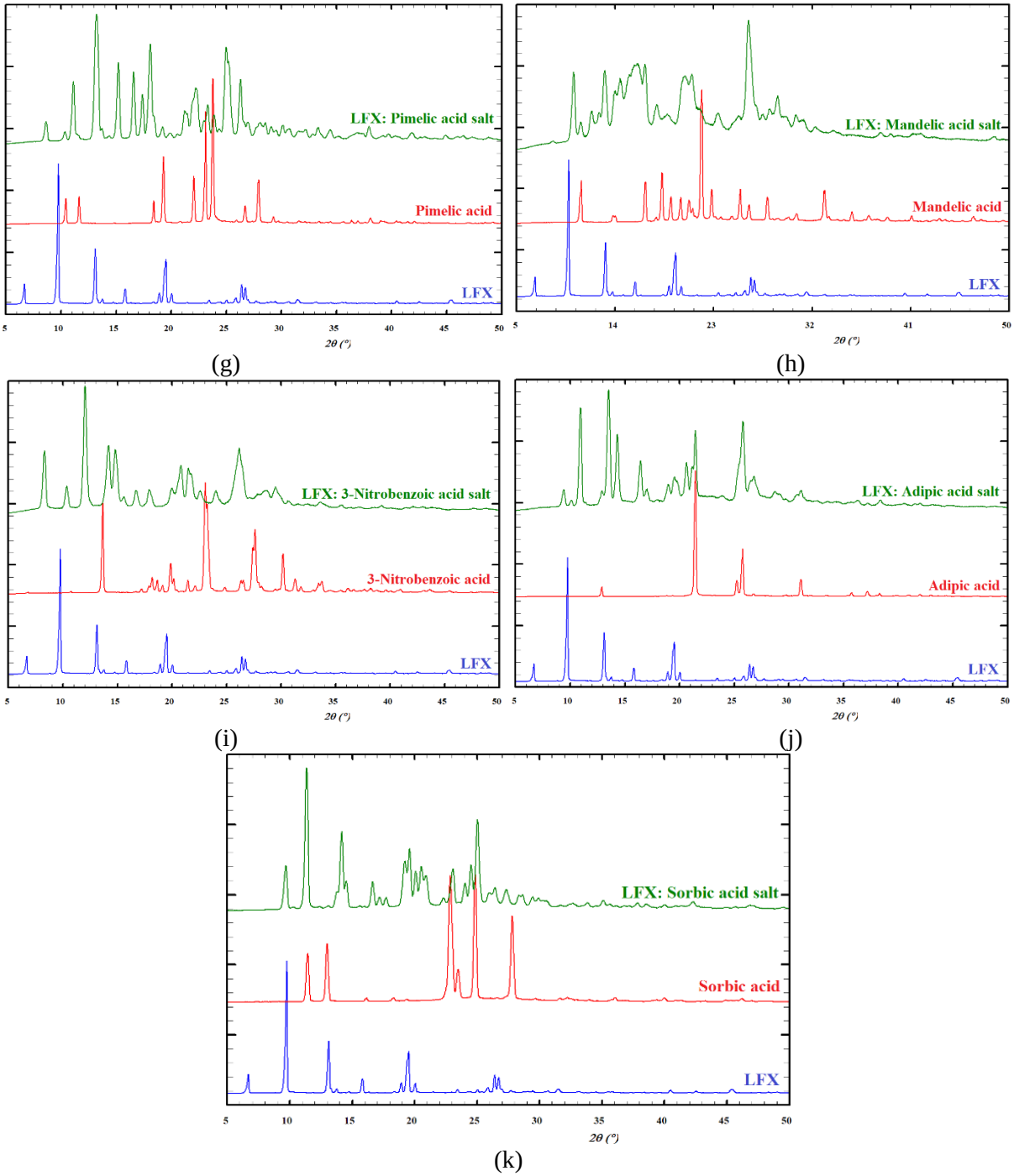

Figure 6.2B: PXRD patterns of salts of LFX in comparison with LFX and coformers.

6.3.3 Thermal Analysis

The DSC thermograms of LFX and all the salts show melting point and melting enthalpy in Table 6.2. We have found different melting/decomposition temperatures for new salts with respect to the parent drug, which advocated the development of new solid phases. The highest melting point is found for LFX: maleic acid salt (233 ^{o}C) and minimum for LFX: pimelic acid salt (128 ^{o}C). The melting enthalpy of salts was higher than LFX, which indicates these salts are more stable than LFX.

Table 6.2: Melting points and melting enthalpies of LFX and their salts.

Name	Melting point of LFX and coformer (ºC)	Melting Point of Salts of LFX (ºC)	Melting enthalpies (J/g)
LFX	151		33.7
D (-) Tartaric Acid	173	232	263.3
Maleic acid	135	233	185.3
Succinic acid	184	216	80.4
Salicylic acid	211	178	196.2
L (-) Malic acid	131	193	153.1
Trans-ferulic acid	172	136	186.7
Pimelic acid	105	128	38.6
Mandelic acid	119	183	58.5
3-Nitrobenzoic Acid	141	162	53.0
Adipic acid	152	176	125.1
Sorbic acid	135	163	74.6

6.3.4 Single Crystal X-ray Analysis

We have grown four single crystals of LFX with D (-) tartaric acid, maleic acid, pimelic acid, and 3-nitrobenzoic acid. Structural parameters of these cocrystal salts are given in following Table 6.3. The cocrystal formation was confirmed through single crystal structural analysis. These single crystals reveal that salt formation occurs by hydrogen bonding with the transfer of acidic proton to the drug molecule. These salts are formed by N–H···O hydrogen bonding. Other salts did not yield single crystals suitable for structure determination.

6.3.4.1 LFX: D (-) Tartaric Acid Salt

LFX salt with D (-) tartaric acid was crystallized in the *C*2 space group. Each asymmetric unit consists of one LFX cations, half D (-) tartrate anions and one water molecule (Figure 6.3a). The acidic hydrogen of the D (-) tartaric acid was found to be transferred to the piperazine nitrogen of LFX and formed a strong hydrogen bond N–H···O (1.900 Å and 2.550 Å) Table 6.4. Intramolecular hydrogen bonding is seen in LFX O–H···O (1.712 Å). LFX arranged antiparallel in a layer along a-axis and connected by week hydrogen bonding C–H···O (2.471 Å, 2.522 Å, 2.604 Å and 2.546 Å) as shown in Figure 6.3b. The crystal packing was shown in Figure 6.3c, which has alternate layers of antiparallel LFX molecules and tartaric acid water channel interacted by hydrogen bonds and van der Waals' forces.

Table 6.3: Crystallographic data on the salts of Levofloxacin.

Data/Salt	LFX: D (-) tartaric acid	LFX: Maleic acid	LFX: Pimelic acid	LFX: 3-Nitrobenzoic acid
Empirical formula	$(C_{18}H_{21}FN_3O_4)^+$ $(C_2H_2O_3)^-$ H_2O	$(C_{18}H_{21}FN_3O_4)^+$ $(C_4H_3O_4)^-$	$8(C_{18}H_{21}FN_3O_4)^+$ $4(C_7H_{10}O_4)^{2-}$ $14(H_2O)$	$(C_{18}H_{21}FN_3O_4)^+$ $(C_7H_4NO_4)^-$ H_2O
CCDC number	1550316	1550314	1550315	2119629
Formula weight	454.43	477.44	882.37	546.50
Crystal system	Monoclinic	Monoclinic	Monoclinic	Monoclinic
Space group	*C*2	$P2_1$	$P2_1$	*C*2
a(Å)	17.405(11)	6.7600(6)	17.552(5)	37.882(4)
b(Å)	6.792(4)	34.605(3)	27.476(7)	6.5866(7)
c(Å)	18.494(11)	9.9057(10)	18.376(5)	9.7900(10)
α(°)	90	90	90	90
β(°)	112.640(8)	105.804(6)	91.218(5)	93.615(2)
γ(°)	90	90	90	90
V(Å^3)	2018(2)	2229.6(4)	8860(4)	2437.9(4)
Z	4	4	2	4
ρ_{calc}(g/cm^{-3})	1.50	1.422	1.418	1.489
Temperature (K)	100.0(2)	200.0(2)	100.0(2)	100.0(2)
μ/ mm^{-1}	0.122	0.115	0.113	0.119
$2\theta_{min,\ max}$ ()	2.35, 24.84	2.22, 24.00	2.22, 25.38	4.31 to 59.998
F (000)	956.0	1000.0	4008.0	1144.0
$h_{min,max}$; $k_{min,max}$; $l_{min,max}$	-20,20; -7,8; -22,22	-8,8; -41,40; -11,11	-20,20; -32,15; -21,21	-52, 47; -9, 9; -13, 13
Total no. of reflections	12331	16139	40337	15447
R_{int}	0.0306	0.0304	0.0603	0.0403
No. of unique reflections	3466	6956	24533	7049
R_1 [I>2σ(I)]	0.044	0.0409	0.083	0.0484
wR2 (all data)	0.108	0.0915	0.221	0.1095
GooF on F^2	1.024	1.001	0.990	1.002
$\Delta\rho_{max,min}$/eÅ^{-3}	0.250, -0.185	0.127, -0.153	1.039, -0.585	0.32/-0.27

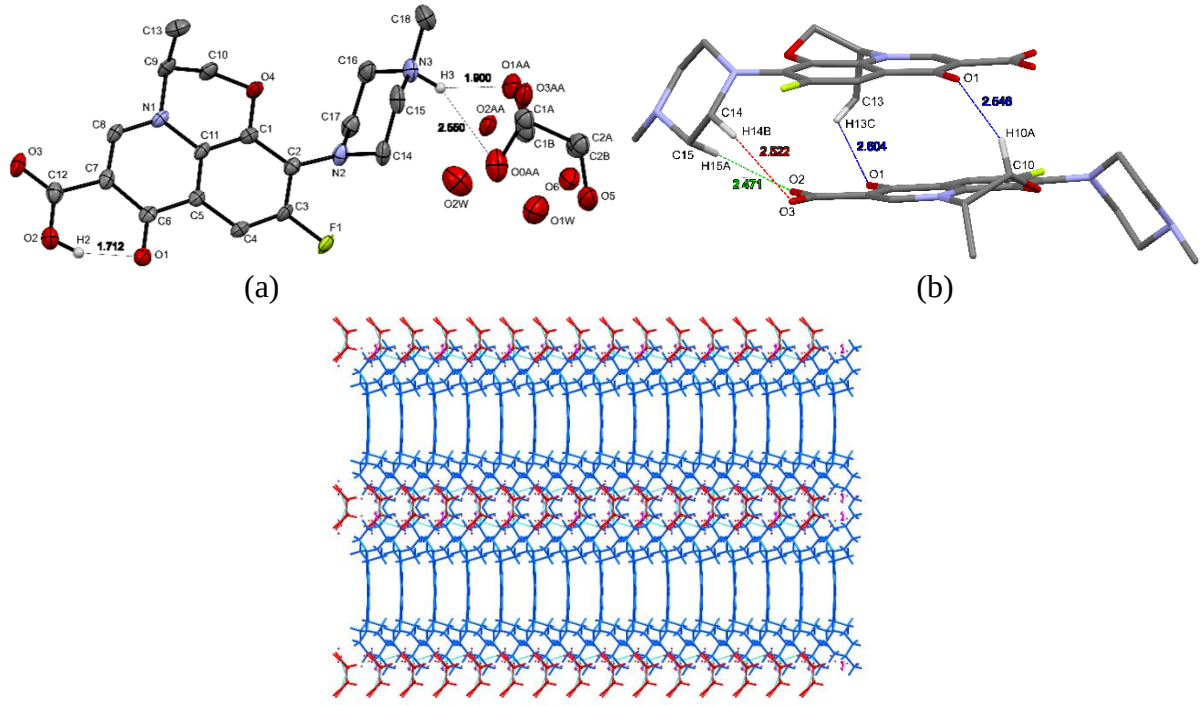

(a) (b)

(c)

Figure 6.3: (a) The asymmetric unit of LFX: D (-) tartaric acid salt; (b) Intermolecular interaction between LFA molecules in LFX layer; (c) Crystal packing diagram of LFX: D (-) tartaric acid salt along 'a' axis.

6.3.4.2 LFX: Maleic Acid Salt

LFX salt with maleic acid was crystallized in the $P2_1$ space group. The asymmetric unit contains two LFX cations and two maleate anions. The acidic hydrogen of the maleic acid was found to be transferred to the piperazine nitrogen of LFX, as shown in Figure 6.4a, and this forms a strong hydrogen bond N–H···O (1.741 Å and 1.748 Å). Intramolecular hydrogen bonding is also seen in maleic acid molecule O–H···O (1.501 Å) and LFX molecule O–H···O (1.732Å and 1.763 Å). LFX molecule is arranged antiparallelly in a layer and connected by weak hydrogen bond C–H···O and van der Waals π – π interactions as displayed in Figure 6.4b. In Crystal packing, we have seen alternative layers of LFX and maleic acid channels in Figure 6.4c. All hydrogen and π···π bonding are given in Table 6.4.

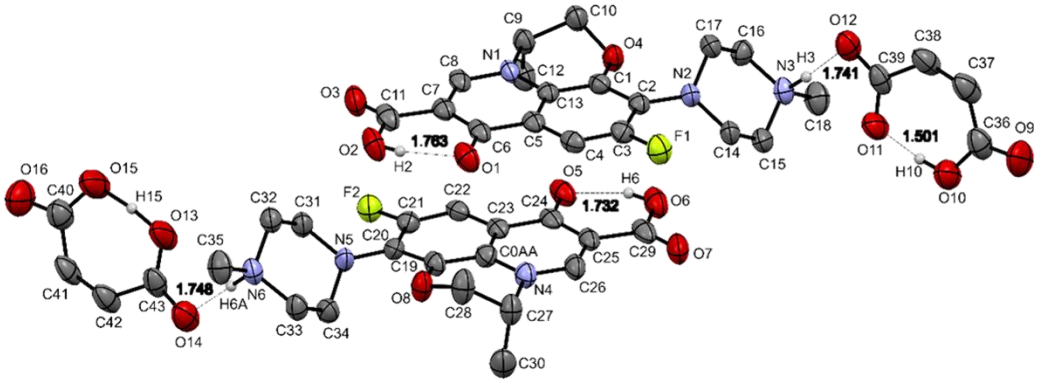

(a)

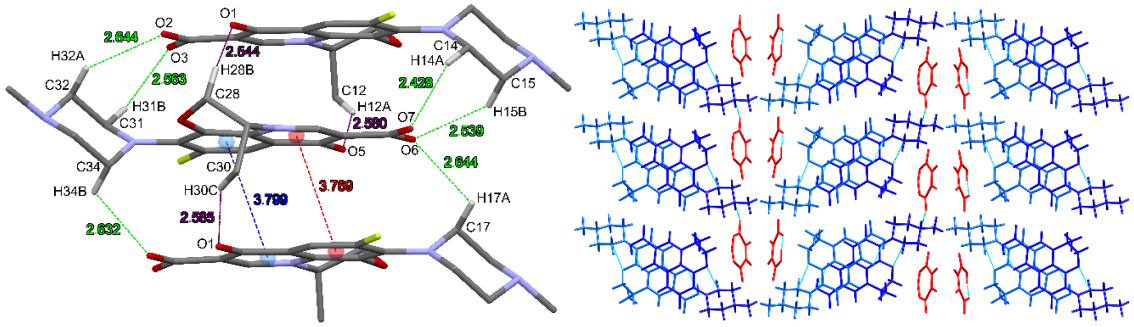

(b) (c)

Figure 6.4: (a) Asymmetric unit of LFX: maleic acid salt; (b) Intermolecular interaction between LFX molecules in a layer of LFX; (c) Crystal packing diagram of LFX: maleic acid salt along 'a' axis.

6.3.4.3 LFX: Pimelic Acid Salt

LFX salt with Pimelic acid was also crystallized in the $P2_1$ space group. Each unit cell contains eight cations of LFX, four dianions of pimelic acid, and fourteen water molecules. The two acidic hydrogens of a pimelic acid were found to be transferred to the piperazine nitrogen of two LFX molecules and formed a strong hydrogen bond, as shown in Figure 6.5a. LFX molecules are arranged antiparallel in a layer and interact with acid and water molecules. In crystal packing, the two drug molecules are stacked onto each other *via* weak C–H···O interactions, and formed alternate layers of LFX and acid water channel shown in Figure 6.5b and 6.5c. All hydrogen bonding is given in Table 6.4.

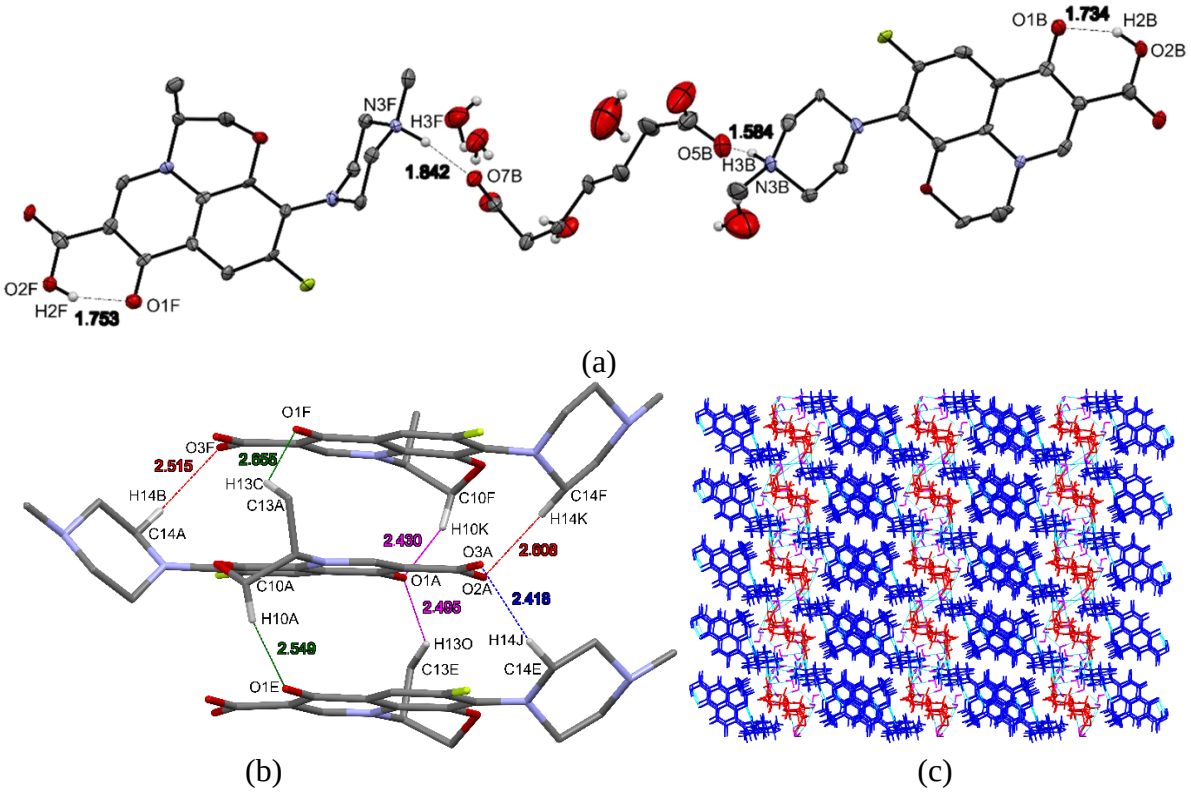

(a)

(b) (c)

Figure 6.5: (a) Depiction of proton transfer in of LFX: Pimelic acid salt; (b) Intermolecular interaction between LFX molecules in a layer of LFX; (c) Crystal packing diagram of LFX: pimelic acid salt along 'b' axis.

6.3.4.4 LFX: 3-Nitrobenzoic Acid Salt

This LFX: 3-nitrobenzoic acid salt crystallizes in the C2 space group. The asymmetric unit contains one molecule of LFX, one molecule of 3-nitrobenzoic acid, and one water molecule in Figure 6.6a. Acidic proton transferred to the piperazine ring of LFX and interacted via water molecule by N1–H1···O9 (1.922Å) and O9–H9A···O5 (1.931Å) hydrogen bond. Intramolecular hydrogen bond O2–H2···O3 (1.731Å) present in LFX molecule. Two LFX molecules interacted by C–H···O hydrogen bonds and van der Waals' force, as seen in Figure 6.6b. Figure 6.6c shows the crystal packing diagram of LFX: 3-nitrobenzoic acid salt along 'c' axis and LFX and 3-nitrobenzoic acid molecules connected through water molecule and found alternatively. All hydrogen bonds are tabulated in Table 6.4.

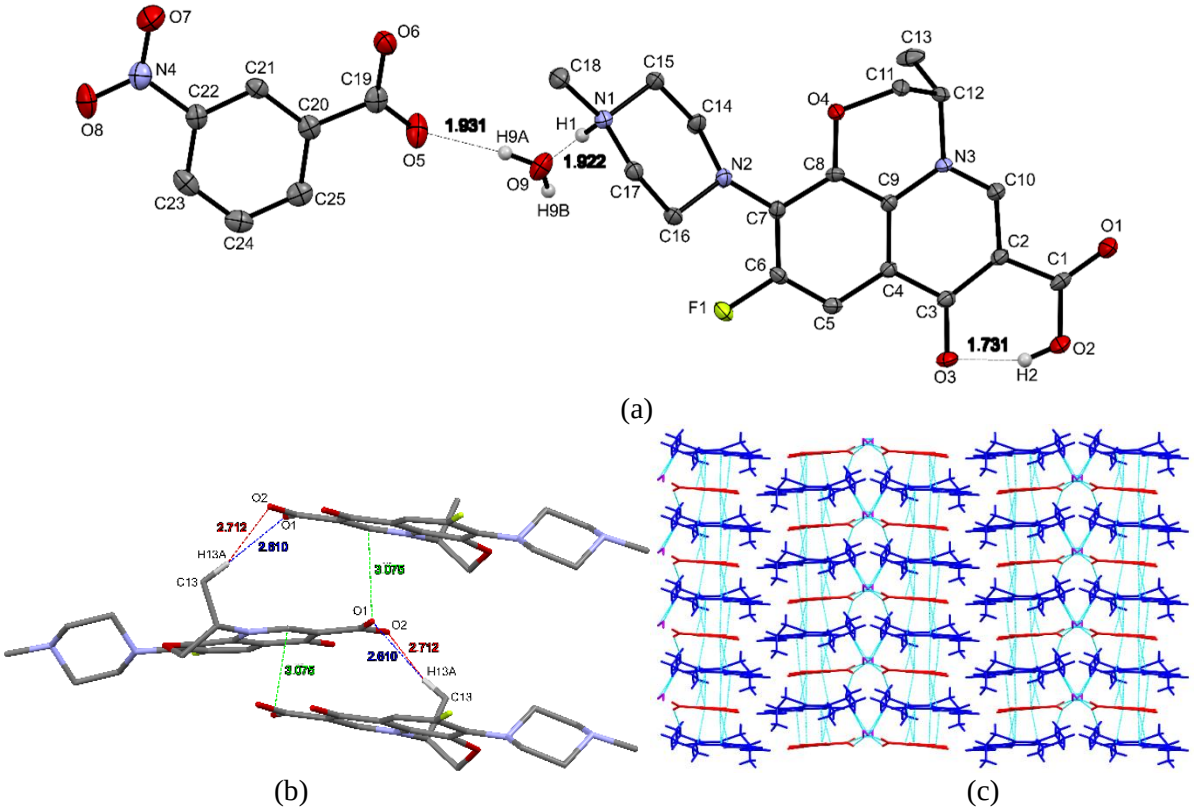

Figure 6.6: (a) Asymmetric unit of LFX: 3-nitrobenzoic acid salt; (b) Intermolecular interaction between LFX molecules in a layer of LFX; (c) Crystal packing diagram of LFX: 3-nitrobenzoic acid salt along 'c' axis.

Table 6.4. Hydrogen bond geometry parameters in LFX salts.

Salts	Interactions	D–H (Å)	H···A (Å)	D···A (Å)	D–H···A (˚)	Symmetry code
LFX: D (-) Tartaric acid	O1W–H1WA···O1W	0.87	1.81	2.636(10)	158	2-x, y, 2-z
	O2–H2···O1	0.84	1.71	2.497(4)	155	x, y, z
	N3–H3···O0AA	1.00	2.55	3.465(9)	152	5/2-x, -½+y, 2-z
	N3–H3···O1AA	1.00	1.90	2.695(8)	134	5/2-x, -½+y, 2-z

	N3–H3···O2AA	1.00	1.70	2.689(7)	171	5/2-x, -½+y, 2-z
	N3–H3···O3AA	1.00	2.56	3.176(8)	120	5/2-x, -½+y, 2-z
	O5–H5···O0AA	0.84	2.12	2.607(10)	117	x, y, z
	C2A–H2A···O1W	1.00	2.20	3.169(16)	164	x, 1+y, z
	C4–H4···F1	0.95	2.44	3.297(4)	150	3-x, y, 3-z
	C8–H8···O3	0.95	2.33	3.216(4)	155	2-x, y, 3-z
	C9–H9···O3	1.00	2.51	3.282(5)	133	2-x, y, 3-z
	C10–H10A···O1	0.99	2.55	3.407(5)	145	5/2-x, -½+y, 3-z
	C13–H13B···O2W	0.98	2.44	3.337(8)	152	2-x, y, 2-z
	C14–H14A···O0AA	0.99	2.60	3.478(8)	148	5/2-x, -½+y, 2-z
	C14–H14B···F1	0.99	2.34	2.834(4)	110	x, y, z
	C14–H14B···O3	0.99	2.52	3.454(5)	157	5/2-x, ½+y, 3-z
	C15–H15A···O2	0.99	2.47	3.249(5)	135	5/2-x, ½+y, 3-z
	C15–H15B···O2W	0.99	2.44	3..389(10)	161	5/2-x, ½+y, 2-z
	C16–H16A···O1AA	0.99	2.53	3.512(8)	174	x, -1+y, z
	C16–H16B···O4	0.99	2.42	3.062(4)	122	x, y, z
	C16–H16B···O1W	0.99	2.55	3.383(9)	142	2-x, y, 2-z
	C17–H17A···O4	0.99	2.44	2.846(5)	104	x, y, z
	C18–H18A···O2W	0.98	2.28	3.221(9)	161	x, y, z
	C18–H18B···O1AA	0.98	2.57	2.932(9)	102	5/2-x, -½+y, 2-z
	C18–H18C···O5	0.98	2.33	3.278(9)	163	2-x, y, 2-z
	C18–H18C···O6	0.98	2.48	3.377(10)	152	2-x, y, 2-z
LFX: Maleic acid	O2–H2···O1	0.84	1.76	2.540(5)	153	x, y, z
	N3–H3···O11	1.00	2.45	3.120(4)	124	-1+x, y, -1+z
	N3–H3···O12	1.00	1.74	2.733(5)	171	-1+x, y, -1+z
	O6–H6···O5	0.84	1.73	2.515(5)	154	x, y, z
	N6–H6A···O13	1.00	2.50	3.161(5)	123	-x, ½+y, -z
	N6–H6A···O14	1.00	1.75	2.734(6)	168	-x, ½+y, -z
	O10–H10···O11	0.94(7)	1.50(7)	2.426(5)	166(5)	x, y, z
	O13–H15···O15	1.24(9)	1.21(8)	2.424(5)	165(6)	x, y, z
	C8–H8···O3	0.95	2.49	2.811(6)	100	x, y, z
	C8–H8···O7	0.95	2.49	3.364(6)	153	x, y, 1+z
	C9–H9···O7	1.00	2.57	3.316(6)	131	x, y, 1+z
	C12–H12A···O5	0.98	2.58	3.397(6)	141	x, y, z
	C14–H14A···F1	0.99	2.30	2.760(5)	107	x, y, z

	C14–H14A···O7	0.99	2.43	3.326(6)	151	x, y, z
	C15–H15B···O6	0.99	2.54	3.327(6)	137	x, y, z
	C17–H17B···O4	0.99	2.28	2.837(6)	114	x, y, z
	C17–H17B···O10	0.99	2.60	3.339(6)	132	-1+x, y, z
	C18–H18C···O9	0.98	2.31	3.271(7)	167	x, y, z
	C26–H26···O3	0.95	2.41	3.274(6)	150	x, y, -1+z
	C26–H26···O7	0.95	2.47	2.795(6)	100	x, y, z
	C27–H27···O3	1.00	2.40	3.234(6)	140	x, y, -1+z
	C28–H28B···O1	0.99	2.54	3.393(6)	144	x, y, z
	C30–H30C···O1	0.98	2.58	3.477(6)	151	1+x, y, z
	C31–H31B···F2	0.99	2.40	2.805(5)	104	x, y, z
	C31–H31B···O3	0.99	2.56	3.512(6)	160	x, y, z
	C34–H34A···O8	0.99	2.32	2.821(6)	110	x, y, z
	C35–H35A···O16	0.98	2.37	3.306(7)	161	-1-x, ½+y, -1-z
LFX: Pimelic acid	O13W–H···O7C	0.87	1.84	2.677(10)	160	x, y, z
	O1W–H1WA···O8A	0.87	1.86	2.709(12)	167	x, y, z
	O1W–H1WB···O7D	0.87	2.44	2.758(12)	102	x, y, z
	O2A–H2A···O1A	0.84	1.75	2.514(8)	150	x, y, z
	O2B–H2B···O1B	0.84	1.73	2.490(8)	149	x, y, z
	O2C–H2C···O1C	0.84	1.78	2.549(8)	152	x, y, z
	O2D–H2D···O1D	0.84	1.76	2.535(8)	153	x, y, z
	O2E–H2E···O1E	0.84	1.72	2.487(10)	151	x, y, z
	O2F–H2F···O1F	0.84	1.75	2.510(8)	149	x, y, z
	O2G–H2G···O1G	0.84	1.72	2.495(10)	152	x, y, z
	O2H–H2H···O1H	0.84	1.74	2.510(8)	151	x, y, z
	O2W–H2WA···O7A	0.87	1.86	2.717(11)	167	x, y, z
	N3A–H3A···O5A	1.00	2.49	3.169(12)	124	-1+x, y, z
	N3A–H3A···O6A	1.00	1.62	2.619(11)	172	-1+x, y, z
	N3B–H3B···O5B	1.00	1.58	2.575(11)	169	3-x, ½+y, 2-z
	N3B–H3B···O6B	1.00	2.58	3.300(11)	128	3-x, ½+y, 2-z
	N3C–H3C···O6C	1.00	1.67	2.665(10)	176	1+x, y, 1+z
	N3D–H3D···O5D	1.00	1.64	2.601(9)	161	-1+x, y, z
	N3E–H3E···O7A	1.00	2.53	3.181(11)	23	x, y, 1+z
	N3E–H3E···O8A	1.00	1.65	2.649(11)	175	x, y, 1+z
	N3F–H3F···O7B	1.00	1.84	2.721(9)	145	2-x, ½+y, 1-z

	N3F–H3F···O7W	1.00	2.59	3.136(12)	114	2-x, ½+y, 1-z
	N3G–H3G···O7C	1.00	1.64	2.636(10)	173	x, y, z
	N3H–H3H···O7D	1.00	2.53	3.137(10)	119	2-x, -½+y, 1-z
	N3H–H3H···O8D	1.00	1.63	2.628(10)	179	2-x, -½+y, 1-z
	O2W–H2WB···O8B	0.87	1.90	2.761(11)	171	x, y, z
	O3W–H3WA···O13W	0.87	2.02	2.876(11)	168	x, y, z
	O3W–H3WB···O2W	0.87	1.93	2.757(11)	159	x, y, z
	O4W–H4WA···O3W	0.87	2.47	2.871(15)	108	x, y, z
	O4W–H4WB···O6A	0.87	2.29	2.973(15)	135	x, y, z
	O5W–H5WA···O5C	0.87	2.34	2.764(11)	110	2-x, ½+y, 1-z
	O5W–H5WB···O5D	0.87	1.91	2.765(10)	167	x, y, z
	O10W–H10Q···O8C	0.87	2.11	2.706(15)	125	x, y, z
	O10W–H10R···O11W	0.87	2.05	2.83(2)	149	x, y, z
	O11W–H11A···O6B	0.87	2.53	3.000(18)	115	2-x, ½+y, 1-z
	O6W–H6WB···O5B	0.87	1.80	2.661(14)	171	x, y, z
	O12W–H12A···O6C	0.87	2.12	2.734(14)	127	x, y, z
	O7W–H7WA···O8B	0.87	1.95	2.724(11)	148	x, y, z
	O13W–H13Y···O8D	0.87	1.88	2.698(10)	155	2-x, -½+y, 1-z
	O7W–H7WB···O13W	0.87	2.01	2.866(12)	168	x, y, z
	O14W–H14Q···O4G	0.87	2.52	3.273(11)	145	x, y, z
	O14W–H14R···O6D	0.87	1.87	2.716(10)	163	x, y, z
	O8W–H8WA···O10W	0.87	1.91	2.745(14)	160	x, y, z
	O8W–H8WB···O7B	0.87	1.93	2.750(10)	157	2-x, ½+y, 1-z
	O9W–H9WA···O8W	0.87	2.00	2.851(16)	164	x, y, z
	C4A–H4A···F1C	0.95	2.50	3.326(10)	145	-1+x, y, z
	C4B–H4B···F1D	0.95	2.47	3.237(10)	138	1+x, y, z
	C4C–H4C···F1A	0.95	2.52	3.347(10)	145	1+x, y, z
	C4D–H4D···F1B	0.95	2.39	3.167(10)	139	-1+x, y, z
	C4F–H4F···F1H	0.95	2.52	3.340(10)	145	2-x, ½+y, 2-z
	C4G–H4G···F1E	0.95	2,45	3.326(10)	154	x, y, z
	C4H–H4H···F1F	0.95	2.51	3.320(10)	144	2-x, -½+y, 2-z
	C8A–H8A···O3A	0.95	2.48	2.805(11)	100	x, y, z
	C8A–H8A···O3C	0.95	2.36	3.226(11)	151	x, y, z
	C8B–H8B···O3D	0.95	2.34	3.233(10)	157	x, y, z
	C8C–H8C···O3A	0.95	2.41	3.276(11)	152	x, y, z

	C8C–H8C···O3C	0.95	2.46	2.792(11)	100	x, y, z
	C8D–H8D···O3B	0.95	2.24	3.130(11)	155	x, y, z
	C8E–H8E···O3E	0.95	2.50	2.820(12)	100	x, y, z
	C8E–H8E···O3G	0.95	2.47	3.378(11)	159	-1+x, y, z
	C8F–H8F···O3F	0.95	2.47	2.803(11)	100	x, y, z
	C8F–H8F···O3H	0.95	2.45	3.303(11)	149	3-x, ½+y, 2-z
	C8G–H8G···O3E	0.95	2.26	3.130(11)	152	1+x, y, z
	C8G–H8G···O3G	0.95	2.50	2.821(12)	100	x, y, z
	C8H–H8H···O3H	0.95	2.49	2.811(11)	100	x, y, z
	C8H–H8H···O3F	0.95	2.42	3.280(10)	150	3-x, -½+y, 2-z
	C9A–H9A···O3C	1.00	2.45	3.184(11)	130	x, y, z
	C9C–H9C···O3A	1.00	2.45	3.211(11)	132	x, y, z
	C9D–H9D···O3B	1.00	2.44	3.242(11)	137	x, y, z
	C9F–H9F···O3H	1.00	2.37	3.179(10)	137	3-x, ½+y, 2-z
	C9G–H9G···O3E	1.00	2.38	3.179(11)	136	1+x, y, z
	C9H–H9H···O3F	1.00	2.43	3.167(10)	130	3-x, -½+y, 2-z
	C10A–H10A···O1E	0.99	2.55	3.417(13)	146	x, y, z
	C10B–H10C···O1F	0.99	2.45	3.354(10)	151	x, y, z
	C10B–H10D···O7D	0.99	2.43	3.335(12)	152	x, y, 1+z
	C10C–H10E···O1G	0.99	2.48	3.380(12)	151	x, y, z
	C10C–H10F···O7A	0.99	2.31	3.075(12)	133	x, y, 1+z
	C10D–H10G···O1H	0.99	2.30	3.207(12)	152	2-x, ½+y, 2-z
	C10F–H10K···O1A	0.99	2.43	3.330(12)	151	2-x, ½+y ,2-z
	C10F–H10L···O5C	0.99	2.53	3.491(12)	164	2-x, ½+y, 1-z
	C10G–H10M···O1B	0.99	2.42	3.310(12)	149	x, y, z
	C10H–H10O···O1C	0.99	2.45	3.330(10)	147	x, y, z
	C13B–H13F···O1G	0.98	2.58	3.330(12)	133	x, y, z
	C13C–H13I···O1H	0.98	2.51	3.267(10)	134	x, y, z
	C13D–H13L···O1E	0.98	2.55	3.128(13)	118	x, y, z
	C13E–H13O···O1A	0.98	2.50	3.315(12)	141	x, y, z
	C13F–H13R···O1B	0.98	2.59	3.354(11)	135	x, y, z
	C13G–H13U···O1C	0.98	2.48	3.205(10)	130	x, y, z
	C13H–H13X···O1D	0.98	2.57	3.349(10)	136	2-x, -½+y, 2-z
	C14A–H14B···F1A	0.99	2.47	2.817(11)	100	x, y, z
	C14A–H14B···O3F	0.99	2.52	3.503(13)	174	2-x, -½+y, 2-z

	C14B–H14D···F1B	0.99	2.37	2.748(11)	102	x, y, z
	C14B–H14D···O3G	0.99	2.34	3.272(11)	156	x, y, z
	C14C–H14F···O3H	0.99	2.55	3.534(13)	175	x, y, z
	C14D–H14H···F1D	0.99	2.29	2.797(11)	111	x, y, z
	C14E–H14J···F1E	0.99	2.34	2.740(12)	103	x, y, z
	C14E–H14J···O3A	0.99	2.42	3.362(13)	159	x, y, z
	C14F–H14K···O4F	0.99	2.40	2.827(10)	105	x, y, z
	C14G–H14M···F1G	0.99	2.44	2.784(11)	100	x, y, z
	C14H–H14O···O2C	0.99	2.55	3.231(12)	126	x, y, z
	C14H–H14O···O4H	0.99	2.44	2.886(11)	107	x, y, z
	C15A–H15B···O6W	0.99	2.57	3.293(16)	130	-1+x, y, z
	C15C–H15F···O5W	0.99	2.53	3.413(13)	148	3-x, -½+y, 2-z
	C15F–H15K···O7W	0.99	2.30	2.966(13)	124	2-x, ½+y, 1-z
	C15F–H15L···O4F	0.99	2.46	3.072(11)	120	x, y, z
	C15G–H15N···O14W	0.99	2.48	3.377(13)	150	x, y, z
	C15H–H15P···O3W	0.99	2.57	3.437(14)	147	x, y, z
	C16C–H16E···O4C	0.99	2.37	3.054(11)	125	x, y, z
	C16D–H16G···O4D	0.99	2.42	3.041(11)	120	x, y, z
	C16D–H16G···O10W	0.99	2.58	3.367(15)	136	x, y, z
	C16E–H16I···O9W	0.99	2.43	3.309(17)	148	x, y, 1+z
	C16F–H16L···O2B	0.99	251	3.260(11)	132	x, y, z
	C16G–H16N···O3W	0.99	2.46	3.346(13)	148	x, y, z
	C17A–H17A···O4A	0.99	2.42	2.907(12)	110	x, y, z
	C17B–H17C···O4B	0.99	2.31	2.854(10)	113	x, y, z
	C17C–H17E···O2G	0.99	2.40	3.321(13)	155	x, y, z
	C17D–H17G···O4D	0.99	2.38	2.806(10)	105	x, y, z
	C17D–H17G···O2H	0.99	2.58	3.338(11)	133	2-x, ½+y, 2-z
	C17E–H17I···O4E	0.99	2.35	2.888(13)	113	x, y, z
	C17F–H17L···F1F	0.99	2.36	2.835(11)	109	x, y, z
	C17G–H17N···O4G	0.99	2.41	2.890(12)	109	x, y, z
	C17H–H17P···F1H	0.99	2.44	2.807(11)	101	x, y, z
	C17H–H17P···O3D	0.99	2.47	3.445(12)	169	2-x, -½+y, 2-z
	C18A–H18C···O6W	0.98	2.13	3.045(18)	155	-1+x, y, z
	C18C–H18I···O5W	0.98	2.41	3.332(13)	157	3-x, -½+y, 2-z
	C18D–H18K···O5A	0.98	2.45	3.367(14)	156	-1+x, y, z

	C18H–H18X···O1W	0.98	2.42	3.336(15)	156	2-x, -½+y, 1-z
	C23C–H23E···O11W	0.99	2.57	3.464(18)	150	x, y, z
LFX: 3-Nitro benzoic acid	N1–H1···O9	0.80(5)	1.92(5)	2.714(4)	171(5)	x, y, z
	O2–H2···O3	0.82	1.73	2.500(3)	155	x, y, z
	O9–H9A···O5	0.81(5)	1.93(5)	2.734(3)	173(5)	x, y, z
	O9–H9B···O9	0.88(10)	2.11(11)	2.672(3)	122(11)	1-x, y, 1-z
	C10–H10···O1	0.93	2.52	2.830(3)	100	x, y, z
	C11–H11B···O2	0.97	2.57	3.355(3)	138	x, y, -1+z
	C13–H13B···O2	0.96	2.52	3.285(3)	137	x, y, -1+z
	C13–H13C···O4	0.96	2.59	2.935(4)	102	x, y, z
	C14–H14B···O4	0.97	2.35	2.932(4)	118	x, y, z
	C23–H23···O1	0.93	2.37	3.109(4)	137	-½+x, -½+y, -1+z

We have compared the simulated PXRD pattern from single-crystal X-ray diffraction data with the recorded PXRD pattern, as shown in Figure 6.7. The simulated PXRD pattern of LFX: D (-) tartaric acid, LFX: pimelic acid and LFX: 3-nitrobenzoic acid did not match the recorded PXRD pattern because single crystal structures have water of crystallization. LFX: maleic acid simulated PXRD pattern matched wait recorded powder pattern because it does not have water molecule in the crystal structure.

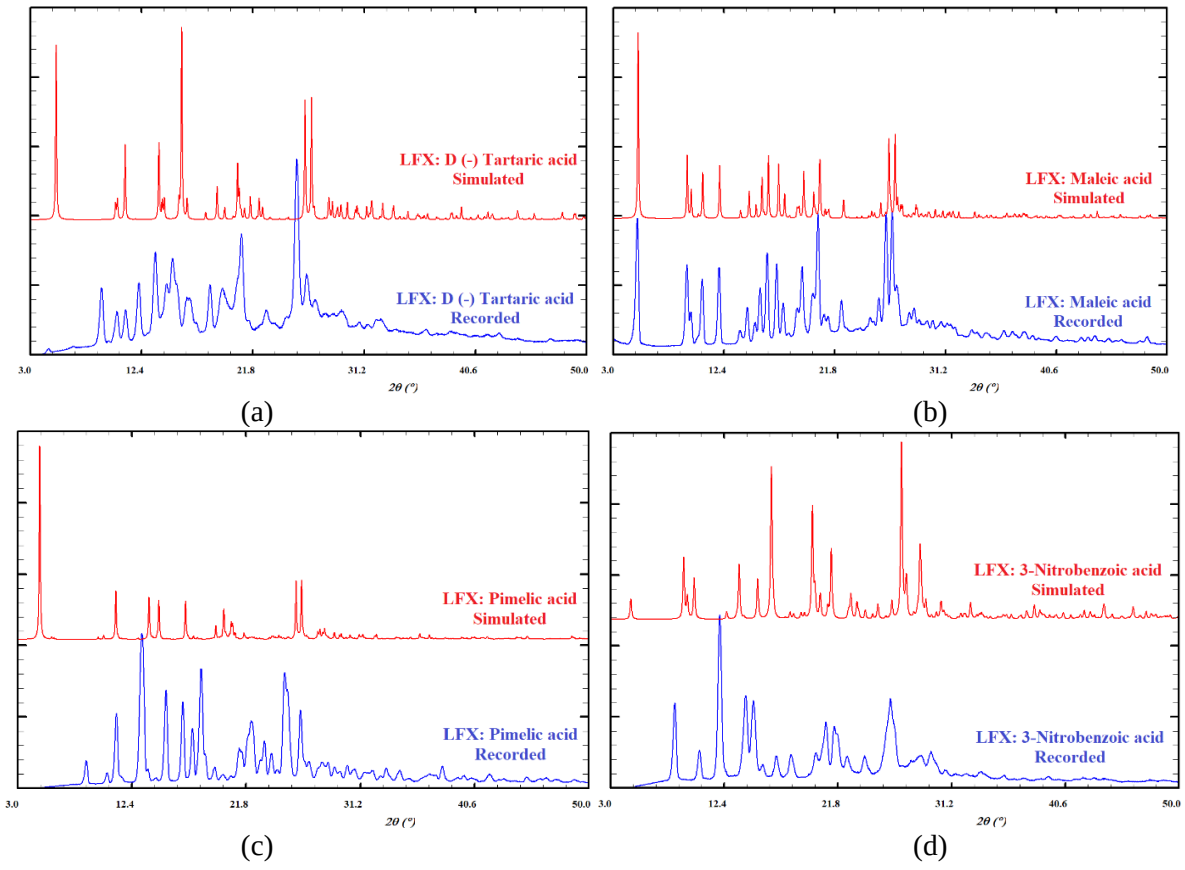

Figure 6.7: PXRD patterns were recorded from powdered samples and simulated from single-crystal X-ray diffraction data.

6.3.5 Hirshfeld Surface Analysis

We have generated Hirshfeld surfaces (HSs) by single-crystal structures to analyze the surface interactions between LFX and surrounding atoms, as shown in Figure 6.8. the acidic proton of the coformers transferred to the piperazine ring of the LFX molecule and connected by the strong hydrogen bond as seen in red color at the Hirshfeld surfaces of the newly formed salts. LFX: 3-nitrobenzoic acid salt is bound by the water molecule inside the unit cell. These strong hydrogen bond interactions of the LFX with corresponding acid molecules are visible in red color on the Hirshfeld surface, and weak interactions are seen in white color.

We can see the fingerprint plots show sharp directional peaks of strong N–H···O bonds. We have displayed all fingerprint plots for all four salts in the supporting file in Figure S6.13 – S6.16 on page number 46 – 49 in the enclosed DVD. Hydrogen atoms played a crucial role in the interaction of the LFX with surrounding molecules. Most HSs interactions are through hydrogen atoms inside and outside of HSs, which shows the highest interaction percentage in surface interaction (Given in the supporting information file, Figure S6.17 on page number 50 – 51 in the enclosed DVD), which supports the presence of N–H···O, O–H···O and C–H···O hydrogen bonds in crystal packing.

6.3.6 Partition Coefficient

We have determined the partition coefficient $log_{10}P$ of LFX and its developed salts by the slow stirring method. This experiment indicated that the salts are more hydrophilic than pure drug LFX except for LFX: trans ferulic acid salt which is less hydrophilic than LFX. Small -ve value of $log_{10}P$ of LFX (-0.39) indicates the hydrophilic nature of pure LFX, but the same for the salts were more negative, indicating higher hydrophilicity of the salts of LFX as shown in Table 6.5. This value supports the increased solubility of the salts of LFX with natural acids. The highest negative value for $log_{10}P$ was found for LFX: salicylic acid salt (-0.84) and lowest negative value with LFX: trans ferulic acid salt (-0.32).

6.3.7 Solubility Studies

The saturation solubility of the LFX and its new salts were determined in PBS7 at 37 ^{o}C and listed in Table 6.6. It is detected that the solubility of the LFX salts with various organic acids is generally much higher than that of the pure drug except LFX: 3-nitrobenzoic acid. Maximum increment in water solubility was seen for LFX: sorbic acid salt (773.21 mg/ mL), and minimum (14.17 mg/ mL) for LFX: salicylic acid salt. A decrease in solubility was observed in LFX: 3-nitrobenzoic acid salt (4.63 mg/ mL).

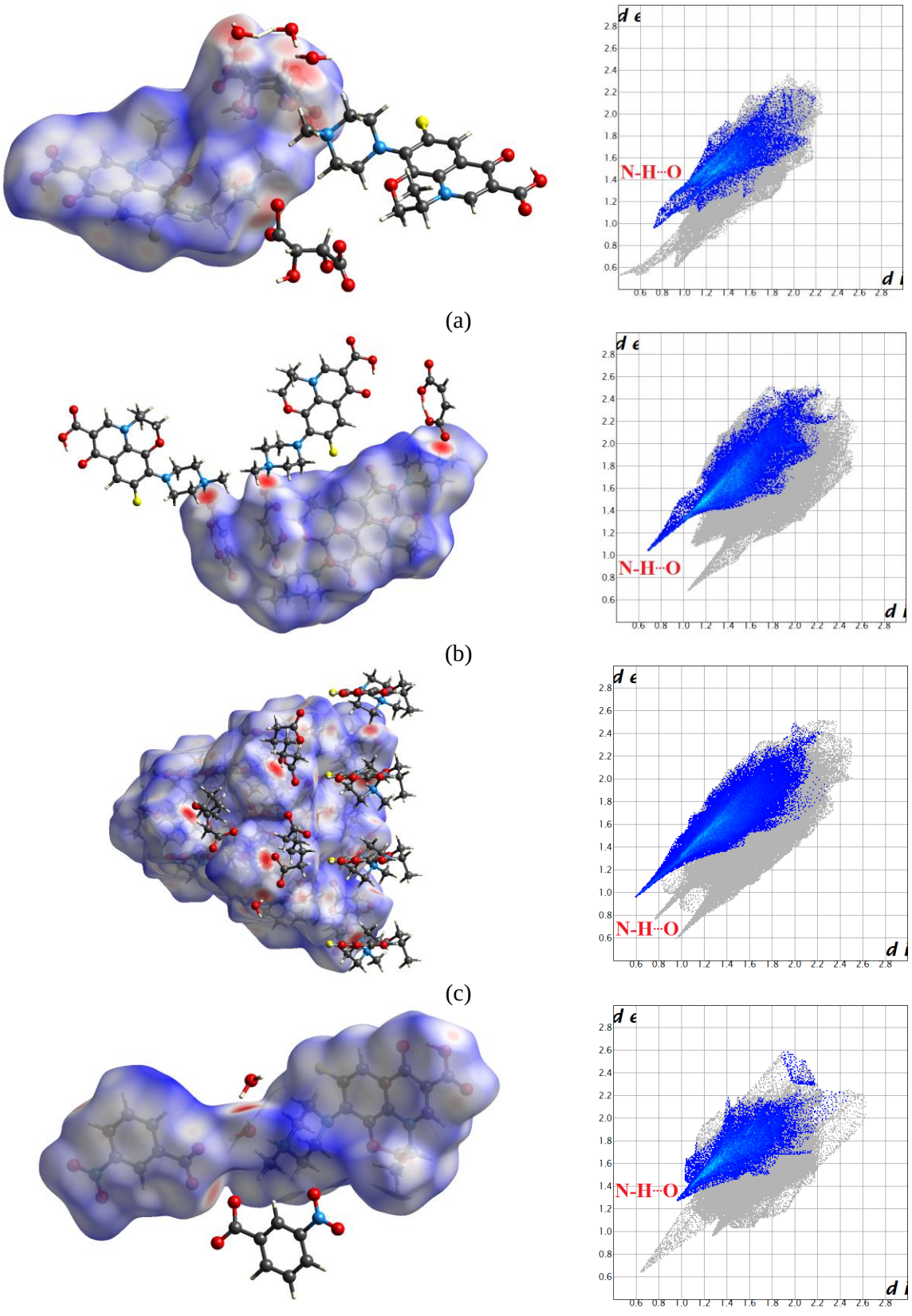

Figure 6.8: Hirshfeld surfaces and fingerprint plot of (a) LFX: D (-) Tartaric acid salt; (b) LFX: Maleic acid salt; (c) LFX: Pimelic acid salt and (d) LFX: 3-Nitrobenzoic acid salt.

Table 6.5: $log_{10}P$ values of LFX and its salts.

Name	$log_{10}P$
LFX	-0.39
D (-) Tartaric acid	-0.56
Maleic acid	-0.49
Succinic acid	-0.54
Salicylic acid	-0.84
L-malic acid	-0.57
Trans ferulic acid	-0.32
Pimelic acid	-0.51
Mandelic acid	-0.44
3-Nitrobenzoic acid	-0.72
Adipic acid	-0.50
Sorbic acid	-0.51

Table 6.6: Saturation Solubility Data of LFX and its salts.

Name	Solubility (mg/mL)
LFX	14.17
LFX: D (-) Tartaric acid	54.36
LFX: Maleic acid	50.26
LFX: Succinic acid	66.94
LFX: Salicylic acid	14.36
LFX: L-malic acid	128.14
LFX: Trans ferulic acid	329.44
LFX: Pimelic acid	287.97
LFX: Mandelic acid	21.75
LFX: 3-Nitrobenzoic acid	4.63
LFX: Adipic acid	405.14
LFX: Sorbic acid	773.21

6.3.8 Intrinsic Dissolution Rate Analysis

We have determined the IDR of the LFX salts and pure drug in PBS7 at 37 ºC. The IDR analysis indicated that the salts of LFX have a faster dissolution rate than the parent drug. Therefore, these salts of LFX could potentially be used in place of the parent drug for future formulations. These salts were stable in ambient air. Hence, the tablets of these salts could be made easily for IDR analysis. The intrinsic dissolution rate for the original drug and the selected salts is given in Table 6.7 LFX: adipic acid salt has shown maximum IDR 17.347 mg $min^{-1}cm^{-2}$, which is 16.7 times higher than LFX.

Table 6.7: IDR analysis of LFX and their salts at 37 ^{o}C.

Name	IDR (j) (mg min^{-1} cm^{-2})
LFX	1.04
LFX: D (-) Tartaric acid	4.13
LFX: Maleic acid	3.28
LFX: Succinic acid	2.43
LFX: Salicylic acid	1.64
LFX: L-malic acid	4.20
LFX: Trans ferulic acid	8.13
LFX: Pimelic acid	5.74
LFX: Mandelic acid	1.05
LFX: 3-Nitrobenzoic acid	1.62
LFX: Adipic acid	17.34
LFX: Sorbic acid	7.12

6.3.9 Minimum Inhibitory Concentration

The minimum inhibitory concentrations (MIC) of the LFX salts, namely LFX: maleic acid, LFX: succinic acid, LFX: L-malic acid, LFX: adipic acid, LFX: sorbic acid and LFX itself, because other salts were found hygroscopic, so we did not choose them for microbiological and biological analysis. The MIC of these salts and LFX were determined for *Escherichia Coli* and *Salmonella Typhimurium* gram-negative bacteria. All the salts showed lower MIC than LFX in *E. Coli* and *S. Typhimurium*, which means these salts are more potent in comparison to LFX. The MICs of the LFX: maleic acid, LFX: succinic acid and LFX: L (-) malic acid salts were observed to be more potent and show less concentration than LFX (in Table 6.8), which indicates that these salts have better efficacy than LFX.

Table 6.8: Minimum Inhibitory Concentration of LFX and its salts in gram negative bacteria.

Name	*E. Coli* (mmol / L)	*S. Typhimurium* (mmol / L)
LFX	11.07×10^{-5}	30.44×10^{-5}
LFX: Maleic acid	8.38×10^{-5}	23.04×10^{-5}
LFX: Succinic acid	8.34×10^{-5}	18.77×10^{-5}
LFX: L-malic acid	10.09×10^{-5}	20.18×10^{-5}
LFX: Adipic acid	9.85×10^{-5}	27.59×10^{-5}
LFX: Sorbic acid	8.45×10^{-5}	23.23×10^{-5}

6.3.10 *In-Vitro* Cell Line Assay

We have selected LFX: maleic acid, LFX: succinic acid and LFX: L-malic acid salts to check their efficacy in clearing off an infection of *S. Typhimurium* as their MICs indicated that they might have better efficacy than LFX. Towards this, we infected a human epithelial cell line, Caco-2, with *S.*

Typhimurium and checked the effect of these salts on the bacterial infection. The concentration at which the bacterial growth was limited to 50 % of the control (where no antibiotic was added) was considered as the Inhibitory concentration or IC_{50}. The IC_{50} values of the LFX: maleic acid, LFX: succinic acid salts were found to be lower than LFX, but LFX: L-malic acid salt showed IC_{50} comparable to LFX (Table 6.9). Interestingly, the IC_{50} value of the derivative LFX: succinic acid salt was 75 % lesser than LFX, as seen in Figure 6.9, indicating that LFX: succinic acid salt is much more potent than LFX because this salt may be invading more in the Caco-2 cells and *S. Typhimurium* bacteria as well.

Table 6.9: IC_{50} values of LFX and its derivatives.

Name	IC_{50}
LFX	0.0682
LFX: Maleic acid	0.06102
LFX: Succinic acid	0.01656
LFX: L-malic acid	0.0763

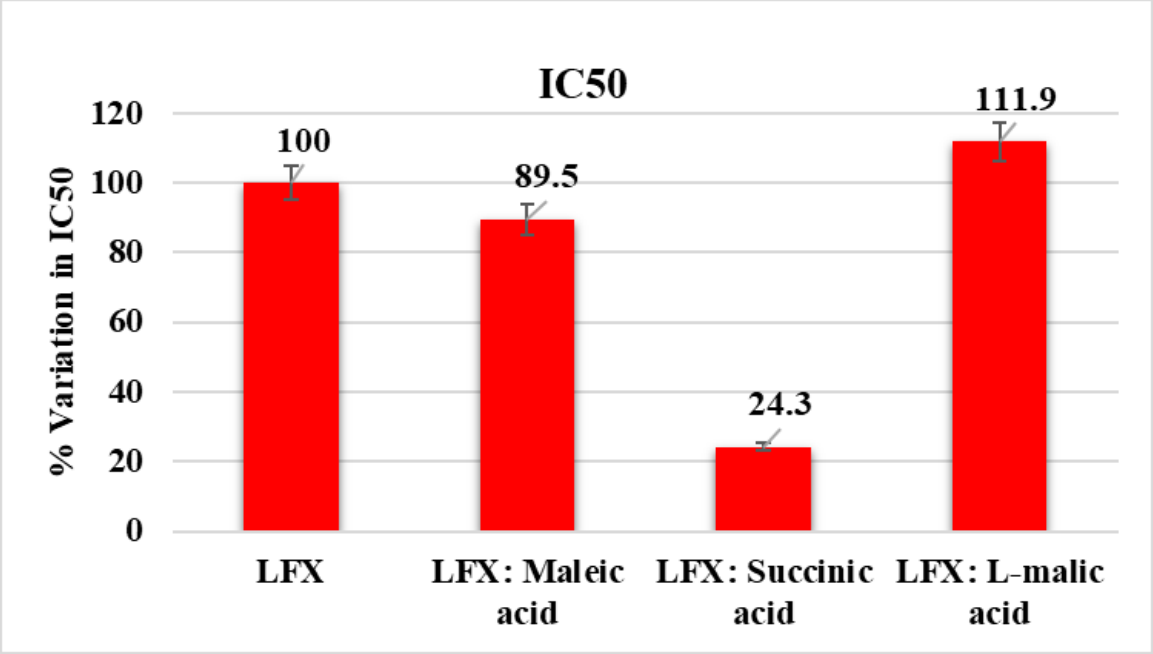

Figure 6.9: Graphical representation of Percentage fluctuations in potent concentrations of LFX and its salts for IC_{50} value.

6.3.11 Oral *in Vivo* Pharmacokinetic Studies

Since the solubility of these derivatives was shown to be better than LFX, the pharmacokinetic parameters of these salts might be better than LFX, thereby improving their efficacy even further. We performed the pharmacokinetic experiment of these derivatives in Balb/c mice via oral route to test this hypothesis. The concentration of plasma drug *versus* time graph for LFX obtained from all the treatments is shown in Figure 6.10.

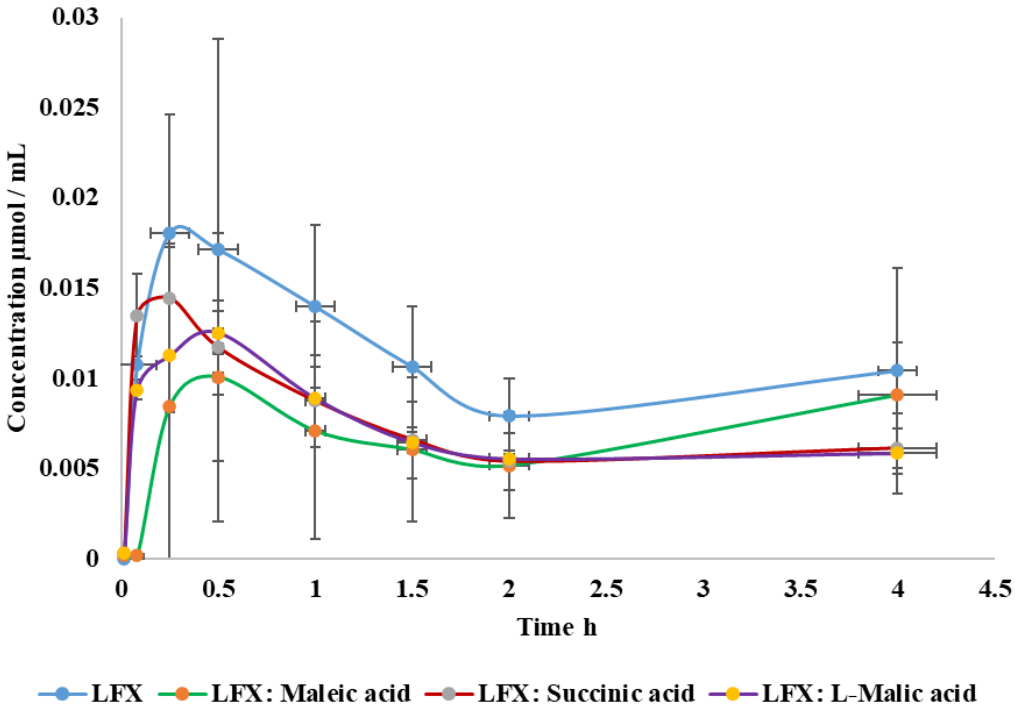

Figure 6.10: Graphical depiction of drug concentration in plasma of LFX and its salts.

It can be inferred from Figure 6.10 that higher drug concentrations were observed in the group receiving the LFX due to its slightly lipophilic nature than that for the groups receiving salts. As shown in Table 6.10, the bioavailable drug fraction was lower to pure LFX by approximately 3–4 times. C_{max} was comparable to LFX in LFX: succinic acid and LFX: L (-) malic acid salts but lower by 41% in LFX: maleic acid salt. $T_{1/2}$ was depressed by 1.87–5.82 times due to its hydrophilic nature. The absorption rate by LFX salts was observed to be approximately 0.69 to 2.45 times faster, and the elimination rate was substantially increased 1.87 to 5.82 times by LFX salts vis-à-vis plain drug, which indicates the hydrophilic nature of salts as seen in log P values also. Interestingly, T_{max} was substantially decreased in the groups receiving salts by 1–2.1 times. The findings are unique and infer the absorption mechanisms for all salts were faster absorbed. Overall, the conducive pharmacokinetic modulation inherits the promise of enhanced drug water solubility and faster action time.

Table 6.10: Tabular Representation of the Various *in Vivo* Pharmacokinetic Parameters.

Pharmacokinetic Parameters	Units	LFX	LFX: Maleic acid	LFX: Succinic acid	LFX: L (-) Malic acid
K_a	1/h	33.77	82.87	56.95	23.54
K	1/h	0.07	0.12	0.38	0.26
$T_{1/2}$	h	10.48	5.60	1.80	2.68
T_{max}	h	0.20	0.095	0.11	0.21
C_{max}	µg/mL	5.01	2.93	4.91	4.10
$[AUC]_0^{\infty}$	µg/mL×h	76.58	23.93	13.19	16.66

6.3.12 Biodistribution Studies

We treated the Balb/c mice orally with these derivatives and quantified their biodistribution and bioavailability in different vital organs, namely the liver, brain, kidney and heart, as shown in Figure 6.11. These graphs show the amount of the drug and its salts as a function of time in various organs after treating the data as per 1 CBM oral pharmacokinetic model; relevant pharmacokinetic parameters were calculated (Table 6.11). The values for K_a, K, $T_{1/2}$ and $[AUC]_0^{\infty}$ were calculated using one compartment-based model oral drug delivery, while C_{max} and T_{max} are reported from the graphs observed in Figure 6.11. We found that absorption and elimination rates of all salts are higher in the heart, kidney, liver and brain. $T_{1/2}$ were decreased for all salts in the brain, so it shows maximum effect in lesser time than LFX but $t_{1/2}$ increased for all salts in the liver, which indicates that salts stay for more time in the liver than LFX (Table 6.11). T_{max} of these salts was reached in a short time or equal time in the heart, kidney and brain, but this time increased in the liver. The decreased bioavailable fraction and increased T_{max} of salts support the bypass of the liver by LFX salts to that of pure drug. C_{max} was achieved much higher than LFX in the kidney and brain whereas lower in the heart and liver. Kidney, liver and brain bioavailability through LFX salts were enhanced compared to that of pure LFX but decreased in the heart.

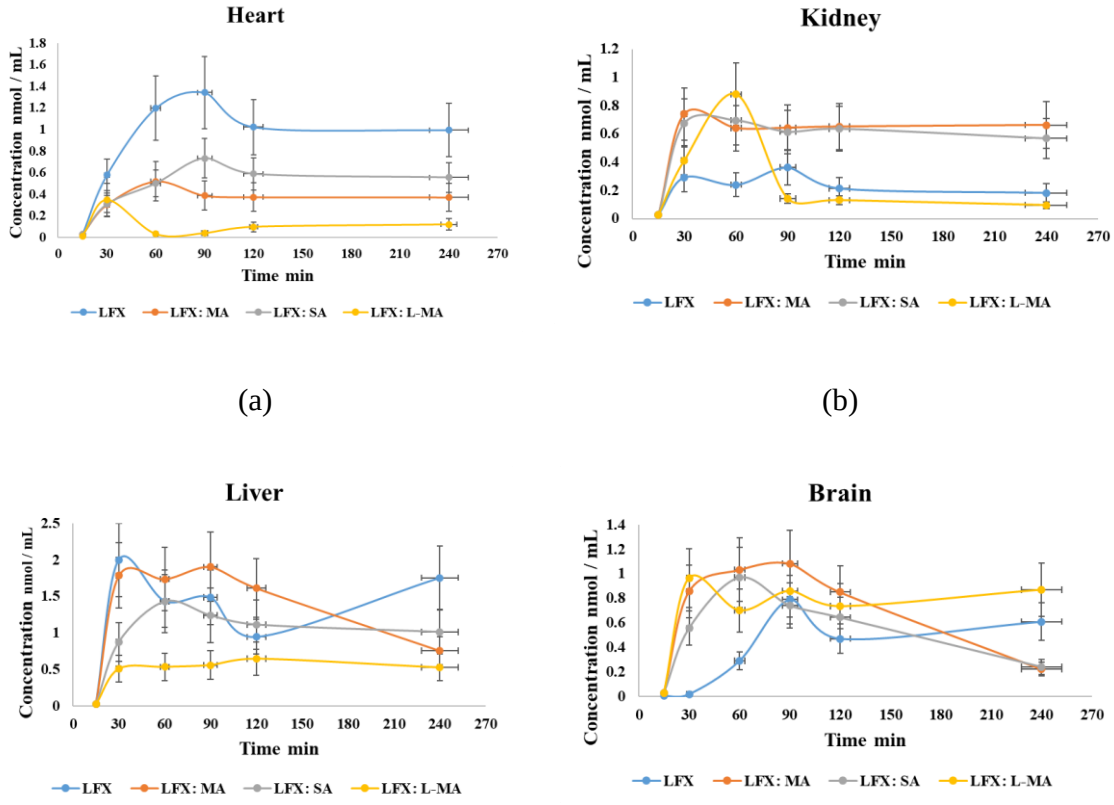

Figure 6.11: Biodistribution of LFX and its salts in heart, kidney, liver and brain in the studied animal group.

Table 6.11: Tabular Representation of the Pharmacokinetic Parameters for Heart, Kidney, Liver, and Brain.

Parameters \ Salts	**K_a**	**K**	**$T_{1/2}$**	**T_{max}**	**C_{max}**	**$[AUC]_0^\infty$**
Units	**1/min**	**1/min**	**min**	**min**	**nmol mL^{-1}**	**nmol mL^{-1} min^{-1}**
Heart						
LFX	0.0496	6.437×10^{-5}	13.97	90	1.34	19358.68
LFX: MA	0.0992	0.0014	8.35	60	0.52	1072.84
LFX: SA	0.3795	0.0071	47.21	90	0.73	257.90
LFX: L-MA	0.7648	0.0668	0.91	30	0.35	12.94
Kidney						
LFX	0.1788	0.0024	3.88	90	0.36	131.97
LFX: MA	1.0005	0.0003	0.69	30	0.74	1982.44
LFX: SA	0.4237	0.0020	3.86	60	0.70	3539.83
LFX: L-MA	0.0359	0.0339	19.30	60	0.88	38.38
Liver						
LFX	1.1076	0.0003	0.63	30	2.00	5701.03
LFX: MA	0.0709	0.0063	18.53	90	1.91	451.79
LFX: SA	0.1245	0.0022	9.86	60	1.43	334.83×10^3
LFX: L-MA	0.1071	0.0011	6.55	120	0.65	312.70×10^3
Brain						
LFX	0.0288	0.0010	24.11	90	0.79	713.33
LFX: MA	0.0618	0.0118	21.94	90	1.08	195.88
LFX: SA	0.3103	0.0057	14.63	60	0.97	201.13
LFX: L-MA	0.6376	0.0010	2.09	30	0.96	448.29×10^3

6.4 Conclusion

We have formed the salts of Levofloxacin with various organic acids using a simple solvent drop assisted grinding method with rational use of ΔpK_a rule of three. These salts are characterized by PXRD and DSC. We found four single crystals of LFX with D (-) tartaric acid, maleic acid, pimelic acid and 3-nitrobenzoic acid and these all are crystallized in chiral space groups *C*2 and $P2_1$. The salts are formed by transferring an acidic proton from the coformers to the piperazine ring of LFX and forming an N–H···O hydrogen bond. The partition coefficient has confirmed the hydrophilic nature of these salts. The majority of the novel salts indicated enhancement in solubility in phosphate buffer solution at pH 7 at 37 °C. The intrinsic dissolution rate study establishes that these salts have significantly higher dissolution rates compared to the parent drug. Most water-soluble non-hygroscopic salts have been

chosen for MIC studies in gram-negative bacteria. These salts have shown significant improvement in MIC in both *E. Coli* and *S. Typhimurium*.

Further, we have calculated the inhibitory concentrations (IC_{50}) by infecting an epithelial cell line, Caco2, with *S. Typhimurium* infection. LFX: succinic acid salt has shown significant improvement in IC_{50} (up to four times of LFX). Pharmacokinetic study of these salts demonstrated that these salts are water-soluble, and considerable progress in pharmacokinetic parameters has been achieved. The novel salts have been tested for their bioavailability *in vivo* using Balb/c mice which indicated that these drugs were better absorbed in the vital organs after being consumed. Since the IC_{50} values of LFX: Maleic acid and LFX: succinic acid salts were also lower, which showed better bio-availability than LFX, it further implies that these would be better drugs candidates than LFX. With the emerging multi-drug resistant (MDR) bacteria, LFX: succinic acid and LFX: maleic acid salts would be better alternatives to LFX.

Concluding Remarks

Pharmaceutical cocrystallization provides an alternative path to modify the physical properties of the active pharmaceutical ingredients in an economical way. We have used the concepts of crystal engineering and utilized the rational of the ΔpK_a rule of three for developing the new cocrystals/salts of three psychiatric drugs (Amoxapine, Doxepin and Zaleplon) and two widely used antibiotics (Ofloxacin and Levofloxacin). We have used these drugs to develop new salts/cocrystals with suitably selected coformers, which are generally regarded as safe for biological use, in a stoichiometric ratio by various experimental methods. We have characterized these new compounds using both powder and single crystal X-ray diffraction technique, differential scanning calorimetry etc.

Hydrogen bond plays a vital role in the development of these new cocrystals/salts. It interlinks the drug molecule with the coformer with or without transferring the acidic proton to the API and with or without the presence of water of crystallization. We have changed the physical properties of the pure medicinal compounds by the formation of cocrystals/salts. We have made a stable solid crystalline phase of liquid drug doxepin at room temperature. Amoxapine and D (-) tartaric acid salt crystallizes in the chiral space group $P2_1$ while the other cocrystals/salts of AMX, DOX, and ZLP go into the non-chiral space group. The chiral drug levofloxacin formed salts in the chiral space group $C2$ and $P2_1$ with the coformers. All these compounds have formed heterosynthons involving the API and the coformers through strong and weak hydrogen bonding. Crystal packing of these compounds reveals the alternative layers of API and acid/acid-water channel by strong and weak hydrogen bonds, van der Waals' forces etc. Hirshfeld surfaces and fingerprint plots also support these surface interactions and strong hydrogen bonding, and hydrogen atom came as a maximum interacting atom in these HSs.

These alternate channels of drug and coformer might be the possible reason for the enhancement in the physical properties like solubility and intrinsic dissolution rate. The saturation solubility of these cocrystals/salts have been improved by many folds than the pure drug in most of the cases. We have recorded a better intrinsic dissolution profile of these compounds than API. These phenomena are supported by the partition coefficient, which indicates the hydrophilic nature of these new cocrystals/salts. The minimum inhibition concentration of the new salts of OFX and LFX was determined. LFX salts show significant results in *E. Coli* and *S. Typhimurium* gram-negative bacteria. As the salts of OFX did not show improved results in *E. Coli*, we did not move further for biological studies with the OFX salts. We have noticed four times potent inhibitory concentration (IC_{50}) in the Caco-2 cell line infected with S. Typhimurium bacteria for the LFX: succinic acid salt than LFX. The pharmacokinetic profile of the LFX salts supports the hydrophilicity of compounds because their rate of absorption and elimination rate was found to increase. The biodistribution profile of these LFX salts indicates that these salts are more bioavailable in the brain and kidney than the heart and liver of the Balb/c mice. So, these salts can be used in brain and kidney infections as an alternative to LFX. LFX:

succinic acid salt has shown better physical as well as biological properties among all the salts of LFX and pure drug LFX. These improved salts/cocrystals can be taken further for their clinical trials and future formulations as an alternative of the pure API with improved physical properties.

References

(1) Bernstein, J.; Henck, J. O. Disappearing and Reappearing Polymorphs - An Anathema to Crystal Engineering? *Mater. Res. Bull.* **1998**, *33*, 119–128.

(2) Desiraju, G. R. Crystal Engineering: From Molecule to Crystal. *J. Am. Chem. Soc.* **2013**, 9952–9967.

(3) Jensen, L. G.; Skautrup, F. B.; Müllertz, A.; Abrahamsson, B.; Rades, T.; Priemel, P. A. Amorphous Is Not Always Better—A Dissolution Study on Solid State Forms of Carbamazepine. *Int. J. Pharm.* **2017**, *522* (1–2), 74–79.

(4) Lee, A. Y.; Erdemir, D.; Myerson, A. S. Crystal Polymorphism in Chemical Process Development. *Annu. Rev. Chem. Biomol. Eng.* **2011**, 259–280.

(5) Yu, L.; Stephenson, G. A.; Mitchell, C. A.; Bunnell, C. A.; Snorek, S. V.; Bowyer, J. J.; Borchardt, T. B.; Stowell, J. G.; Byrn, S. R. Thermochemistry and Conformational Polymorphism of a Hexamorphic Crystal System. *J. Am. Chem. Soc.* **2000**, *122* (4), 585–591.

(6) Wang, C. X.; Yang, G. W. Thermodynamics of Metastable Phase Nucleation at the Nanoscale. *Mater. Sci. Eng. R Rep.* **2005**, 157–202.

(7) York, P. Solid-State Properties of Powders in the Formulation and Processing of Solid Dosage Forms. *Int. J. Pharm.* **1983**, 1–28.

(8) Duchêne, D.; Ponchel, G. Principle and Investigation of the Bioadhesion Mechanism of Solid Dosage Forms. *Biomaterials.* **1992**, *13* (10), 709–714.

(9) Petereit, H. U.; Weisbrod, W. Formulation and Process Considerations Affecting the Stability of Solid Dosage Forms Formulated with Methacrylate Copolymers. *Eur. J. Pharm. Biopharm.* **1999**, 15–25.

(10) Gerhardt, A. H. Moisture Effects on Solid Dosage Forms—Formulation, Processing, and Stability. *J. GXP Compliance.* **2009**, *13* (1), 58–67.

(11) Khatri, P.; Shah, M. K.; Vora, N. Formulation Strategies for Solid Oral Dosage Form Using 3D Printing Technology: A Mini-Review. *J. Drug Deliv. Sci. Technol.* **2018**, 148–155.

(12) Fuenmayor, E.; Forde, M.; Healy, A. V.; Devine, D. M.; Lyons, J. G.; McConville, C.; Major, I. Material Considerations for Fused-Filament Fabrication of Solid Dosage Forms. *Pharmaceutics.* **2018**, *10* (2), 1–27.

(13) Salamanca, C. H.; Barrera-Ocampo, A.; Lasso, J. C.; Camacho, N.; Yarce, C. J. Franz Diffusion Cell Approach for Pre-Formulation Characterisation of Ketoprofen Semi-Solid Dosage Forms. *Pharmaceutics.* **2018**, *10* (3).

(14) Glass, B. D.; Haywood, A. Stability Considerations in Liquid Dosage Forms Extemporaneously Prepared from Commercially Available Products. *J. Pharm. Pharm. Sci.* **2006**, *9* (3), 398–426.

(15) Davis, S. S.; Hardy, J. G.; Taylor, M. J.; Whalley, D. R.; Wilson, C. G. A Comparative Study of the Gastrointestinal Transit of a Pellet and Tablet Formulation. *Int. J. Pharm.* **1984**, *21* (2), 167–177.

(16) Conway, B. R. Solid Dosage Forms. *Pharmaceutical Sciences Encyclopedia.* **2010**, 1–31.

(17) Gotoh, K. Powder Characteristics for Index of Powder Unit Operation. *J. Taiwan Inst. Chem. Eng.* **2018**, *90*, 4–8.

(18) Ali, H. S.; Suliman, R. S. R.; Elhaj, B. M. A.; Suliman, R. S. R.; Saad Ali, H.; Saad Suliman, R.; A Elhaj, B. M.; Suliman, R. S. R. Pharmaceutical Powder Dosage Forms: A Review. *Int. J. Pharm. Clin. Res.* **2019**, *11* (1), 20–22.

(19) CALVERT, R. Report on the Use of Charcoal Powder as a Substitute for Cinchona. *New Engl. J. Med. Surg. Collat. Branches Sci.* **1815**, *4* (1), 86–88.

(20) Strickley, R. G.; Iwata, Q.; Wu, S.; Dahl, T. C. Pediatric Drugs - Review of Commercially Available Oral Formulations. *J. Pharm. Sci*. **2008**, 1731–1774.

(21) Tsuneji, N.; Yuji, N.; Naoki, N.; Yoshiki, S.; Kunio, S. Powder Dosage Form of Insulin for Nasal Administration. *J. Control. Release* **1984**, *1* (1), 15–22.

(22) Barnhart, S. D. Thin Film Oral Dosage Forms. *Modified-Release Drug Delivery Technology*, **2008**, *1*, 209–216.

(23) Milne, I.; Bayer, M.; Cardle, L.; Shaw, P.; Stephen, G.; Wright, F.; Marshall, D. Tablet-next Generation Sequence Assembly Visualization. *Bioinformatics*. **2009**, 401–402.

(24) Kerz, T.; Paret, G.; Herff, H. Routes of Drug Administration. *Card. Arrest Sci. Pract. Resusc. Med.* **2007**, *I* (I), 614–638.

(25) Zaman, N. N.; Sopyan, I. Tablet Manufacturing Process Method and Defect Of Tablets. *Maj. Farmasetika* **2020**, *5* (2), 24368–24374.

(26) Gavi, E.; Reynolds, G. K. System Model of a Tablet Manufacturing Process. *Comput. Chem. Eng.* **2014**, *71*, 130–140.

(27) Syed, S. M. A d v a n c e s i n B i o r e s e a r c h Mini-Tablet : A Review. **2016**, 5–10.

(28) Verma, S.; Tippavajhala, V. K. A Review on the Polymers for Vegetarian Soft Gel Capsule Films. *Res. J. Pharm. Technol*. **2017**, 3217–3222.

(29) Srividya, B.; Reddy, C. S. C. S. P. Capsules And It'S Technology: An Overview. *Int. J. Pharm. Drug Anal.* **2014**, *2* (9), 727–733.

(30) Qiu, Y.; Chen, Y.; Zhang, G. G. Z.; Yu, L.; Mantri, R. V. Developing Solid Oral Dosage Forms. *Pharmaceutical Theory and Practice*. **2016**.

(31) Javadzadeh, Y.; Siahi-Shadbad, M. R.; Barzegar-Jalali, M.; Nokhodchi, A. Enhancement of Dissolution Rate of Piroxicam Using Liquisolid Compacts. *Farmaco* **2005**, *60* (4), 361–365.

(32) Kline & Company. Solubility Enhancement in Pharmaceutical Oral Solid Dosage Forms: Global Market Analysis and Opportunities https://klinegroup.com/reports/solubility_enhancement_pharmaceutical_oral_solid_dosage_forms/ (accessed May 31, 2021).

(33) Paus, R.; Prudic, A.; Ji, Y. Influence of Excipients on Solubility and Dissolution of Pharmaceuticals. *Int. J. Pharm.* **2015**, *485* (1–2), 277–287.

(34) Aggarwal, S.; Gupta, G.; Chaudhary, S. SOLID DISPERSION AS AN EMINENT STRATEGIC Approach in Solubility Enhancement of Poorly Soluble Drugs. *Int. J. Pharm. Sci. Res.* **2010**, *1* (8), 1–13.

(35) Dahan, A.; Wolk, O.; Kim, Y. H.; Ramachandran, C.; Crippen, G. M.; Takagi, T.; Bermejo, M.; Amidon, G. L. Purely in Silico BCS Classification: Science Based Quality Standards for the World's Drugs. *Mol. Pharm.* **2013**, *10* (11), 4378–4390.

(36) L, B. A.; K., S. S.; V, P. S. Enhancement of Solubility: A Pharmaceutical Overview. *Der Pharm. Lett.* **2010**, *2* (2), 310–318.

(37) Panchagnula, R.; Thomas, N. S. Biopharmaceutics and Pharmacokinetics in Drug Research. *Int. J. Pharm*. **2000**, 131–150.

(38) Warren, F. Handbook of Pharmaceutical Excipients. *Am. J. Heal. Pharm.* **1987**, *44* (8), 1946–1948.

(39) Vadlamudi, M. K.; Dhanaraj, S. Significance of Excipients to Enhance the Bioavailability of Poorly Water-Soluble Drugs in Oral Solid Dosage Forms: A Review. *Mat. Sci. Eng.* **2017,** *263*, 022023.

(40) Verma, V.; Sharma, P.; Sharma, J.; Kaur Lamba, A.; Lamba, H. S. Development, Characterization and Solubility Study of Solid Dispersion of Quercetin by Solvent Evaporation Method. *Mat. Today: Proceedings*. **2017**; *4*, 10128–10133.

(41) Craig, D. Q. M. The Mechanisms of Drug Release from Solid Dispersions in Water-Soluble Polymers. *Int. J. Pharm*. **2002**, 131–144.

(42) Sharma, D.; Soni, M.; Kumar, S.; Gupta, G. Solubility Enhancement – Eminent Role in Poorly Soluble Drugs. *Res. J. Pharm. Technol.* **2009**, *2* (2), 220–224.

(43) Desiraju, G. R. Crystal Engineering: A Holistic View. *Angew. Chem. Int. Ed*. **2007**, 8342–8356.

(44) Aitipamula, S.; Banerjee, R.; Bansal, A. K.; Biradha, K.; Cheney, M. L.; Choudhury, A. R.; Desiraju, G. R.; Dikundwar, A. G.; Dubey, R.; Duggirala, N.; Ghogale, P. P.; Ghosh, S.; Goswami, P. K.; Goud, N. R.; Jetti, R. R. K. R.; Karpinski, P.; Kaushik, P.; Kumar, D.; Kumar, V.; Moulton, B.; Mukherjee, A.; Mukherjee, G.; Myerson, A. S.; Puri, V.; Ramanan, A.; Rajamannar, T.; Reddy, C. M.; Rodriguez-Hornedo, N.; Rogers, R. D.; Row, T. N. G.; Sanphui, P.; Shan, N.; Shete, G.; Singh, A.; Sun, C. C.; Swift, J. A.; Thaimattam, R.; Thakur, T. S.; Kumar Thaper, R.; Thomas, S. P.; Tothadi, S.; Vangala, V. R.; Variankaval, N.; Vishweshwar, P.; Weyna, D. R.; Zaworotko, M. J. Polymorphs, Salts, and Cocrystals: What's in a Name? *Cryst. Growth Des*. **2012**, 2147–2152.

(45) Bailey Walsh, R. D.; Bradner, M. W.; Fleischman, S.; Morales, L. A.; Moulton, B.; Rodríguez-Hornedo, N.; Zaworotko, M. J. Crystal Engineering of the Composition of Pharmaceutical Phases. *Chem. Commun.* **2003**, *0* (2), 186–187.

(46) EMA. Reflection Paper on the Use of Cocrystals and Other Solid State Forms of Active Substances in Medicinal Products. *Eur. Med. Agency* **2015**, *44* (May), 1–10.

(47) Wood, P. A.; Feeder, N.; Furlow, M.; Galek, P. T. A.; Groom, C. R.; Pidcock, E. Knowledge-Based Approaches to Co-Crystal Design. *CrystEngComm* **2014**, *16* (26), 5839–5848.

(48) Shan, N.; Zaworotko, M. J. The Role of Cocrystals in Pharmaceutical Science. *Drug Discovery Today*. **2008**, 440–446.

(49) Cruz-Cabeza, A. J. Acid–Base Crystalline Complexes and the PKa Rule. *CrystEngComm* **2012**, *14* (20), 6362.

(50) Sarma, B.; Nath, N. K.; Bhogala, B. R.; Nangia, A. Synthon Competition and Cooperation in Molecular Salts of Hydroxybenzoic Acids and Aminopyridines. *Cryst. Growth Des.* **2009**, *9* (3), 1546–1557.

(51) Cruz-Cabeza, A. J. Acid-Base Crystalline Complexes and the PKa Rule. *CrystEngComm* **2012**, *14* (20), 6362–6365.

(52) Desiraju, G. R. Crystal Engineering: From Molecule to Crystal. *J. Am. Chem. Soc*. **2013**, 9952–9967.

(53) Eddaoudi, M.; Moler, D. B.; Li, H.; Chen, B.; Reineke, T. M.; O'Keeffe, M.; Yaghi, O. M. Modular Chemistry: Secondary Building Units as a Basis for the Design of Highly Porous and Robust Metal-Organic Carboxylate Frameworks. *Acc. Chem. Res.* **2001**, *34* (4), 319–330.

(54) Jones, J. T. A.; Hasell, T.; Wu, X.; Bacsa, J.; Jelfs, K. E.; Schmidtmann, M.; Chong, S. Y.; Adams, D. J.; Trewin, A.; Schiffman, F.; Cora, F.; Slater, B.; Steiner, A.; Day, G. M.; Cooper, A. I. Modular and Predictable Assembly of Porous Organic Molecular Crystals. *Nature* **2011**, *474* (7351), 367–371.

(55) Salmon, D. J. Building Co-Crystals with Molecular Sense and Supramolecular Sensibility Highlight. *Cryst. Eng.* **2005**, *7* (72), 439–448.

(56) Thomas, J. M. Crystal Engineering: Origins, Early Adventures and Some Current Trends. *CrystEngComm* **2011**, *13* (13), 4304.

(57) Desiraju, G. R. A Bond by Any Other Name. *Angew. Chemie - Int. Ed.* **2011**, *50* (1), 52–59.

(58) Hathwar, V. R.; Thakur, T. S.; Guru Row, T. N.; Desiraju, G. R. Transferability of Multipole Charge Density Parameters for Supramolecular Synthons: A New Tool for Quantitative Crystal Engineering. *Cryst. Growth Des.* **2011**, *11* (2), 616–623.

(59) Kastelic, J.; Lah, N.; Kikelj, D.; Leban, I. A 1:1 Cocrystal of Fluconazole with Salicylic Acid. *Acta Crystallogr. Sect. C Cryst. Struct. Commun.* **2011**, *67* (9), o370–o372.

(60) Aitipamula, S.; Vangala, V. R.; Chow, P. S.; Tan, R. B. H. Cocrystal Hydrate of an Antifungal Drug, Griseofulvin, with Promising Physicochemical Properties. *Cryst. Growth Des.* **2012**, *12* (12), 5858–5863.

(61) Yan, Y.; Chen, J. M.; Geng, N.; Lu, T. B. Improving the Solubility of Agomelatine via Cocrystals. *Cryst. Growth Des.* **2012**, *12* (5), 2226–2233.

(62) Mannava, M. K. C.; Suresh, K.; Nangia, A. Enhanced Bioavailability in the Oxalate Salt of the Anti-Tuberculosis Drug Ethionamide. *Cryst. Growth Des.* **2016**, *16* (3), 1591–1598.

(63) Clarke, H. D.; Hickey, M. B.; Moulton, B.; Perman, J. A.; Peterson, M. L.; Wojtas, Ł.; Almarsson, Ö.; Zaworotko, M. J. Crystal Engineering of Isostructural Quaternary Multicomponent Crystal Forms of Olanzapine. *Cryst. Growth Des.* **2012**, *12* (8), 4194–4201.

(64) Thakuria, R.; Nangia, A. Olanzapinium Salts, Isostructural Solvates, and Their Physicochemical Properties. *Cryst. Growth Des.* **2013**, *13* (8), 3672–3680.

(65) Karanam, M.; Dev, S.; Choudhury, A. R. New Polymorphs of Fluconazole: Results from Cocrystallization Experiments. *Cryst. Growth Des.* **2012**, *12* (1), 240–252.

(66) Karanam, M.; Choudhury, A. R. Structural Landscape of Pure Enrofloxacin and Its Novel Salts: Enhanced Solubility for Better Pharmaceutical Applicability. *Cryst. Growth Des.* **2013**, *13* (4), 1626–1637.

(67) Almarsson, Ö.; Zaworotko, M. J. Crystal Engineering of the Composition of Pharmaceutical Phases. Do Pharmaceutical Co-Crystals Represent a New Path to Improved Medicines? *Chem. Comm*. **2004**, 1889–1896.

(68) Cheney, M. L.; Weyna, D. R.; Shan, N.; Hanna, M.; Wojtas, L.; Zaworotko, M. J. Coformer Selection in Pharmaceutical Cocrystal Development: A Case Study of a Meloxicam Aspirin Cocrystal That Exhibits Enhanced Solubility and Pharmacokinetics. *J. Pharm. Sci.* **2011**, *100* (6), 2172–2181.

(69) Cheney, M. L.; Weyna, D. R.; Shan, N.; Hanna, M.; Wojtas, L.; Zaworotko, M. J. Supramolecular Architectures of Meloxicam Carboxylic Acid Cocrystals, a Crystal Engineering Case Study. *Cryst. Growth Des.* **2010,** *10*, 4401–4413.

(70) Smith, A. J.; Kavuru, P.; Wojtas, L.; Zaworotko, M. J.; Shytle, R. D. Cocrystals of Quercetin with Improved Solubility and Oral Bioavailability. *Mol. Pharm.* **2011**, *8* (5), 1867–1876.

(71) Duggirala, N. K.; Perry, M. L.; Almarsson, Ö.; Zaworotko, M. J. Pharmaceutical Cocrystals: Along the Path to Improved Medicines. *Chem. Commun.* **2016**, *52* (4), 640–655.

(72) Shan, N.; Perry, M. L.; Weyna, D. R.; Zaworotko, M. J. Impact of Pharmaceutical Cocrystals: The Effects on Drug Pharmacokinetics. *Expert Opin. Drug Metab. Toxicol*. **2014**, 1255–1271.

(73) Friščić, T.; Jones, W. Benefits of Cocrystallisation in Pharmaceutical Materials Science: An Update. *J. Pharm. Pharmacol*. **2010**, 1547–1559.

(74) Brittain, H. G. Cocrystal Systems of Pharmaceutical Interest: 2009. *Profiles Drug Subst. Excip. Relat. Methodol.* **2011,** *36*, 361–381.

(75) Brittain, H. G. Cocrystal Systems of Pharmaceutical Interest: 2010. *Cryst. Growth Des*. **2012**, 1046–1054.

(76) Brittain, H. G. Cocrystal Systems of Pharmaceutical Interest: 2011. *Cryst. Growth Des.* **2012**, *12* (11), 5823–5832.

(77) Brittain, H. G. Pharmaceutical Cocrystals: The Coming Wave of New Drug Substances. *J. Pharm. Sci.* **2013**, *102* (2), 311–317.

(78) Cohen, B. M.; Harris, P. Q.; Altesman, R. I.; Cole, J. O. Amoxapine: Neuroleptic as Well as Antidepressant? *Am. J. Psychiatry* **1982**, *139* (9), 1165–1167.

(79) Ban, T. A.; Fujimori, M.; Petrie, W. M.; Ragheb, M.; Wilson, W. H. Systematic Studies with Amoxapine, a New Antidepressant. *Int. Pharmacopsychiatry* **1982**, *17* (1), 18–27.

(80) Lydiard, R. B.; Gelenberg, A. J. Amoxapine — An Antidepressant With Some Neuroleptic Properties?: A Review of Its Chemistry, Animal Pharmacology and Toxicology, Human Pharmacology, and Clinical Efficacy. *Pharmacother. J. Hum. Pharmacol. Drug Ther.* **1981**, *1* (3), 163–178.

(81) Stewart D., Stavness C., King G., Antle B., L. M. A Critical Appraisal Of. *EmbasePhysical Occup. Ther. Pediatr.* **2006**, *42* (6), 238–242.

(82) Kinney, J. L.; Evans, R. L. J. Evaluation of Amoxapine. *Clin. Pharm.* **1982**, *1* (5), 417–424.

(83) Wander, T. J.; Nelson, A.; Haruo Okazaki; Richelson, E. Antagonism by Antidepressants of Serotonin S1 and S2 Receptors of Normal Human Brain in Vitro. *Eur. J. Pharmacol.* **1986**, *132* (2–3), 115–121.

(84) Richelson, E.; Nelson, A. Antagonism by Neuroleptics of Neurotransmitter Receptors of Normal Human Brain in Vitro. *Eur. J. Pharmacol.* **1984**, *103* (3–4), 197–204.

(85) Cells, G.; Graveleau, C.; Paust, H.-J.; Schmidt-grimminger, D.; Mukhopadhyay, A. K. Presence of a 5-HT 7 Receptor Positively Coupled to Adenylate Cyclase Activation in Human. *J. Clin. Endocrinol. Metab.* **2009**, *85* (3), 1277–1286.

(86) Apiquian, R.; Ulloa, E.; Fresan, A.; Loyzaga, C.; Nicolini, H.; Kapur, S. Amoxapine Shows Atypical Antipsychotic Effects in Patients with Schizophrenia: Results from a Prospective Open-Label Study. *Schizophr. Res.* **2003**, *59* (1), 35–39.

(87) Braga, D.; Curzi, M.; Dichiarante, E.; Giaffreda, S. L.; Grepioni, F.; Maini, L.; Palladino, G.; Pettersen, A.; Polito, M. Making Crystals from Crystals: A Solid-State Route to the Engineering of Crystalline Materials, Polymorphs, Solvates and Co-Crystals; Considerations on the Future of Crystal Engineering. *NATO Sci. Peace Secur. Ser. B Phys. Biophys.* **2008**, 131–156.

(88) Almarsson, Ö.; Zaworotko, M. J. Crystal Engineering of the Composition of Pharmaceutical Phases. Do Pharmaceutical Co-Crystals Represent a New Path to Improved Medicines? *Chem. Comm*. **2004**, 1889–1896.

(89) Khankari, R. K.; Grant, D. J. W. Pharmaceutical Hydrates. *Thermochim. Acta* **1995**, *248* (C), 61–79.

(90) Childs, S. L.; Stahly, G. P.; Park, A. The Salt-Cocrystal Continuum: The Influence of Crystal Structure on Ionization State. *Mol. Pharm.* **2007**, *4* (3), 323–338.

(91) Sun, Y.; Zhu, L.; Wu, T.; Cai, T.; Gunn, E. M.; Yu, L. Stability of Amorphous Pharmaceutical Solids: Crystal Growth Mechanisms and Effect of Polymer Additives. *AAPS J*. **2012**, 380–388.

(92) FDA. Substances Added to Food (Formerly EAFUS). **2020**, 7–8.

(93) Good, D. J.; Naír, R. H. Solubility Advantage of Pharmaceutical Cocrystals. *Cryst. Growth Des.* **2009**, *9* (5), 2252–2264.

(94) Aakeröy, C. B.; Forbes, S.; Desper, J. Using Cocrystals to Systematically Modulate Aqueous Solubility and Melting Behavior of an Anticancer Drug. *J. Am. Chem. Soc.* **2009**, *131* (47), 17048–17049.

(95) Jung, M. S.; Kim, J. S.; Kim, M. S.; Alhalaweh, A.; Cho, W.; Hwang, S. J.; Velaga, S. P. Bioavailability of Indomethacin-Saccharin Cocrystals. *J. Pharm. Pharmacol.* **2010**, *62* (11), 1560–1568.

(96) Wang, C.; Paul, S.; Sun, D. J.; Nilsson Lill, S. O.; Sun, C. C. Mitigating Punch Sticking Propensity of Celecoxib by Cocrystallization: An Integrated Computational and Experimental Approach. *Cryst. Growth Des.* **2020**, *20* (7), 4217–4223.

(97) Calvo, M. B.; Garcia, M. J.; Pedraz, J. L.; Dominguez-Gil, A. Bioavailability of Amoxapine in Experimental Animals. *Boll. Chim. Farm.* **1986**, *125* (8), 307–311.

(98) Tamblyn, K. C.; Conner, D. E. Bactericidal Activity of Organic Acids against Salmonella Typhimurium Attached to Broiler Chicken Skin. *J. Food Prot.* **1997**, *60* (6), 629–633.

(99) Dolomanov, O. V.; Bourhis, L. J.; Gildea, R. J.; Howard, J. A. K.; Puschmann, H. OLEX2: A Complete Structure Solution, Refinement and Analysis Program. *J. Appl. Crystallogr.* **2009**, *42* (2), 339–341.

(100) Sheldrick, G. M. Crystal Structure Refinement with SHELXL. *Acta Crystallogr. Sect. C Struct. Chem.* **2015**, *71* (1), 3–8.

(101) Sheldrick, G. M. A Short History of SHELX. *Acta Crystallogr. Sect. A: Found. Cryst*. **2008**, 112–122.

(102) Macrae, C. F.; Bruno, I. J.; Chisholm, J. A.; Edgington, P. R.; McCabe, P.; Pidcock, E.; Rodriguez-Monge, L.; Taylor, R.; Van De Streek, J.; Wood, P. A. Mercury CSD 2.0 - New Features for the Visualization and Investigation of Crystal Structures. *J. Appl. Cryst*. **2008**, 466–470.

(103) Spackman, M. A.; Jayatilaka, D. Hirshfeld Surface Analysis. *CrystEngComm* **2009**, *11* (1), 19–32.

(104) Spackman, M. A.; McKinnon, J. J. Fingerprinting Intermolecular Interactions in Molecular Crystals. *CrystEngComm* **2002**, *4* (66), 378–392.

(105) M. J. Turner, J. J. McKinnon, S. K. Wolff, D. J. Grimwood, P. R. Spackman, D. Jayatilaka, M. A. S. Crystal Explorer. **2017**.

(106) Ropel, L.; Belvèze, L. S.; Aki, S. N. V. K.; Stadtherr, M. A.; Brennecke, J. F. Octanol-Water Partition Coefficients of Imidazolium-Based Ionic Liquids. *Green Chem.* **2005**, *7* (2), 83–90.

(107) Reddy, J. S.; Ganesh, S. V.; Nagalapalli, R.; Dandela, R.; Solomon, K. A.; Kumar, K. A.; Goud, N. R.; Nangia, A. Fluoroquinolone Salts with Carboxylic Acids. *J. Pharm. Sci.* **2011**, *100* (8), 3160–3176.

(108) Joshi, M.; Roy Choudhury, A. Salts of Amoxapine with Improved Solubility for Enhanced Pharmaceutical Applicability. *ACS Omega* **2018**, *3* (2), 2406–2416.

(109) Higuchi, T.; Connors, K. A. Phase Solubility Techniques. *Adv. Anal. Chem. Instrum.* **1965**, *4*,

117–212.

(110) Aakeröy, C. B.; Fasulo, M. E.; Desper, J. Cocrystal or Salt: Does It Really Matter? *Mol. Pharm.* **2007**, *4* (3), 317–322.

(111) Cruz-Cabeza, A. J. Acid–Base Crystalline Complexes and the PKa Rule. *CrystEngComm* **2012**, *14* (20), 6362.

(112) Tetko, I. V.; Gasteiger, J.; Todeschini, R.; Mauri, A.; Livingstone, D.; Ertl, P.; Palyulin, V. A.; Radchenko, E. V.; Zefirov, N. S.; Makarenko, A. S.; Tanchuk, V. Y.; Prokopenko, V. V. Virtual Computational Chemistry Laboratory - Design and Description. *J. Comput. Aided. Mol. Des.* **2005**, *19* (6), 453–463.

(113) Owen, R. T. Selective Histamine H1 Antagonism: A Novel Approach to Insomnia Using Low-Dose Doxepin. *Drugs of Today*. **2009**, 261–267.

(114) Wu, J.; Chang, F.; Zu, H. Efficacy and Safety Evaluation of Citalopram and Doxepin on Sleep Quality in Comorbid Insomnia and Anxiety Disorders. *Exp. Ther. Med.* **2015**, *10* (4), 1303–1308.

(115) Kouwenhoven, T. A.; van de Kerkhof, P. C. M.; Kamsteeg, M. Use of Oral Antidepressants in Patients with Chronic Pruritus: A Systematic Review. *J. Am. Acad. Dermatol.* **2017**, *77* (6), 1068-1073.e7.

(116) Eschler, D. C.; Klein, P. A. An Evidence-Based Review of the Efficacy of Topical Antihistamines in the Relief of Pruritus. *J. Drugs Dermat.* **2010**, 992–997.

(117) Wörz, R.; Berlin, J. Behandlung Chronischer Schmerzsyndrome Mit Antidepressiva. *Der Schmerz* **1989**, *3* (1), 1–7.

(118) Casale, R.; Symeonidou, Z.; Bartolo, M. Topical Treatments for Localized Neuropathic Pain. *Curr. Pain Headache Rep.* **2017**.

(119) Hershey, L. A.; Bednarczyk, E. M. Treatment of Headache in the Elderly. *Curr. Treat. Options Neurol.* **2013**, *15* (1), 56–62.

(120) Koch, H. J.; Jürgens, T. P. Antidepressants in Long-Term Migraine Prevention. *Drugs*. **2009**, 1–19.

(121) Feighner, J. P. Mechanism of Action of Antidepressant Medications. *J. Clin. Psy.* **1999**, 4–13.

(122) Hobbs, D. C. Distribution and Metabolism of Doxepin. *Biochem. Pharmacol.* **1969**, *18* (8), 1941–1954.

(123) Meyer-Barner, M.; Meineke, I.; Schreeb, K.; Gleiter, C. Pharmacokinetics of Doxepin and Desmethyldoxepin: An Evaluation with the Population Approach. *Eur. J. Clin. Pharmacol.* **2002**, *58* (4), 253–257.

(124) Yan, J. H.; Hubbard, J. W.; McKay, G.; Korchinski, E. D.; Midha, K. K. Absolute Bioavailability and Stereoselective Pharmacokinetics of Doxepin. *Xenobiotica.* **2002**, *32* (7), 615–623.

(125) Bruker, APEX3. SAINT, SADABS and XP. Bruker AXS Inc., Madison, Wisconsin, USA.

(126) CrysAlisPRO. Oxford Diffraction /Agilent Technologies UK Ltd, Yarnton, England.

(127) Raza, K.; Thotakura, N.; Kumar, P.; Joshi, M.; Bhushan, S.; Bhatia, A.; Kumar, V.; Malik, R.; Sharma, G.; Guru, S. K.; Katare, O. P. C60-Fullerenes for Delivery of Docetaxel to Breast Cancer Cells: A Promising Approach for Enhanced Efficacy and Better Pharmacokinetic Profile. *Int. J. Pharm.* **2015**, *495* (1), 551–559.

(128) Dement, W. C.; Miles, L. E.; Carskadon, M. A. “White Paper” on Sleep and Aging. *J. Am.*

Geriatr. Soc. **1982**, *30* (1), 25–50.

(129) Foley, D. J.; Monjan, A. A.; Brown, S. L.; Simonsick, E. M.; Wallace, R. B.; Blazer, D. G. Sleep Complaints among Elderly Persons: An Epidemiologic Study of Three Communities. *Sleep.* **1995**, *18* (6), 425–432.

(130) Mellinger, G. D.; Balter, M. B.; Uhlenhuth, E. H. Insomnia and Its Treatment: Prevalence and Correlates. *Arch. Gen. Psychiatry.* **1985**, *42* (3), 225–232.

(131) Roth, T.; Ancoli-Israel, S. Daytime Consequences and Correlates of Insomnia in the United States: Results of the 1991 National Sleep Foundation Survey. II. *Sleep.* **1999**, *22* (SUPPL. 2).

(132) Morgan, K.; Dallosso, H.; Ebrahim, S.; Arie, T.; Fentem, P. H. Prevalence, Frequency, and Duration of Hypnotic Drug Use among the Elderly Living at Home. *Br. Med. J. (Clin. Res. Ed).* **1988**, *296* (6622), 601.

(133) Moran, M. G.; Thompson, T. L.; Nies, A. S. Sleep Disorders in the Elderly. *Am. J. Psy.* **1988**, 1369–1378.

(134) Vitiello, M. V. Sleep Disorders and Aging: Understanding the Causes. *J. Gerontol. A Biol. Sci. Med. Sci.* **1997**, 89–98.

(135) Scharf, M. B.; Mayleben, D. W.; Kaffeman, M.; Krall, R.; Ochs, R. Dose Response Effects of Zolpidem in Normal Geriatric Subjects. *J. Clin. Psychiatry* **1991**, *52* (2), 77–83.

(136) Weitzel, K. W.; Wickman, J. M.; Augustin, S. G.; Strom, J. G. Zaleplon: A Pyrazolopyrimidine Sedative-Hypnotic Agent for the Treatment of Insomnia. *Clin. Ther.* **2000**, *22* (11), 1254–1267.

(137) Dooley, M.; Plosker, G. L. Zaleplon: A Review of Its Use in the Treatment of Insomnia. *Drugs.* **2000**, 413–445.

(138) Sanger, D. J.; Morel, E.; Perrault, G. Comparison of the Pharmacological Profiles of the Hypnotic Drugs, Zaleplon and Zolpidem. *Eur. J. Pharmacol.* **1996**, *313* (1–2), 35–42.

(139) Beer, B.; Ieni, J. R.; Wu, W. -H; Clody, D.; Amorusi, P.; Rose, J.; Mant, T.; Gaudreault, J.; Cato, A.; Stern, W. A Placebo-Controlled Evaluation of Single, Escalating Doses of CL 284,846, a Non-Benzodiazepine Hypnotic. *J. Clin. Pharmacol.* **1994**, *34* (4), 335–344.

(140) Rosen, A. S.; Fournié, P.; Darwish, M.; Danjou, P.; Troy, S. M. Zaleplon Pharmacokinetics and Absolute Bioavailability. *Biopharm. Drug Dispos.* **1999**, *20* (3), 171–175.

(141) Renwick, A. B.; Mistry, H.; Ball, S. E.; Walters, D. G.; Kao, J.; Lake, B. G. Metabolism of Zaleplon by Human Hepatic Microsomal Cytochrome P450 Isoforms. *Xenobiotica* **1998**, *28* (4), 337–348.

(142) Drover, D. R. Comparative Pharmacokinetics and Pharmacodynamics of Short-Acting Hypnosedatives: Zaleplon, Zolpidem and Zopiclone. *Clin. Pharmacokinet.* **2004**, 227–238.

(143) Lipinski, C. Poor Aqueous Solubility - An Industry Wide Problem in Drug Discovery. *Am. Pharm. Rev.* **2002**, *5* (3), 82–85.

(144) Chen, J.; Sarma, B.; Evans, J. M. B.; Myerson, A. S. Pharmaceutical Crystallization. *Cryst. Growth Des.* **2011**, *11* (4), 887–895.

(145) Rodríguez-Hornedo, N. Cocrystals: Molecular Design of Pharmaceutical Materials. *Mol. Pharm.* **2007**, 299–300.

(146) Malik, I. A.; Abbas, Z.; Karim, M.; Malik, I. A. Randomised Comparison of Oral Ofloxacin Alone with Combination of Parenteral Antibiotics in Neutropenic Febrile Patients. *Lancet.* **1992**, *339* (8801), 1092–1096.

(147) Horstkötter, C.; Blaschke, G. Stereoselective Determination of Ofloxacin and Its Metabolites in

Human Urine by Capillary Electrophoresis Using Laser-Induced Fluorescence Detection. *J. Chromatogr. B Biomed. Sci. Appl.* **2001**, *754* (1), 169–178.

(148) Morrissey, I.; Hoshino, K.; Sato, K.; Yoshida, A.; Hayakawa, I.; Bures, M. G.; Shen, L. L. Mechanism of Differential Activities of Ofloxacin Enantiomers? *Antimicrob. Agents Chemother.* **1996**, *40* (8), 1775–1784.

(149) Monk, J. P.; Campoli-Richards, D. M. Ofloxacin: A Review of Its Antibacterial Activity, Pharmacokinetic Properties and Therapeutic Use. *Drugs.* **1987**, *33* (4), 346–391.

(150) Mahapatra, S.; Venugopala, K. N.; Guru Row, T. N. A Device to Crystallize Organic Solids: Structure of Ciprofloxacin, Midazolam, and Ofloxacin as Targets. *Cryst. Growth Des.* **2010**, *10* (4), 1866–1870.

(151) National Center for Biotechnology Information. PubChem Database. Ofloxacin, CID=4583, https://pubchem.ncbi.nlm.nih.gov/compound/4583 (accessed Apr 27, 2019).

(152) Ball, P. Quinolone Generations: Natural History or Natural Selection? *J. Antimicrob. Chemother.* **2012**, *46* (suppl_3), 17–24.

(153) Ibsen, H. H.; Møller, B. R.; Halkier-Sørensen, L.; From, E. Treatment of Nongonococcal Urethritis: Comparison of Ofloxacin and Erythromycin. *Sex. Transm. Dis.* **1989**, *16* (1), 32–35.

(154) Mogabgab, W. J.; Holmes, B.; Murray, M.; Beville, R.; Lutz, F. B.; Tack, K. J. Randomized Comparison of Ofloxacin and Doxycycline for Chlamydia and Ureaplasma Urethritis and Cervicitis. *Chemotherapy.* **1990**, *36* (1), 70–76.

(155) DeAbate, C. A.; Henry, D.; Bensch, G.; Jubran, A.; Chodosh, S.; Harper, L.; Tipping, D.; Talbot, G. H. Sparfloxacin vs Ofloxacin in the Treatment of Acute Bacterial Exacerbations of Chronic Bronchitis: A Multicenter, Double-Blind, Randomized, Comparative Study. *Chest.* **1998**, *114* (1), 120–130.

(156) Gentry, L. O.; Rodriguez-Gomez, G.; Kohler, R. B.; Khan, F. A.; Rytel, M. W. Parenteral Followed by Oral Ofloxacin for Nosocomial Pneumonia and Community-Acquired Pneumonia Requiring Hospitalization. *Am. Rev. Respir. Dis.* **2011**, *145* (1), 31–35.

(157) Louw, G. E.; Warren, R. M.; Gey Van Pittius, N. C.; Leon, R.; Jimenez, A.; Hernandez-Pando, R.; McEvoy, C. R. E.; Grobbelaar, M.; Murray, M.; Van Helden, P. D.; Victor, T. C. Rifampicin Reduces Susceptibility to Ofloxacin in Rifampicin-Resistant Mycobacterium Tuberculosis through Efflux. *Am. J. Respir. Crit. Care Med.* **2011**, *184* (2), 269–276.

(158) Ji, B.; Grosset, J. Ofloxacin for the Treatment of Leprosy. *Acta Leprol.* **1991**, *7* (4), 321–326.

(159) Peipert, J. F.; Sweet, R. L.; Walker, C. K.; Kahn, J.; Rielly-Gauvin, K. Evaluation of Ofloxacin in the Treatment of Laparoscopically Documented Acute Pelvic Inflammatory Disease (Salpingitis). *Infect. Dis. Obstet. Gynecol.* **1999**, *7* (3), 138–144.

(160) Todd, P. A.; Faulds, D. Ofloxacin: A Reappraisal of Its Antimicrobial Activity, Pharmacology and Therapeutic Use. *Drugs.* **1991**, *42* (5), 825–876.

(161) Ariyarit, C.; Panikabutra, K.; Chitwarakorn, A.; Wongba, C.; Buatiang, A. Efficacy of Ofloxacin in Uncomplicated Gonorrhoea. *Infection.* **1986**, *14* (4 Supplement), S311–S313.

(162) Jüngst, G.; Mohr, R. Side Effects of Ofloxacin in Clinical Trials and in Postmarketing Surveillance. *Drugs.* **1987**, *34* (1), 144–149.

(163) Borrmann, L.; Tang-Liu, D. D.; Kann, J.; Nista, J.; Lin, E. T.; Frank, J. Ofloxacin in Human Serum, Urine, and Tear Film after Topical Application. *Cornea.* **1992**, *11* (3), 226–230.

(164) Förster, C.; Kociok, K.; Shakibaei, M.; Merker, H. J.; Vormann, J.; Günther, T.; Stahlmann, R. Integrins on Joint Cartilage Chondrocytes and Alterations by Ofloxacin or Magnesium

Deficiency in Immature Rats. *Arch. Toxicol.* **1996**, *70* (5), 261–270.

(165) Lipinski, C. A. Drug-like Properties and the Causes of Poor Solubility and Poor Permeability. *J. Pharmacol. Toxicol. Methods.* **2000**, *44* (1), 235–249.

(166) Datta, S.; Grant, D. J. W. Crystal Structures of Drugs: Advances in Determination, Prediction and Engineering. *Nat. Rev. Drug Discov*. **2004**, 42–57.

(167) Douroumis, D.; Fahr, A. Drug Delivery Strategies for Poorly Water-Soluble Drugs. *Taylor & Francis*, **2013**, 4.

(168) Krishnaiah, Y. S. . Pharmaceutical Technologies for Enhancing Oral Bioavailability of Poorly Soluble Drugs. *J. Bioequiv. Availab.* **2010**, *02* (02), 1–5.

(169) Trask, A. V.; Motherwell, W. D. S.; Jones, W. Physical Stability Enhancement of Theophylline via Cocrystallization. *Int. J. Pharm.* **2006**, *320* (1–2), 114–123.

(170) Gart, E. V; Suchodolski, J. S.; Welsh, T. H.; Alaniz, R. C.; Randel, R. D.; Lawhon, S. D. Salmonella Typhimurium and Multidirectional Communication in the Gut. *Front. Microbiol.* **2016**, *7*, 1827.

(171) Limwikrant, W.; Higashi, K.; Yamamoto, K.; Moribe, K. Characterization of Ofloxacin-Oxalic Acid Complex by PXRD, NMR, and THz Spectroscopy. *Int. J. Pharm.* **2009**, *382* (1–2), 50–55.

(172) Lee, H. G.; Zhang, G. G. Z.; Flanagan, D. R. Cocrystal Intrinsic Dissolution Behavior Using a Rotating Disk. *J. Pharm. Sci.* **2011**, *100* (5), 1736–1744.

(173) Hoogkamp-Korstanje, J. A. A. In-Vitro Activities of Ciprofloxacin, Levofloxacin, Lomefloxacin, Ofloxacin, Pefloxacin, Sparfloxacin and Trovafloxacin against Gram-Positive and Gram-Negative Pathogens from Respiratory Tract Infections. *J. Antimicrob. Chemother.* **1997**, *40* (3), 427–431.

(174) Radi, A.; El-Sherif, Z. Determination of Levofloxacin in Human Urine by Adsorptive Square-Wave Anodic Stripping Voltammetry on a Glassy Carbon Electrode. *Talanta.* **2002**, *58* (2), 319–324.

(175) Sarkar, S.; Sengupta, M.; SenGupta, M.; Chakraborty, A.; Ghosh, S.; Mukhopadhyay, S. In Vitro Activity of Levofloxacin against Lower Respiratory Tract Pathogens. *J. Basic Clin. Pharm.* **2015**, *6* (3), 89.

(176) Davis, R.; Bryson, H. M. Levofloxacin: A Review of Its Antibacterial Activity, Pharmacokinetics and Therapeutic Efficacy. *Drugs.* **1994**, *47* (4), 677–700.

(177) Gorman, E. M.; Samas, B.; Munson, E. J. Understanding the Dehydration of Levofloxacin Hemihydrate. *J. Pharm. Sci.* **2012**, *101* (9), 3319–3330.

(178) Furet, Y. X.; Deshusses, J.; Pechere, J. C. Transport of Pefloxacin across the Bacterial Cytoplasmic Membrane in Quinolone-Susceptible Staphylococcus Aureus. *Antimicrob. Agents Chemother.* **1992**, *36* (11), 2506–2511.

(179) Hayakawa, I.; Atarashi, S.; Yokohama, S.; Imamura, M.; Sakano, K.; Furukawa, M. Synthesis and Antibacterial Activities of Optically Active Ofloxacin. *Antimicrob. Agents Chemother.* **1986**, *29* (1), 163–164.

(180) Jones, W.; Motherwell, W. D. S.; Trask, A. V. Pharmaceutical Cocrystals: An Emerging Approach to Physical Property Enhancement. *MRS Bull.* **2006**, *31* (11), 875–879.

(181) Hickey, M. B.; Peterson, M. L.; Scoppettuolo, L. A.; Morrisette, S. L.; Vetter, A.; Guzmán, H.; Remenar, J. F.; Zhang, Z.; Tawa, M. D.; Haley, S.; Zaworotko, M. J.; Almarsson, Ö. Performance Comparison of a Co-Crystal of Carbamazepine with Marketed Product. *Eur. J. Pharm. Biopharm.* **2007**, *67* (1), 112–119.

(182) Joshi, M.; Roy Choudhury, A. Salts of Amoxapine with Improved Solubility for Enhanced Pharmaceutical Applicability. *ACS Omega.* **2018**, *3* (2), 2406–2416.

(183) Kitaoka, H.; Wada, C.; Moroi, R.; Hakusui, H. Effect of Dehydration on the Formation of Levofloxacin Pseudopolymorphs. *Chem. Pharm. Bull.* **1995**, *43* (4), 649–653.

(184) Drevenšek, P.; Košmrlj, J.; Giester, G.; Skauge, T.; Sletten, E.; Sepčić, K.; Turel, I. X-Ray Crystallographic, NMR and Antimicrobial Activity Studies of Magnesium Complexes of Fluoroquinolones - Racemic Ofloxacin and Its S-Form, Levofloxacin. *J. Inorg. Biochem.* **2006**, *100* (11), 1755–1763.

(185) Sousa, I.; Claro, V.; Pereira, J. L.; Amaral, A. L.; Cunha-Silva, L.; De Castro, B.; Feio, M. J.; Pereira, E.; Gameiro, P. Synthesis, Characterization and Antibacterial Studies of a Copper(II) Levofloxacin Ternary Complex. *J. Inorg. Biochem.* **2012**, *110*, 64–71.

(186) Singh, S. S.; Thakur, T. S. New Crystalline Salt Forms of Levofloxacin: Conformational Analysis and Attempts towards the Crystal Structure Prediction of the Anhydrous Form. *CrystEngComm* **2014**, *16* (20), 4215–4230.

(187) Friščić, T.; Fábián, L.; Burley, J. C.; Jones, W.; Motherwell, W. D. S. Exploring Cocrystal-Cocrystal Reactivity via Liquid-Assisted Grinding: The Assembling of Racemic and Dismantling of Enantiomeric Cocrystals. *Chem. Commun.* **2006**, No. 48, 5009–5011.

(188) Bruker, A. V. 0 Data Collection and Processing Software. *Bruker AXS Inc., Madison, Wisconsin, USA.* **2008**.

(189) Bourhis, L. J.; Dolomanov, O. V.; Gildea, R. J.; Howard, J. A. K.; Puschmann, H. The Anatomy of a Comprehensive Constrained, Restrained Refinement Program for the Modern Computing Environment - Olex2 Dissected. *Acta Crystallogr. Sect. A Found. Crystallogr.* **2015**, *71* (1), 59–75.

(190) Macrae, C. F.; Edgington, P. R.; McCabe, P.; Pidcock, E.; Shields, G. P.; Taylor, R.; Towler, M.; Van De Streek, J. Mercury: Visualization and Analysis of Crystal Structures. *J. Appl. Crystallogr.* **2006**, 453–457.

(191) Suto, M. J.; Domagala, J. M.; Roland, G. E.; Mailloux, G. B.; Cohen, M. A. Fluoroquinolones: Relationships between Structural Variations, Mammalian Cell Cytotoxicity, and Antimicrobial Activity. *J. Med. Chem.* **1992**, *35* (25), 4745–4750.

(192) Sheikh, N. W.; Tripathi, A. S.; Chitra, V.; Choudhury, A.; Dewani, A. P. Development and Validation of RP-HPLC Assay for Levofloxacin in Rat Plasma and Saliva: Application to Pharmacokinetic Studies. *African J. Pharm. Pharmacol.* **2011**, *5* (13), 1612–1618.

(193) Kumar, P.; Sharma, G.; Kumar, R.; Malik, R.; Singh, B.; Katare, O. P.; Raza, K. Stearic Acid Based, Systematically Designed Oral Lipid Nanoparticles for Enhanced Brain Delivery of Dimethyl Fumarate. *Nanomedicine.* **2017**, *12* (23), 2607–2621.

(194) Kumar, P.; Sharma, G.; Kumar, R.; Singh, B.; Malik, R.; Katare, O. P.; Raza, K. Promises of a Biocompatible Nanocarrier in Improved Brain Delivery of Quercetin: Biochemical, Pharmacokinetic and Biodistribution Evidences. *Int. J. Pharm.* **2016**, *515* (1–2), 307–314.

Publications from Thesis

1. **Joshi M.**, Choudhury A. R. Salts of Amoxapine with Improved Solubility for Enhanced Pharmaceutical Applicability. *ACS Omega*. **2018**, 3, 2, 2406-2416.
2. **Joshi M.**, Choudhury A. R. Salts of amoxapine with improved solubility for enhanced pharmaceutical applicability. *Acta Crystallogr. A.* **2017**, A70, C208.
3. **Joshi M.**, Choudhury A. R. Salt of Amoxapine with D (-) Tartaric acid: Synthesis, Structural and Physical Analysis. *CrystEngComm.* **2022**. (Submitted)
4. **Joshi M.,** Choudhury A. R. Development of Novel Solid Phase Salts of Antidepressant Drug Doxepin from Liquid Phase: Improved Physicochemical Properties. *Mol. Pharm.* **2022**. (Submitted)
5. **Joshi M.,** Choudhury A. R. Cocrystals of Hypnotic Drug Zaleplon: Synthesis, Structural and Physicochemical Studies. *Mol. Pharm.* **2022**. (Submitted)
6. **Joshi M.**, Verma I., Gulati A., Mukhopadhaya A., Choudhury A R. Salts of Ofloxacin with Enhanced Physical and Micro-Biological Properties. *J. Mol. Sturt.* **2022**. (Submitted)
7. **Joshi M.**, Gulati A., Verma I., Raza K., Mukhopadhaya A., Choudhury A. R. Synthesis and Characterization of salts of Levofloxacin: Physical, Microbiological and Pharmacokinetic Overview. *Acta Crystallogr. B.* **2022**. (Submitted)
8. **Joshi M.**, Choudhury A. R. Progressive approach of supermolecules towards the advancement of antimicrobial drugs; Pharmaceutical Applications of Supramolecules. *Springer Nature*. **2022**. (Book Chapter)

Publications from Collaboration

1. Mahato S., Rawal P., Devadkar A. K., **Joshi M.**, Choudhury A. R., Biswas B., Gupta P., Panda T. K. Hydroboration and reductive amination of ketones and aldehydes with HBpin by a bench stable Pd (II)-catalyst. *Org. Biomol. Chem.*, **2022**.
2. Mahato S., Mondal A., Das M., **Joshi M.**, Ray P., Choudhury A. R., Reddy C. M., Biswas B. De novo synthesis of hybrid d-f block metal complex salts for electronic charge transport applications. *Dalton Trans.* **2022**.
3. Rokkam S. K., Yadav M., **Joshi M.,** Choudhury A. R., Sahal D., Golakoti N. R. Synthesis, *in vitro* anti-plasmodial potency, *in silico* cum SPR binding with inhibition of *Pf*Pyridoxal synthase, and rapid parasiticidal action by 3,5-Bis {(E) arylidene}-N-methyl-4-piperidones. *New J. Chem.* **2021,** 45, 22150-22165.
4. Mahato R. K., Das S., **Joshi M.,** Choudhury A. R., Misra A., Biswas B. Biomimics of phenazine oxidase activity of a cobalt (III)-dipyridylamine complex: Spectroscopic, structural, and computational studies. *Appl. Organomet. Chem.* **2021**, e6483.
5. Mukherjee S., Pal C. K., Kotakonda M., **Joshi M.,** Shit M., Ghosh P., Choudhury A. R., Biswas B. Solvent induced distortion in a square planner copper(II) complex containing an azo-functionalized Schiff base: Synthesis, crystal structure, *in-vitro* fungicidal and anti-proliferative, and catecholase activity. *J. Mol. Struc.* **2021**, 1245, 131057.

6. Biswas B., Banerjee N., **Joshi M.**, Armaković S., Armaković S. J., Das H. S., Choudhury A. R. Unprecedented Copper(II) Coordination Induced Nucleophilic Cleavage of Quinoxaline Heterocycle: Structural and Computational Studies. *CrystEngComm.* **2021**, **23**, 5078-5086.

7. De J., Yadav R. K., Yadav R. S., Gupta S. P., **Joshi M.**, Choudhury A. R., Jayakumar J., Jou J. H., Cheng C. H., Pal S. K. Molecular Engineering for the Development of a Discotic Nematic Mesophase and Solid-State Emitter in Deep-Blue OLEDs. *J. Org. Chem.* **2021**, 86, 10, 7256–7262.

8. Mudi P. K., Mahato R. K., **Joshi M.**, Shit M., Choudhury A. R., Das H. S., Biswas B. Copper (II) complexes with a benzimidazole functionalized Schiff base: Synthesis, crystal structures, and role of ancillary ions in phenoxazinone synthase activity. *Appl. Organomet. Chem.* **2021**, 35, 6, e6211.

9. Roy S., Paul P., Karar M., **Joshi M.**, Paul S., Choudhury A. R., Biswas B. Cascade detection of fluoride and bisulphate ions by newly developed hydrazine functionalised Schiff bases. *J. Mol. Liq.* **2021**, 326, 115293.

10. P A. P., **Joshi M.**, Verma D., Jadhav S., Choudhury A. R., Jana D. Layered $Cs_4CuSb_2Cl_{12}$ Nanocrystals for Sunlight-Driven Photocatalytic Degradation of Pollutants. *ACS Appl. Nano Mater.* **2021**, 4, 2, 1305–1313.

11. Mahato S., Meheta N., Kotakonda M., **Joshi M.**, Shit M., Choudhury A. R., Biswas B. Synthesis, structure, polyphenol oxidase mimicking and bactericidal activity of a zinc-schiff base complex. *Polyhedron*. **2021**, 194, 114933.

12. Singh A., Maji A., **Joshi M.**, Choudhury A. R., Ghosh K. Designed pincer ligands supported Co(II)-based catalysts for dehydrogenative activation of alcohols: Studies on N-alkylation of amines, α-alkylation of ketones and synthesis of quinolines. *Dalton Trans.* **2021**, 50, 8567-8587.

13. Chatterjee A., Kaur G., **Joshi M.**, Choudhury A. R., Ghosh R. pH dependent catecholase activity of Fe(II) complexes of type $[Fe(L)]X_2$ [L = N-(phenyl-pyridin-2-yl-methylene)-ethane-1,2-diamine; X = $ClO4^-$ (1), $PF6^-$ (2)]: Role of counter anion on turnover number. *Inorganica Chim. Acta*. **2020**, 513, 119933.

14. Mahato S., Meheta N., Kotakonda M., **Joshi M.**, Ghosh P., Shit M., Choudhury A. R., Biswas B. Ligand directed synthesis of a unprecedented tetragonalbipyramidal copper (II) complex and its antibacterial activity and catalytic role in oxidative dimerisation of 2-aminophenol. *Appl. Organomet. Chem.* **2020**, 34, 11, e5935.

15. Tamang N., Ramamoorthy G., **Joshi M.**, Choudhury A. R., Kumar S., Golakoti N. R., Doble M. Diarylidenecyclopentanone derivatives as potent anti-inflammatory and anticancer agents. *Med. Chem. Res.* **2020**, 29, 9, 1579–1589.

16. Pal C. K., Mahato S., **Joshi M.**, Paul S., Choudhury A. R., Biswas B. Transesterification activity by a zinc (II)-schiff base complex with theoretical interpretation. *Inorganica Chim. Acta*. **2020**, 506, 119541.

17. Mudi P. K., Bandopadhyay N., **Joshi M.**, Shit M., Paul S., Choudhury A. R., Biswas B. Schiff base triggering synthesis of copper (II) complex and its catalytic fate towards mimics of phenoxazinone synthase activity. *Inorganica Chim. Acta*. **2020**, 505, 119468.

18. Mudi P. K., Mahato R. K., **Joshi M.**, Paul S., Choudhury A. R., Biswas B. Synthesis and structural characterization of a linkage isomer to a mononuclear Nickel (II) complex:

Experimental and computational depiction of phosphoesterase efficiency. *J. Mol. Struct.* **2020**, 1200, 127083.

19. Santra B., Kumar V., Kalita P., Gupta V., Mandal D., Chandra A., **Joshi M.**, Choudhury A. R., Jana A., Chandrasekhar V. Molecular di-and tetra-nuclear zinc (II) phosphates with sterically hindered aryl phosphate mono esters ligands. *Polyhedron.* **2019**, 172, 216-225.

20. Kachwal V., **Joshi M.**, Mittal V., Choudhury A. R., Laskar I. R. Strategic design and synthesis of AIEE (Aggregation Induced Enhanced Emission) active push-pull type pyrene derivatives for the ultrasensitive detection of explosives. *Sensing and Bio-Sensing Research.* **2019**, 23, 100267.

21. Chowdhury B., Karar M., Paul S., **Joshi M.**, Choudhury A. R., Biswas B. Salen type ligand as a selective and sensitive nickel (II) ion chemosensor: a combined investigation with experimental and theoretical modelling. *Sens. Actuators B Chem.* **2018**, 276, 560-566.

22. Chowdhury B., Bhowmik B., Sahu A., **Joshi M.**, Paul S., Choudhury A. R., Biswas B. Phenoxazinone synthase and antimicrobial activity by a bis (1, 3-diamino-2-propanolate) cobalt (III) complex. *J. Chem. Sci.* **2018**, 130, 12, 1-12.

23. Garai M., Das A., **Joshi M.**, Paul S., Shit M., Choudhury A. R., Biswas B. Synthesis and spectroscopic characterization of a photo-stable tetrazinc (II)–Schiff base cluster: A rare case of ligand centric phenoxazinone synthase activity. *Polyhedron.* **2018**, 156, 223-230.

24. Das S., Sahu A., **Joshi M.**, Paul S., Shit M., Choudhury A. R., Biswas B. Ligand-Centered Radical Activity by a Zinc-Schiff-Base Complex towards Catechol Oxidation. *ChemSelect.* **2018**, 3, 38, 10774-10781.

25. De A., Sahu A., Paul S., **Joshi M.**, Choudhury A. R., Biswas B. Structural and luminescent properties of a new 1D Cadmium (II) coordination polymer: A combined effort with experiment & theory. *J. Mol. Struct.* **2018**, 1167, 187-193.

26. Sahoo S. C., **Joshi M.**, Pan S. C. Diastereoselective Desymmetrization of Prochiral Cyclopentenediones via Cycloaddition Reaction with *N*-Phenacylbenzothiazolium Bromides. *J. Org. Chem.* **2017**, 82, 23, 12763-12770.

Publication from M. Pharm. Project, CURAJ Ajmer

1. Misra C., **Joshi M.**, Raza K. Do fullerenes have the potential to cross the threshold for drug delivery?. *Chem. Rev.*, **2022**. (Submitted)

2. **Joshi M.**, Kumar P., Kumar R., Sharma G., Singh B., Katare O. P., Raza K. Aminated carbon-based "cargo vehicles" for improved delivery of methotrexate to breast cancer cells. *Mater. Sci. Eng. C Mater. Biol. Appl.* **2017**, 75, 1376-1388.

3. Raza K., Thotakura N., Kumar P., **Joshi M.**, Bhushan S., Bhatia A., Kumar V., Malik R., Sharma G., Guru S. K., Katare O. P. C_{60}-fullerenes for delivery of docetaxel to breast cancer cells: a promising approach for enhanced efficacy and better pharmacokinetic profile. *Int. J. Pharm.* **2015**, 495, 1, 551-559.